学位申請論文

Research on the chemopreventive effect of approved drugs on colorectal cancer and its mechanisms
(既存薬を利用した大腸がん予防と
その作用機序解明)

2020 年 3 月

<ruby>鱧屋<rt>はもや</rt></ruby> <ruby>隆博<rt>たかひろ</rt></ruby>

Contents   Pages

Abbreviations

APC	adenomatous polyposis coli
AP-1	activator protein-1
ART	artesunate
COX	cyclooxygenase
CRC	colorectal cancer
EM	erythromycin
FBS	fetal bovine serum
FDA	Food and Drug Administration
GAPDH	glyceraldehyde-3-phosphate dehydrogenase
IL	interleukin
IS	internal standard
LC/MS	liquid chromatography/mass spectrometry
LEF1	lymphoid enhancer factor
NF-κB	nuclear factor-kappaB
NOX	NADPH oxidase
NRF2	nuclear respiratory factor 2
NLS	nuclear localization signal
Min	multiple intestinal neoplasia
PBS	phosphate-buffered saline
PCR	polymerase chain reaction
ppm	parts per million
RNA	ribonucleic acid
RT-PCR	reverse transcription-polymerase chain reaction
RCs	reactive carbonyl species
SD	standard deviation
SRM	selected reaction monitoring
TCF	T-cell factor
TNF	tumor necrosis factor

1. 要旨

〈序論〉

　1981 年以降、日本における死因の 1 位は、変わることなく悪性腫瘍(がん)である。また、近年の高齢化や食生活の変化などにより、がんの罹患者数は増加しており早急に有効ながん対策を施行する必要がある。がんの治療においては、近年第 4 の柱として免疫療法が注目されているが、どの疾患においても予防が一番有効であり、未然に防ぐ予防という観点から研究を行なうことが今後重要である。現在、比較的成果が報告されているがん予防研究としては、胃がんに対するヘリコバクター・ピロリ菌の除去や大腸がんに対する低用量アスピリン投与などが挙げられる。また、子宮頸がんワクチンの効果も期待されるが、日本における接種率は極端に低い。ヘリコバクター・ピロリ菌や子宮頸がんワクチンなど感染症対策は政策レベルにまで達しているが、未だがん化学予防剤と呼ばれる薬は研究レベルに留まっている。その要因として考えられるのが、薬剤開発には高額な資金と膨大な時間を有するが、がん予防薬を開発後の利潤が明らかに低いことが挙げられる。この要因を打破するための一つの方法として、現在市販されている既存薬の中からがん予防に効果的な薬をドラッグリポジショニングの考えを用いて見出す方法がある。この方法は、薬剤開発において課題として挙げられる投与量と副作用についての情報が豊富であることから、長期的な服用が想定される予防薬開発に応用することは最適であると考えられる。

　国立がん研究センター 予防研究部の武藤倫弘グループでは、以前ヒト大腸がん由来細胞である DLD-1 細胞および HCT116 細胞を用いて大腸発がんの初期段階に寄与すると考えられている細胞増殖/分化・炎症・酸化ストレスの 3 つの状態を指標とした既存薬のがん化学予防剤スクリーニングを行なった。スクリーニングの対象薬剤として、東京大学創薬機構が管理する約 1280 種類の既存薬ライブラリーを用い、各細胞を処理した際に 3 つの指標を抑制する効果を複合的に評価することで複数のがん予防剤の候補を見出した。本研究において、私は

このスクリーニングによって選択された薬剤の中から安全性が高く、炎症抑制効果の強かったエリスロマイシン及び細胞増殖/分化の抑制効果が強かったアルテスネイトに着目し、これら二つの薬剤について *in vitro* 及び *in vivo* にてがん予防効果の検証と作用機序の解明を行なった。

〈第一部：エリスロマイシンを用いた腸発がん抑制効果の検討〉

エリスロマイシンは、マクロライド系の抗生物質と知られ、慢性びまん性汎細気管支炎の治療薬として臨床で広く用いられている。また、抗炎症や抗酸化ストレス作用を有することがいくつかのがん細胞を用いた研究で報告が挙げられているが、大腸がんに対する予防効果に関しては報告がない。そこで、まずヒト大腸がん由来細胞である SW48 および HCT116 細胞を用い、エリスロマイシンを添加した際の抗炎症作用にについて検討を行なった。その結果、エリスロマイシンは炎症性サイトカインである IL-1βや TNFα 添加(がん組織が前炎症状態にあると考えられているため、疑似的な慢性炎症状態を作成)により活性化された NF-κB の転写活性とその下流因子(IL-6, COX-2)の mRNA 発現レベルを抑制することを見出した。さらに、家族性大腸腺腫モデルマウスである Min マウスに対し、5 週齢から 13 週齢の 8 週間 500 ppm のエリスロマイシンを混餌にて投与を行なった。Min マウスはがん抑制遺伝子 *Apc* に変異より Wnt シグナルが過剰活性化しているマウスであり、小腸を中心に腺腫(前がん病変)が多発することが報告されている。その結果、投与 8 週後において、小腸近位部位における腸ポリープの生成数が非投与群に比べて減少していた。また、腸ポリープ部位において炎症関連因子(IL-6 や COX-2)の抑制が確認された。さらに、酸化ストレスの変化については、肝臓および血液サンプルにおける活性カルボニル化合物(過酸化脂質の分解により生成される生体内の酸化ストレスマーカー)の存在量を評価し、エリスロマイシンを投与することで、この化合物の減少が確認された。以上の結果より、エリスロマイシンは炎症の抑制や抗酸化ストレス作用により、大腸がんを予防する能力があることを見出した。

〈第二部：アルテスネイトを用いた腸発がん抑制効果の検討〉

　アルテスネイトは、2015年に中国の研究者である Tu Youyou 博士が抗マラリア薬として開発した薬剤であり、現在、抗マラリア薬として世界的に使用されており、ノーベル賞を受賞する功績となった薬剤である。また、近年、抗がん作用があることが報告されているが、その作用機序等は未だ明らかにはなっていない。そこで、私はスクリーニングの結果をもとに、アルテスネイトをがん予防薬としても開発できると考え、アルテスネイトの大腸がんの原因となる Wnt シグナルに与える影響について検討を行なった。その結果、ヒト大腸がん由来細胞である DLD-1 および HCT116 細胞において、アルテスネイトは Wnt シグナルが調節する TCF/LEF の転写活性およびその下流因子(c-Myc, cyclin D1)の mRNA 及びタンパク発現を抑制した。

　in vitro の結果を *in vivo* で確認するために、Min マウスに対してアルテスネイトの混餌投与を行なった。その結果、腸ポリープ生成数の抑制及び腸ポリープ部位における細胞増殖関連因子(c-Myc, cyclin D1)の mRNA 発現の抑制が確認された。以前の研究において、Wnt シグナルの抑制効果としてβ-catenin の存在量もしくはリン酸化の亢進などが報告されているが、アルテスネイト処理では、これらの影響が見られなかった。このため、アルテスネイトが作用する特異的なタンパク質があると考え、それの同定を試みた。今回、ナノ磁性微粒子である FG ビーズを用いてアルテスネイト結合磁気ビーズを作成し、結合したタンパクを mass spectrometry にて同定した。次に、同定した複数のタンパクについて、それらをコードする遺伝子をノックダウンし、その薬剤効果を評価することにより、核移行関連タンパクRAN をアルテスネイト結合タンパクとして同定した。さらに、アルテスネイトによる Wnt シグナルの抑制効果が RAN のノックダウンにより抑制されることからアルテスネイトによる Wnt シグナルの抑制に RAN が寄与していることが示唆された。Wnt シグナル下流における転写因子 TCF/LEF の活性化には TCF の細胞質から核内への移行が必要である。Western blot および細胞蛍光免疫染色によりアルテスネイト投与後の TCF1 の核内量が減少してい

ることが分かった。このことは、アルテスネイトが RAN の機能を阻害すること
で TCF/LEF の転写活性を抑制している可能性を示している。以上の結果より、
アルテスネイトは大腸がんにおいて RAN の機能を抑制することで、過剰な Wnt
シグナルが及ぼす細胞増殖を抑制すると考えられた。

〈結論〉

　最後に本研究では、既存薬ライブラリーのスクリーニングによって単離され
た薬剤から選択したエリスロマイシン及びアルテスネイトが *in vitro* 及び *in vivo*
実験にて大腸発がんの抑制効果があることを示した。エリスロマイシンは、炎
症や抗酸化ストレス作用介して腸発がん抑制作用を示すことが明らかになった。
また、アルテスネイトは、タンパク質の核移行を制御する RAN を介して過剰な
Wnt シグナルを抑制し、腸発がん抑制作用を示すことが明らかになった。

2. Abstract

The major cause of death in Japan since 1981 is cancer. Moreover, the number of cancer patients is increasing due to an aging society and changes in diet through the spread of western dietary habits. Therefore, it is important to control cancer immediately. In recent years, cancer prevention research has become more important. In this study, I investigated the anti-carcinogenic effects of two drugs, erythromycin (EM) and artesunate (ART). These two drugs were selected from a previous screening system of ours to detect cancer prevention agents among FDA approved drugs.

EM, a macrolide antibiotic, has been shown to exert pleiotropic effects, such as anti-inflammatory and anti-oxidative effects, on mammalian cells. In the present study, I aimed to evaluate the preventive effects of EM on intestinal carcinogenesis. I first confirmed that EM suppresses the transcriptional activity of nuclear factor-kappaB (NF-κB) and activator protein-1 (AP-1) and the expression of its downstream targets, interleukin (IL)-6 and cyclooxygenase (COX)-2, in human colon cancer cells. Next, I fed 5-week-old male *Apc* mutant Min mice a diet containing 500 ppm EM for 13 weeks. EM treatment significantly reduced the number of proximal intestinal polyps to 70.9% of the untreated control value. Moreover, EM reduced the levels of IL-6 and COX-2 mRNA expression in intestinal polyps. Although the levels of hepatic NADPH oxidase mRNA decreased, EM treatment did not affect the levels of oxidative stress markers, reactive carbonyl species, in the liver of Min mice. My results suggest that EM suppresses intestinal polyp development in Min mice, in part by attenuating local inflammation, and indicate that EM is useful as a chemopreventive agent.

ART, an antimalarial drug, has been shown to suppress inflammation via inhibiting NF-κB signaling, and induces apoptosis by overproducing reactive oxygen

species in colorectal cancer (CRC) cells. In the present study, I aimed to evaluate the preventive effects of ART on intestinal carcinogenesis. I first confirmed that ART suppresses the transcriptional activity of T-cell factor/lymphoid enhancer-binding factor and the expression of its downstream targets, c-Myc and Cyclin D1 in human CRC cells. Next, I fed 5-week-old male Min mice a diet containing 5 or 10 ppm ART for 13 weeks. ART treatment significantly reduced the number of distal intestinal polyps to 79.2% and 71.3% of the untreated control value. Moreover, ART reduced the levels of c-Myc and Cyclin D1 mRNA expression in intestinal polyps. Next, I searched for ART-binding protein using FG beads. As a result of mass spectrometry analysis, a nuclear translocation-related protein, RAN, was identified as a candidate. When RAN was knocked down using siRNA in CRC cells, the ART-suppressed Wnt signaling suppression disappeared. Moreover, the amount of TCF1/TCF7 in the nucleus was reduced by ART. My results suggest that ART suppresses excessive Wnt pathway and intestinal polyp development *in vitro* and *in vivo*. Therefore, I assumed that these inhibitory effects were caused by ART binding to RAN to inhibit its function.

The two drugs, EM and ART, used in this study have been shown to suppress intestinal carcinogenesis through inhibiting regulatory factors involved in carcinogenesis.

3. Introduction

Colorectal cancer (CRC) is the second leading cause of cancer death (881,000 deaths) worldwide, with an estimated incidence of 1.8 million in 2018 (1). Thus, it is important to establish useful methods for preventing it. One approach is to use chemopreventive agents that meet the following criteria: i) having convenient dosing schedules, ii) easy administration, iii) low cost and iv) most importantly, few side effects (2). To find useful preventive drug candidates, I previously developed a high throughput drug screening system using a reporter gene assay, and estimated a "validated library" consisting of 1280 drugs approved by the FDA (3). In this study, targeting signaling pathways were evaluated that suppress inflammation (NF-κB signaling), cell proliferation/differentiation (Wnt/β-catenin signaling) and oxidative stress (Nrf2 signaling). I selected two highly safe drugs (EM and ART) from the screening results.

EM is known as one of macrolide drugs. Macrolides are commonly used antibiotics that have good oral bioavailability and limited side effects, and exhibit prolonged tissue persistence. Macrolides bind to bacterial 50S ribosomes, not to eukaryotic cells, leading to the inhibition of transpeptidation or nascent peptide translocation, and thus cause a limited number of side effects. It has been reported that long-term low-dose use (400–600 mg/day for 6 months to 2 years) of EM, a macrolide antibiotic with a 14-membered ring, is effective against diffuse panbronchiolitis and does not cause severe side effects (4, 5).

Acute inflammation is one of the body's protective responses. On the other hand, chronic inflammation could be a risk for carcinogenesis. This prolonged inflammation situation includes infections by certain viruses, bacteria and parasites, or foreign bodies. The NF-κB pathway plays an important role in inflammation-related

7

signaling. The canonical NF-κB pathway responds to a variety of stimuli, such as cytokines. Moreover, nuclear translocation of NF-κB induces inflammation-related factors, such as IL-6 and COX-2 (6). IL-6 and COX-2 are well-known cancer promoters. Thus, it is important to develop cancer chemopreventive agents that target the canonical NF-κB pathway.

Recently, EM has been reported to exert anti-inflammatory and anti-oxidative effects on mammalian cells *in vitro* and *in vivo*, in addition to exerting antimicrobial effects, by modulating the secretion of pro-inflammatory cytokines, such as IL-6, IL-1β and tumor necrosis factor (TNF) α (7), and inhibiting their oxidant burst by inhibiting neutrophil NADPH oxidase (NOX) activation (8). NOX is an enzyme that produces reactive oxides. EM has been reported to suppress mRNA expression of IL-8 by inhibiting NF-κB and AP-1 activity on bronchial epithelial cells (9). Of note, NF-κB and AP-1 dysregulation have been suggested to promote carcinogenesis (10-12). It has been established that both inflammation and oxidative stress status play pivotal roles in colorectal carcinogenesis. However, the preventive effects of erythromycin on intestinal carcinogenesis have not yet been elucidated.

In this study, I demonstrated that EM weakly but significantly suppressed NF-κB and AP-1 transcriptional activity and pro-inflammatory cytokine expression, and decreased intestinal tumorigenesis in *Apc* mutant Min mice, a model of familial adenomatous polyposis. Intestinal tissue of Min mouse is known to be pro-inflammatory status, and therefore, this mouse is often used to evaluate anti-inflammatory effect. In addition, EM administration reduced the mRNA expression levels of hepatic NADPH oxidase in Min mouse.

ART is a semisynthetic derivative of artemisinin, a compound isolated from the

plant *Artemesia annua*. It is clinically used as an antimalarial drug worldwide. To date, ART has reported to possess an anti-cancer function through suppression of inflammation via inhibiting NF-κB signaling and induces apoptosis by overproducing reactive oxygen species in CRC cells (13, 14). Moreover, ART is reported to inhibit carcinogenesis in 1, 2 dimethylhydrazine (DMH)-induced rat colorectal cancer model (15). However, the preventive effects of ART on hereditary intestinal carcinogenesis have not yet been elucidated.

Tissue homeostasis is kept by the balance of cell proliferation and differentiation. However, genetic mutations caused by environmental factors break down homeostasis, induce excessive cell proliferation and develop neoplastic tissue. Most CRCs are caused by mutation of APC, a tumor suppressor gene, and ~80% of CRCs are associated with abnormal canonical Wnt/β-catenin signaling pathways (16). Abnormal Wnt signaling causes unexpected β-catenin nuclear translocation and promotes TCF/LEF transcriptional activity, resulting in progress of CRC with induction of excessive cell proliferation-related factors such as c-Myc and Cyclin D1 (17). Thus, it is important to develop cancer chemopreventive agents that target abnormal canonical Wnt/β-catenin signaling pathways. Therefore, I used *Apc*-mutant mice, a model of familial adenomatous polyposis, to clarify the effects of ART on intestinal polyp development that due to activation of Wnt/β-catenin signaling. Moreover, as the main part of this study, the mechanism of action of artesunate were investigated in detail with revealing novel ART binding partner.

In the present study, inhibition of intestinal carcinogenesis by suppressing each signaling (NF-κB pathway by erythromycin, Wnt/β-catenin pathway by artesunate) is demonstrated.

9

4. Materials and Methods

Chemicals.

Erythromycin and artesunate were purchased from Tokyo Chemical Industry Co., Ltd. (Tokyo, Japan) (Figures 1A and 1B). Acrolein, crotonaldehyde, dansyl hydrazine (DH), glyoxal, 2,4-decadienal (DDE), heptadecanal, hexadecanal, 2,4-nonadienal (NDE), octadecanal, 2-octenal, pentadecanal, tetradecanal and 2-undecenal were also purchased from Tokyo Chemical Industry (Tokyo, Japan). Acetaldehyde, p-Toluenesulfonic acid (p-TsOH) and the RCs, including propanal, pentanal, butanal, 2-hexenal, hexanal, 2-heptenal, heptanal, octanal, 2-nonenal, nonanal, decanal, undecanal, dodecanal and tridecanal, were obtained from Sigma-Aldrich (St. Louis, MO, USA). 4-Hydroxy-2-hexenal (HHE), 4-hydroxy-2-nonenal (HNE) and 4-oxo-2-nonenal (ONE) were purchased from Cayman Chemical Company (Ann Arbor, MI, USA). p-Benzyloxybenzaldehyde (p-BOBA) was purchased from Wako Pure Chemical Industries (Osaka, Japan). 8-Heptadecenal (8-HpDE), 8,11-heptadecadienal (8,11-HpDDE) and 8,11,14-heptadecatrienal (8,11,14-HpDTE) were synthesized using a previously described method (18, 19). Secosterol-A and B were synthesized according to a procedure reported by Wentworth *et al*. (20). Stock solutions of the reactive carbonyl species (RCs) and an internal standard (IS) (p-BOBA, 10 μM) were prepared separately in acetonitrile and stored at –20°C prior to use.

Synthesis of ART-OMe 【*For ART experiments*】

To a stirred solution of artesunate (ART, 1.15 g, 2.99 mmol) in MeOH (45 mL) 2 M TMS-CHN$_2$ in *n*-hexane (1.5 mL, 3 mmol) was added at room temperature. After being stirred for 1 h, the reaction mixture was concentrated *in vacuo* to give ART-OMe (1.19

g, 2.99 mmol). ^{1}H NMR (CD$_3$OD, 500 MHz) δ 5.76 (d, J = 9.8 Hz, 1H), 5.53 (s, 1H), 3.67 (s, 3H), 2.74-2.65 (m, 4H), 2.46 (m, 1H), 2.33 (ddd, J = 14.6, 13.5, 4.0 Hz, 1H), 2.05 (ddd, J = 14.6, 4.8, 3.0 Hz, 1H), 1.92 (m, 1H), 1.78 (dddd, J = 13.3, 3.5, 3.5, 3.5 Hz, 1H), 2.05 (dddd, J = 13.1, 3.3, 3.3, 3.3 Hz, 1H), 1.62 (ddd, J = 13.8, 4.4, 4.4 Hz, 1H), 1.53-1.37 (m, 3H), 1.36 (s, 3H), 1.26 (ddd, J = 11.5, 11.5, 6.7 Hz, 1H), 1.04 (dddd, J = 12.9, 12.9, 12.9, 3.5 Hz, 1H), 0.97 (d, J = 6.4 Hz, 3H), 0.87 (d, J = 7.2 Hz, 3H); ^{13}C NMR (CD$_3$OD, 125 MHz) δ 174.4, 172.8, 105.6, 93.7, 92.9, 81.3, 52.9, 52.2, 46.6, 38.2, 37.3, 35.3, 33.0, 30.0, 29.4, 25.9, 25.8, 22.8, 20.6, 12.3; HRESIMS m/z 421.1832 [M+Na]$^+$ calcd. for C$_{20}$H$_{30}$O$_8$Na, 421.1833.

Synthesis of redART-OMe 【For ART experiments】

A mixture of ART-OMe (730 mg, 1.83 mmol) and 10% Pd/C (52 mg) in MeOH (6 mL) was stirred for 2 days under a hydrogen atmosphere and then insoluble material was removed by filtration. The filtrate was concentrated *in vacuo* and purified by silica gel column chromatography (n-hexane/acetone = 10/1) to give redART-OMe (58.6 mg, 0.153 mmol). ^{1}H NMR (CD$_3$OD, 500 MHz) δ 5.71 (d, J = 6.4 Hz, 1H), 5.34 (s, 1H), 3.67 (s, 3H), 2.68-2.58 (m, 4H), 1.92-1.80 (m, 3H), 1.76 (dddd, J = 13.2, 3.1, 3.1, 3.1 Hz, 1H), 1.67 (m, 1H), 1.59 (m, 1H), 1.50 (s, 3H), 1.34-1.16 (m, 4H), 1.06 (m, 1H), 0.98 (d, J = 7.4 Hz, 3H), 0.92 (d, J = 6.1 Hz, 3H); ^{13}C NMR (CD$_3$OD, 125 MHz) δ 174.4, 173.5, 109.5, 97.2, 97.0, 83.3, 52.3, 46.7, 42.3, 36.4, 35.5, 35.2, 31.7, 30.3, 29.5, 24.3, 23.7, 23.0, 19.1, 15.1; HRESIMS m/z 405.1881 [M+Na]$^+$ calcd. for C$_{20}$H$_{30}$O$_7$Na, 405.1884.

Cell culture

DLD-1, HCT116, HCT15 and SW48 cells, human colon adenocarcinoma cell lines, were purchased from the American Type Culture Collection (Manassas, VA, USA). The DLD-1, HCT116, HCT15 and SW48 cells were maintained in DMEM supplemented with 10% FBS and antibiotics (100 µg/ml streptomycin and 100 U/ml penicillin) at 37 °C with 5% CO_2.

Animal experiment protocol.

Male C57BL/6-$Apc^{Min/+}$ mice (Min mice) were purchased from Jackson Laboratory (Bar Harbor, ME, USA). The mice (n = 3 - 4) were housed in plastic cages with sterilized softwood chips as bedding in a barrier-sustained animal room maintained at 24 ± 2°C and 55% humidity under a 12 h light/dark cycle. EM was mixed with AIN-76A powdered basal diet (CLEA Japan, Inc., Tokyo, Japan) at concentrations of 500 ppm. Seven male Min mice aged 5 weeks were given 0 and 500 ppm erythromycin for 8 weeks. ART was mixed with AIN-76A powdered basal diet (CLEA Japan, Inc., Tokyo, Japan) at concentrations of 5 or 10 ppm. Twelve male Min mice aged 5 weeks were given 5 or 10 ppm artesunate for 8 weeks. All animals housed in the same cage were included in the same treatment group. Food and water were available *ad libitum*. The animals were observed daily for clinical symptoms and mortality. Body weight and food consumption were measured weekly. At the time of sacrifice, the mice were anesthetized, and blood samples were collected from their abdominal veins. Their intestinal tracts were removed and separated into the small intestine, cecum and colorectum. The small intestine was divided into proximal segments (4 cm in length), and the remaining segments contained middle and distal halves. The number of polyps in the proximal segments were counted and dissected under a stereoscopic microscope

12

at the time of sacrifice (21, 22). The remaining intestinal mucosa (the part without polyps) in the proximal segments was removed by scraping, and the specimens were stored at $-80°C$ until quantitative real-time PCR analysis was conducted. The other regions were opened longitudinally and fixed flat between sheets of filter paper in 10% buffered formalin. Later, the number, size and intestinal distribution of the polyps were assessed with a stereoscopic microscope. All experiments were performed according to the "Guidelines for Animal Experiments in the National Cancer Center" and were approved by the Institutional Ethics Review Committee for Animal Experimentation of the National Cancer Center. The animal protocol was designed to minimize pain and discomfort to the animals. All animals were euthanized for tissue collection by isoflurane overdose.

Transient luciferase assays for NF-κB and AP-1 promoter transcriptional activity
【*For EM experiments*】

To measure NF-κB and AP-1 promoter transcriptional activity, HCT116 and SW48 cells were seeded in 96-well plates ($2×10^4$ cells/well). After 24 h incubation, the cells were transiently transfected with 200 ng/well pGL4.32 [luc2P/NF-κB-RE/Hygro] (Promega, Madison, WI, USA) or pAP-1-Luc (Signosis Inc., Santa Clara, CA, USA) reporter plasmid and 10 ng/well pGL4.73 [hRluc/SV40] control plasmid (Promega) using Polyethylenimine MAX MW 40,000 (PolyScience, Warrington, PA, USA). The transfected cells were cultured for an additional 24 h and then treated with EM for 24 h. Firefly and Renilla luciferase activity levels were determined using the Bright GLO and Renilla GLO Luciferase Assay Systems (Promega), respectively. For the TNFα and IL-1β experiment, TNFα and IL-1β were administered at the same time as EM. The

luciferase activity percentages for each treatment were calculated from triplicate well data, and the values were normalized to those of Renilla luciferase activity. Data are expressed as the mean ± SD (n = 3).

Transient luciferase assays for TCF/LEF promoter transcriptional activity 【For ART experiments】

To measure TCF/LEF promoter transcriptional activity, DLD-1 and HCT116 cells were seeded in 96-well plates (2×10^4 cells/well). After 24 h incubation, the cells were transiently transfected with 200 ng/well pGL4.49 [luc2P/TCF-LEF/Hygro] (Promega, Madison, WI, USA) reporter plasmid and 10 ng/well pGL4.73 [hRluc/SV40] control plasmid (Promega) using Polyethylenimine MAX MW 40,000 (PolyScience, Warrington, PA, USA). The transfected cells were cultured for an additional 24 h and then treated with ART for 24 h. Firefly and Renilla luciferase activity levels were determined using the Bright GLO and Renilla GLO Luciferase Assay Systems (Promega). The luciferase activity percentages for each treatment were calculated from triplicate well data, and the values were normalized to those of Renilla luciferase activity. Data are expressed as the mean ± SD (n = 3).

Luciferase assays for NF-κB promoter transcriptional activity in stable transfectants 【For EM experiments】

To measure NF-κB transcriptional activity, HCT116 cells were transfected with pGL4.32 [luc2P/NF-κB-RE/Hygro] (Promega, Madison, WI, USA) reporter plasmids using Polyethylenimine MAX MW 40,000 (PolyScience, Warrington, PA, USA). The transfected cells were cultured for an additional 24 h. Cells stably expressing

NF-κB-Luc were treated with hygromycin and cloned. These cells were referred to as HCT116-NF-κB-Luc cells. HCT116-NF-κB-Luc cells were seeded in 96-well plates (2×10^4 cells/well). After a 24-h incubation, the cells were treated with EM and 10 ng/mL TNFα (Perotec, NJ, USA) for 24 h. Firefly luciferase activity levels were determined using the Bright GLO Luciferase Assay System (Promega). Basal NF-κB luciferase activity in the control was set as 1.0. Data are expressed as the mean ± SD (n = 4).

Luciferase assays for TCF/LEF promoter transcriptional activity in stable transfectants 【For ART experiments】

To measure TCF/LEF transcriptional activities, DLD-1, HCT116, HCT15 and SW48 cells were transfected with pGL4.49 [luc2P/TCF-LEF/Hygro] (Promega, Madison, WI, USA) reporter plasmids using Polyethylenimine MAX MW 40,000 (Polyscience, Warrington, PA, USA). Cells stably expressing TCF/LEF-Luc were treated with hygromycin and cloned. These cells are referred to as DLD-1-TCF/LEF-Luc cells, HCT116-TCF/LEF-Luc cells, HCT15-TCF/LEF-Luc cells and SW48-TCF/LEF-Luc cells, respectively. For the artesunate experiments, the DLD1-TCF/LEF-Luc cells, HCT116-TCF/LEF-Luc cells, HCT15-TCF/LEF-Luc cells and SW48-TCF/LEF-Luc cells were seeded in 96-well plates (2×10^4 cells/well). After 24 h preincubation, the cells were treated with ART for 24h. Firefly luciferase activity levels were determined using the Bright GLO Luciferase assay system (Promega). Basal TCF/LEF luciferase activity in the control was set as 1.0. Data are expressed as the mean ± SD ($n = 4$).

Quantitative real-time polymerase chain reaction (PCR) analyses

Total RNA was isolated using RNAiso Plus (TaKaRa, Japan) and 1 µg aliquots in a final volume of 20 µL were used for cDNA synthesis using a High Capacity cDNA Reverse Transcription Kit (Applied Biosystems). Real-time PCR was carried out using the CFX96/384 PCR Detection System (BIO RAD, Tokyo, Japan) and Fast Start Universal SYBR Green Mix (Roche Diagnostics, Mannheim, Germany), according to the manufacturers' instructions. The designed gene primer sequences used to evaluate human and mouse mRNA levels are shown in Table 1. To assess the specificity of each primer set used to evaluate human mRNA levels, the melting curves of the amplicons generated by the PCR reactions were analyzed.

Extraction and analysis of reactive carbonyl species 【*For EM experiments*】

Mouse liver (20 mg) samples were homogenized in 200 µL of sodium phosphate buffer (50 mM, pH 7.4) containing 0.5 mM EDTA and 20 µM BHT. The liver homogenates were mixed with an IS (p-BOBA) (20 pmol) and 400 µL of a chloroform/methanol (2:1, v/v) solution. The resulting mixture was vigorously agitated for 1 min and then centrifuged at 15,000 rpm for 10 min, and the organic phase was collected. The remaining precipitate and aqueous phases were then mixed with 400 µL of the chloroform/methanol solution (2:1, v/v), and the resulting mixture was centrifuged at 15,000 rpm for 10 min to obtain the organic phase. The combined organic phases were mixed with 100 µL of acetonitrile containing 50 µg of DH and 10 µg of p-toluenesulfonic acid and incubated for 4 h at ambient temperature in the absence of light. The mixtures were then evaporated to dryness *in vacuo* to yield the corresponding derivatized residues. These residues were dissolved in 200 µL of acetonitrile, and 5 µL of each sample was injected into the LC/MS system. The details regarding RCs analysis

by LC/MS were described previously (23, 24)

Western blot analysis 【*For ART experiments*】

DLD1 and HCT116 cells were seeded at a density of 2×10^5/well in 24-well plates, and incubated with 0.5, 1, 2.5, 5 and 10 µM artesunate for 24 h. After treatment, cells were lysed in RIPA buffer [50 mM Tris-HCl (pH8.0), 150 mM NaCl, 1% Triton-X, 0.5% Deoxycholic acid, 0.1% Sodium dodecyl sulfate]. After 30 min incubation in RIPA buffer, the remaining cells were excluded by centrifuge at 15,000 rpm for 30 min. Protein lysate was mixed for 5 min at 95°C in sample buffer [125 M Tris–HCl (pH 6.8), 10% 2-mercaptoethanol, 20% glycerol, 4% sodium dodecyl sulfate]. Fifteen µg protein lysate was loaded into each well for SDS-PAGE. After electrophoresis, proteins were blotted onto a polyvinylidene difluoride membranes (Millipore, MA, USA). The primary anti-bodies are shown in Table 2 and were used at a 1:1,000 dilution. Peroxidase-conjugated secondary anti-bodies for anti-rabbit and anti-mouse IgG were obtained from GE Healthcare (Buckingham shire, UK). Blots were developed with ECL western blotting detection reagents (GE Healthcare).

Preparation of artesunate-fixed beads 【*For ART experiments*】

Magnetic FG beads with NH_2 were purchased from Tamagawa Seiki (Nagano, Japan). The beads were mixed with artesunate in DMF containing 1-hydroxybenzotriazole (HOBt) at 37°C for 24h, washed twice with DMF, and then twice with deionized water. The resulting beads were stored at 4°C.

Purification and identification of artesunate-binding proteins using artesunate-fixed

beads 【*For ART experiments*】

HCT116 cells were lysed with binding buffer (50 mM Tris-HCl [pH8.0], 150 mM NaCl, 1% NP-40, 1 mM DTT, 0.5 mM PMSF) for 30 min at 4°C and centrifuged. The supernatants were used as whole cell lysate of HCT116 cells. The lysates were incubated with different concentrations of empty beads or artesunate-fixed beads for 4h at 4°C. The bound proteins were eluted with Laemmli dye, and silver-stained after being subjected to SDS-PAGE.

Liquid chromatography/tandem mass spectrometry (LC/MS) analysis 【*For ART experiments*】

The protein samples were separated by 12.5% SDS-PAGE and subjected to in-gel digestion using trypsin (25). Peptides were analyzed by a LTQ-Orbitrap-XL mass spectrometer (Thermo Scientific) combined with nano-flow HPLC system (AMR). Protein identification was performed with the Mascot software package (version 2.5.1; Matrix Science). The MS/MS spectra were searched for against the Homo sapiens protein database (20,205 sequences in the Swiss prot_2015_09.fasta file) in SwissProt, using the following parameters – 1 missed cleavage; variable modifications: oxidation (Met) and phospho (Ser, Thr and Tyr); peptide tolerance: 10 ppm; MS/MS tolerance: 0.8 Da; peptide charge: 2+, 3+ and 4+.

Design of short-interfering RNA 【*For ART experiments*】

The siRNA duplexes were designed to target the corresponding sequences of human gene mRNA. A scramble siRNA was used as a control. siRNA molecules were synthesized by FlexiPlate siRNA (QIAGEN). The designed gene-siRNA and the

control-siRNA sequences are shown in Table 3.

siRNA transfection 【***For ART experiments***】

The transfections were performed using Lipofectamine 2000 (Invitrogen) according to the manufacture's protocol. Briefly, 2.0×10^5 cells / 24-well culture plate were cultured with complete DMEM plus 10% FBS, treated with 10% OPTI-MEM and 2 μL lipofectamine 2000 for 3 days, and then western blot analysis and luciferase assay were performed.

Immunofluorescence staining 【***For ART experiments***】

DLD-1 cells and HCT116 cells (3×10^4 cells/well) were seeded in 8 well-chamber slides. After 24 h pre-incubation, the cells were treated with 10 μM artesunate for 24h. The cells were then washed with PBS and fixed with 4% paraformaldehyde for 15 min at room temperatures. The cells were permeabilized with 0.5% Triton X-100 for 15 min. The cells were treated with anti-TCF1/TCF7 and anti-β-catenin antibody (1:250) overnight at 4℃. After this, the cells were washed with PBS three times, and incubated with Alexa 594-labeled anti-rabbit and Alexa 488-labeled anti-mouse secondary antibody (1:500) at room temperature for 1 h.

Statistical analyses

The results are expressed as the mean ± SD according to the statistical analyses performed using Dunnett's test. Differences were considered to be statistically significant at *$p < 0.05$, **$p < 0.01$ and ***$p < 0.001$.

5. Inhibition of intestinal carcinogenesis by erythromycin

5 – 1. Results

Suppression of NF-κB and AP-1 promoter transcriptional activity by erythromycin

NF-κB and AP-1 promoter transcriptional activities were examined following 24 h of EM treatment (100, 200 and 400 μM) in HCT116 cells and SW48 cells (Figures 2 and 3). First, I confirmed NF-κB promoter transcriptional activity using HCT116-NF-κB-Luc cells in a simplified method. Four hundred μM EM treatment for 24 h decreased NF-κB promoter transcriptional activity by 11% ($p<0.05$), compared with the untreated control value (Figure 2A). Furthermore, to evaluate the action of EM in a chronic inflammatory condition, a simulated inflammatory condition was created using cytokines (TNFα and IL-1β). As a result, 100, 200 and 400 μM EM treatment for 24 h decreased TNFα-stimulated NF-κB promoter transcriptional activity by 14% ($p<0.05$), 17% ($p<0.05$) and 21% ($p<0.01$), respectively, compared with the cytokines-stimulated plus untreated EM value (Figure 2B).

Next, I evaluated NF-κB promoter transcriptional activity in cells that transiently expressed NF-κB-Luciferase plasmid vector. In HCT116 cells, EM treatment slightly decreased NF-κB and AP-1 promoter transcriptional activities in a dose-dependent manner (Figures 2C and D). Four hundred μM EM treatment for 24 h decreased NF-κB and AP-1 promoter transcriptional activity by 29% ($p<0.01$) and 18% ($p<0.01$), respectively, compared with the untreated control value. Even in cells stimulated with 10 ng/mL TNFα and 10 ng/ml IL-1β, EM decreased NF-κB transcriptional activity in a dose-dependent manner (Figures 3A and 3B). NF-κB inhibitor, 5HPP-33, was used as a positive control. Four hundred μM EM treatment for 24 h decreased TNFα-stimulated and IL-1β-stimulated NF-κB promoter transcriptional

activity by 21% ($p<0.05$) and 22% ($p<0.05$) compared with the cytokines-stimulated plus untreated EM value, respectively.

In other CRC cells, SW48 cells, EM treatment slightly decreased TNFα-stimulated or IL-1β-stimulated NF-κB promoter transcriptional activities in a dose-dependent manner (Figures 3C and 3D). Four hundred μM EM treatment for 24 h decreased TNFα-stimulated and IL-1β-stimulated NF-κB promoter transcriptional activity by 26% ($p<0.05$) and 31% ($p<0.01$) compared with the cytokines-stimulated plus untreated EM value, respectively.

Suppression of mRNA expression of inflammation-related factors by erythromycin in human colon cancer cells

To clarify the effects of EM on the downstream targets of NF-κB and AP-1, mRNA expression of inflammation-related factors was evaluated in HCT116 cells following 24 h of 100, 200 and 400 μM EM treatment with and without 10 ng/mL TNFα. EM significantly suppressed IL-6 and COX2 mRNA expression with and without TNFα treatment (Figure 4).

Suppression of intestinal polyp formation by erythromycin in Min mice

Administration of 500 ppm EM to Min mice for 8 weeks did not affect body weight, food intake or clinical symptoms throughout the experimental period. There was no difference in average daily food intake between the 0 and 500 ppm groups of Min mice. In addition, no changes in organ weights that may have been attributable to toxicity were observed. Table 3 summarizes the data regarding the numbers and distributions of intestinal polyps in the basal diet control group and EM-treated group. The majority of

polyps developed in the small intestine, while only a few developed in the colon. Treatment with 500 ppm EM decreased the total number of polyps to 72.6% of the untreated control value (Table 3). A reduction in the number of polyps to 70.9% of the untreated control value ($p<0.01$ *vs* control group) was observed in the proximal segment of the small intestine (Table 4). No significant differences in the numbers of polyps were observed in the other segment of the small intestine or the colon following EM treatment (Table 4). Figure 5 shows the size distributions of the intestinal polyps in the basal diet and EM-treated groups. EM treatment significantly reduced the numbers of polyps whose diameters were less than 0.5 mm (Figure 5).

Suppression of inflammation-related genes expression by erythromycin in the intestinal polyps of Min mice

To clarify the mechanisms underlying EM-mediated suppression of intestinal polyp formation, expressions of inflammation-related genes in the non-polyp portions (mucosa) and polyp portions of the intestine were investigated (Figure 6). Real-time PCR revealed that treatment with 500 ppm EM for 8 weeks significantly decreased IL-6 and COX-2 mRNA expression in the intestinal polyp segments by 38% ($p<0.05$) and 28% ($p<0.01$), compared with the untreated control values, respectively. In the non-polyp portions (mucosa), no difference of IL-6 and COX-2 mRNA expression between the EM treatment and non-treatment mice groups was observed.

EM decreased NADPH oxidase mRNA expression in hepatic, but not in intestinal in Min mice

One of the factors inducing inflammation in the living body is oxidative stress. Thus, I

attempted to elucidate the oxidative stress-related mechanisms underlying the suppression of intestinal polyp formation. I first examined expression of the NADPH oxidase subunit (NOX-1, NOX-2 and p22^{phox}) in the non-polyp portions (mucosa) and polyp portions of the intestine and found that NOX-1, NOX-2 and p22^{phox} mRNA expression was unchanged by EM treatment (Figure 7A, 7B and 7C). I then examined the effects of EM on liver NADPH oxidase expression because I could not rule out the possibility that general oxidative stress may affect local intestinal polyp development. Real-time PCR revealed that 500 ppm EM treatment for 8 weeks significantly suppressed NOX-1, NOX-2 and p22^{phox} mRNA expression in the liver by 31% ($p<0.05$), 21% ($p<0.001$) and 47% ($p<0.001$), respectively, compared with untreated control values (Figures 7D, 7E and 7F).

Decreases in the levels of oxidative stress-related markers in Min mice treated with erythromycin

To confirm the effects of EM on oxidative stress, I used liquid chromatography/mass spectrometry (LC/MS) and measured the levels of reactive carbonyl species (RCs) in the livers of Min mice treated with or without EM. RCs are molecular markers generated by oxidative stress *in vivo*. LC/MS detected 182 and 184 peaks in the samples taken from non-treated and 500 ppm EM-treated Min mice, respectively (Figure 8). In these samples, known RCs and unknown RCs are detected. The expression levels of 31 known RCs are shown in Table 5. Of the 184 peaks detected in the samples taken from EM-treated Min mice, 90 tended to have lower levels and 74 tended to have higher levels, compared to the peaks detected in the samples taken from non-treated Min mice (Figure 9). Moreover, 13 were at significantly lower levels and 17 were at significantly

higher levels, compared to the peaks detected in the samples taken from non-treated Min mice (Figure 9). Thus, I could not determine whether oxidative stress affects intestinal tumorigenesis of the Min mice.

5 – 2. Discussion

In the present study, I assessed the effectiveness of EM as a CRC chemopreventive agent by evaluating its ability to suppress inflammation- and oxidative stress-related transcription factor activities. I then confirmed that EM weakly inhibited intestinal polyp development in Min mice. I also confirmed that the expression levels of the downstream targets of NF-κB and AP-1, such as IL-6 and COX-2, were decreased in the polyp portions of the intestine. Moreover, EM administration also reduced the mRNA expression levels of hepatic NADPH oxidase (Figure 10).

I investigated the effects of EM on NF-κB and AP-1 transcriptional activity because both transcriptional factors play an important role in colorectal carcinogenesis. Moreover, activation of both NF-κB and AP-1 induce the expression of inflammatory cytokines, growth factors and inflammation-related enzymes, such as COX-2 and IL-6. Both COX-2 and IL-6 have been shown to play important roles in colorectal carcinogenesis (26, 27). In our *in vitro* study using HCT116 cells, EM treatment clearly suppressed COX-2 and IL-6 mRNA expression in both the presence and the absence of TNFα stimulation. However, its weak inhibition of NF-κB and AP-1 transcriptional activity does not explain its suppression of COX-2 and IL-6 mRNA expression. We surmised that both the IL-6 and COX-2 genes possess a NF-κB and AP-1 responsible element (28, 29) in their promoter region, and additional activation of the responsible element could synergistically enhance resultant gene expression. For example, it has

been reported that red raspberries inhibit both NF-κB and AP-1 transcriptional activity, and both inhibitions synergistically suppress COX-2 and IL-6 mRNA expression in RAW264.7 cells (30). Of course, I cannot exclude other possibilities regarding the independence of IL-6 / COX-2 and NF-κB / AP-1 transcriptional activity at this point. Of note, it has been reported that EM (0.1-1000 nM) suppressed IL-1β-stimulated synovial cells expressing COX-2 mRNA and IL-1β-induced p38 MAPK phosphorylation, but NF-κB DNA binding activity did not affect by EM (31). The effects of EM on NF-κB transcriptional activity should be confirmed using several cell lines in the future.

It has been reported that inflammatory factors such as COX-2 are up-regulated in stroma cells in intestinal polyps/adenomas of *Apc*-mutant mice. However, when they transform to adenocarcinomas, the expression of COX-2 is apparent in the epithelial cells of a tumor. COX-2 and IL-6 mRNA expression was clearly suppressed in the polyp portions of the intestines of Min mice, which may have affected local tumor growth and may explain the decreases in polyp numbers elicited by EM treatment. Moreover, activation of NF-κB signaling is regulated by a phosphorylation of upstream IKKα/β and IkBα (Figure 10). However, it is reported that EM does not affect IkBα phosphorylation and its degradation (32). Thus, it is expected that EM inhibits other step(s) of NF-κB pathway. Although EM exhibits antibacterial activity by blocking the function of 50S ribosome in bacterial, a target molecule in mammalian cell have not been clarified. Clarithromycin has similar structure to EM, and is also suppresses NF-κB pathway in lung epithelial cells (33). How clarithromycin inhibits the NF-κB signaling has not been clarified, but these drug might target similar molecule in mammalian cell (33).

This is the first report showing that EM can suppress intestinal polyp formation in mice. Some other macrolides are known to have anti-cancer effects and are part of a group of anti-cancer chemotherapy drugs classified as "antitumor antibiotics." For instance, mitomycin-C is used in the treatment of many cancers, such as anal, bladder, breast, cervical, colorectal, head-and-neck, and non-small cell lung cancer (34). Rapamycin is used to treat renal cell cancer, neuroendocrine tumors and metastatic breast cancer by inhibiting mammalian target of rapamycin (mTOR) activation (35). Bryostatin and epothilone have also been used to treat cancer, and many other macrolides, such as exiguolide, are under investigation (36). Among macrolides, EM has the fewest side effects. Therefore, it can be expected in the future as a highly safe anti-cancer effect

EM treatment tends to reduce polyp development in the colon and small intestine, but only significantly in the proximal portion of the small intestine. Similar to EM effect, LPL inducers NO-1886 and PPAR ligand also significantly reduce the number of intestinal polyps particularly in the proximal part of the intestine (37, 38). On the other hand, some other agents, such as indomethacin (a COX inhibitor), nimesulide (a COX-2 selective inhibitor), sesamol, (a COX-2 suppressor) and apocynin (an NADPH oxidase inhibitor) have been shown to reduce the numbers of intestinal polyps in the middle to distal parts of the small intestine (39-41). I surmised that localized EM absorption or some unknown EM functions played a role in its effects on proximal intestinal polyp development. EM is widely used on an antibacterial drug. Previous studies reported that bacteria-free mouse develops few carcinogen-induced colon tumor compared to those of mouse examined in normal condition (42). On the other hand, long-term administration of antibacterial agents was shown to promote colon

carcinogenesis (43). Therefore, whether gut flora affect intestinal carcinogenesis is still under debate.

I also analyzed the expression of NADPH oxidase (NOX) components, such as NOX1, NOX2 and $p22^{phox}$, in the liver and intestine, as EM has been reported to inhibit neutrophil NOX activation. The NADPH oxidase inhibitor apocynin also suppresses intestinal polyp development in Min mice (44). Interestingly, the expression of hepatic NOX1, NOX2 or $p22^{phox}$ but not intestinal NOX1, NOX2 or $p22^{phox}$, was suppressed in the mice group treated with EM. Thus, I evaluated the levels of oxidative stress markers, RCs, in the liver of EM-treated Min mice. However, EM administration did not affect the levels of the liver RCs. Thus, it is not conclusive whether EM suppresses oxidative stress or not.

In conclusion, this study demonstrated that EM suppresses the development of intestinal polyps in Min mice, in part by attenuating local inflammation. My findings suggest that EM is a useful chemopreventive agent in the aspect of drug repositioning.

6. Inhibition of intestinal carcinogenesis by artesunate

6 – 1. Results

Suppression of TCF/LEF promoter transcriptional activity by artesunate treatment

For the second screening, I investigated the effects of ART on TCF/LEF promoter transcriptional activity in several cells. The DLD-1-TCF/LEF-Luc cells and HCT116-TCF/LEF-Luc cell cells were treated with 0.5, 1, 2.5, 5 and 10 µM ART for 24 hours, and it was found that all of them decreased TCF/LEF promoter transcriptional activity in a dose-dependent manner (Figure 11). In DLD1-TCF/LEF-Luc cells, 0.5 and 1µM ART treatment decreased TCF/LEF promoter transcriptional activity by 20% ($p<0.01$) and 50% ($p<0.001$), respectively, and doses more than 2.5 µM decreased it by >75% ($p<0.001$) compared with the activity in the ART-untreated cell (Figure 11A). In HCT116-TCF/LEF-Luc cells, 0.5 µM ART treatment decreased TCF/LEF promoter transcriptional activity by 84% ($p<0.001$), and other doses over 1 µM decreased it by >95% ($p<0.001$) (Figure 11B).

DLD-1-TCF/LEF-Luc and HCT116-TCF/LEF-Luc are cloned cells. Therefore, it is necessary to evaluate in unselected cells. I evaluated TCF/LEF promoter transcriptional activity in cells that transiently expressed TCF/LEF-Luciferase vector. Moreover, the results from the transient transfection of reporter plasmid in DLD-1 and HCT116 cells also supported the previous results that 1, 2.5, 5 and 10 µM ART treatment for 24 hours decreased TCF/LEF promoter transcriptional activity (Figures 11C and 11D).

Suppression of cell proliferation-related factor mRNA and protein expression by artesunate treatment

To clarify the effects of ART on downstream targets of TCF/LEF, the mRNA expression levels of c-Myc and Cyclin D1, both proliferation-related factors highly expressed in cancer, were evaluated in the DLD-1 and HCT116 cells. Treatment of 2.5, 5 and 10 μM ART for 24 h in the DLD-1 cells decreased c-Myc mRNA expression levels by 22.9%, 20.1% and 33.8% ($p<0.01$), respectively, compared with the activity in the ART-untreated cell (Figure 12A). In addition, Cyclin D1 mRNA expression levels of 2.5, 5 and 10 μM ART treatment for 24 h were decreased by 35.0%, 44.7% and 51.4% ($p<0.01$), respectively (Figure 12C). In the HCT116 cells, treatment with 2.5, 5 and 10 μM ART decreased c-Myc mRNA expression levels by 61.8%, 61.0% and 70.2% ($p<0.001$), respectively (Figure 12B). In addition, Cyclin D1 mRNA expression levels of 2.5, 5 and 10 μM ART treatment for 24 h were decreased by 29.6%, 28.5% and 26.2% ($p<0.001$), respectively (Figure 12D).

Moreover, the protein expression levels of c-Myc and Cyclin D1 were evaluated in DLD-1 and HCT116 cells. In both cells, ART decreased the protein expression levels of c-Myc and Cyclin D1 in a dose-dependent manner (Figures 13A and 13B).

Suppression of intestinal polyp formation by artesunate in Min mice

Administration of 5 or 10 ppm ART to Min mice for 8 weeks did not affect body weight, food intake or clinical symptoms throughout the experimental period. There was no difference in average daily food intake between the 0, 5 and 10 ppm groups of Min mice (Figure 14). In addition, no changes in the major organ weights that may have been attributable to drug toxicity were observed (Table 6). Table 7 summarizes the number of intestinal polyps per mouse in the ART 0 ppm (control)-, 5 ppm- and 10

ppm-ART-treated groups.

The majority of polyps developed in the small intestine, while only a few developed in the colorectum (Table 7). Treatment with 10 ppm ART decreased the total number of polyps to 74.0% of the untreated control value ($p<0.05$ vs control group) (Table 7). A decrease in the number of polyps to 79.2% and 71.3% was observed in the distal segment of the intestine with the administration of 5 and 10 ppm ART, respectively (Table 7). Figure 15 shows the size distributions of the intestinal polyps in the ART 0 ppm-, 5 ppm- and 10 ppm-treated mice. Ten ppm ART treatment significantly decreased the numbers of polyps sized between 1.0 and 1.5 mm in diameter.

Suppression of Wnt signaling regulated gene expression by artesunate in the intestinal polyps of Min mice

To clarify the mechanisms underlying ART-mediated suppression of intestinal polyp formation, Wnt signaling regulated gene expression in the non-polyp portions (mucosa) and polyp portions of the intestine was investigated. Real-time PCR revealed that treatment with 10 ppm ART for 8 weeks significantly suppressed c-Myc and Cyclin D1 mRNA expression in the intestinal polyp segments by 31.4% and 27.2% ($p<0.05$), respectively, compared with 0 ppm ART treatment. In the mucosa, no difference in c-Myc and Cyclin D1 mRNA expression between the ART treatment and non-treatment mice group was observed (Figures 16A and 16B).

Inhibition of TCF1/TCF7 nuclear translocation by artesunate treatment

So far, I confirmed that ART has a certain inhibitory effect on TCF/LEF transcriptional activity and its downstream gene expression. From the next experiment, I aimed to

clarify its mechanism. Nuclear translocation of β-catenin and the TCF family plays a central role on the Wnt/β-catenin. To clarify the effect of ART on Wnt/β-catenin regulator protein, such as β-catenin, TCF1/TCF7, LEF1 (TCF7L3) and TCF4 (TCF7L2), I evaluated these protein expression levels in the DLD-1 and HCT116 cells after 0.5, 1, 2.5 5 and 10 μM ART treatment for 24 hours (Figure 17). ART treatment did not affect the total β-catenin and non-phospho β-catenin (active form) that regulates transcription protein expression levels in either DLD-1 or HCT116 cells (Figures 17A and 17B). ART treatment decreased the TCF1/TCF7 protein expression levels in a dose-dependent manner in DLD-1 and HCT116 cells (Figures 17C and 17D). In addition, LEF1 also decreased in a dose-dependent manner in DLD-1 cells and it has been reported that LEF1 is hardly expressed in HCT116 cells (45, 46), and it seems that this result did not reach the detection level. (Figure 17C and 17D). On the other hand, expression of TCF4 was not affected by ART treatment in either DLD1 or HCT116 cells (Figure 17C and 17D).

As TCF/LEF is activated after its translocation from the cytosol into the nucleus, I examined the expression levels of TCF/LEF in cytoplasmic and nuclear fractions. As a result, ART clearly decreased the protein expression levels of TCF1/TCF7 in nuclear fractions (Figures 18A and 18B).

To visualize the TCF1/TCF7 localization, HCT116 and DLD-1 cells were treated with 10 μM ART for 24 hours and stained with anti-TCF1/TCF7 antibodies. Amount of TCF1/TCF7 protein localization was sustained in the cytoplasm by ART treatment compared to that of the untreated control (Figures 19A and 19C). Furthermore, to evaluate in more detail, it quantified about the localization area (for cytoplasm and nucleus respectively) of TCF1/TCF4 in cells. In HCT116 cells, quantitative evaluation

31

of the result revealed the TCF1/TCF7 nuclei (location of dot-like) were decreased 39.6% ($p<0.05$), and conversely, cytoplasmic TCF1/TCF7 increased 5-fold ($p<0.001$) (Figure 19B). In DLD-1 cells, the TCF1/TCF7 nuclei (location of dot-like) were decreased 64.3% ($p<0.001$), and conversely, cytoplasmic TCF1/TCF7 increased 1.6-fold ($p<0.05$) (Figure 19D).

Identification of an artesunate-binding proteins

As ART had no effect on β-catenin and TCF4 expression levels (Figure 17), I assumed that there are other target proteins regulated by ART. Thus, I aimed to identify proteins that bind to ART. Before searching for ART-binding proteins, I wondered about the structural site of ART responsible for suppressing TCF/LEF transcriptional activity. To this end, I synthesized ART-OMe (structure in which hydroxyl group contained in carboxyl group was changed to methyl group) and redART-OMe (structure in which hydroxyl group contained in carboxyl group was changed to methyl group and peroxide structure was changed to ether structure) from ART (Figure 20). Among them, ART-OMe decreased TCF/LEF promoter transcriptional activity in both DLD-1-TCF/LEF-Luc cells and HCT116-TCF/LEF-Luc cells (Figure 21). In the other hands, redART-OME did not change TCF/LEF promoter transcriptional activity in both DLD-1-TCF/LEF-Luc cells and HCT116-TCF/LEF-Luc cells (Figure 21) This result suggested that the peroxide structure of ART is important for the suppression of TCF/LEF transcriptional activity, and the structure should not be blocked by magnetic FG beads, used in the next experiment.

To identify the proteins that bind to ART, ART was covalently conjugated to the beads with HOBt, (Figure 22A) and ART-fixed beads were incubated with whole

cell lysate of HCT116 cells. And the protein solution obtained using empty beads or ART-fixed beads were electrophoresed. As shown in Figure 22B, several proteins from the HCT116 cell lysate were bound to the ART-fixed beads. These binding proteins were identified by mass spectrometry (MS). The top 50 proteins detected only with ART-fixed beads are shown in Tables 8. From the data obtained by MS analysis, 30 candidate proteins were selected by evaluating the peptide coverage and peak pattern. Therefore, to select the proteins that may be involved in the Wnt/β-catenin, I knocked down the genes that encode candidate proteins with siRNA. I assumed that the knock down of proteins that bind to ART could inhibit the TCF/LEF promoter transcriptional activity, similar to ART treatment. To evaluate whether the experimental method is valid, I examined the effect of ART on LEF1 (Wnt/β-catenin signaling related protein) knockdown. As the result, LEF1 knockdown canceled the suppressive effect of ART on TCF/LEF transcriptional activity (Figures 23A and 23B) If there was Wnt/β-catenin signaling related protein among the candidate proteins, the suppressive effect of ART on TCF/LEF transcriptional activity must be lost. According to this hypothesis, I evaluated the difference of the TCF/LEF promoter transcriptional activity between no treatment in candidate gene knock-down cells and ART treatment in candidate gene knock-down cells (Figures 24 and 25). In Figure 26A, the values dividing the luciferase activities in cells treated with ART by those in the gene knock-down cells were shown as heat map. I focused on ras-related nuclear protein (RAN), which were more important in both DLD-1 and HCT116 cells. As confirmation, the existence of RAN was checked by immunoblotting in the whole lysate and cell extracts from the ART-fixed beads of DLD-1 and HCT116 cells. As the result, RAN was detected in the ART-fixed beads (Figure 26B), Finally, RAN, a well-known nucleus transportation protein, was identified

as a strong candidate of the ART-binding proteins.

Artesunate affected to the TCF/LEF promoter transcriptional activity through RAN

Since RAN was found to be a candidate ART binding protein, we first examined the effects of ART on RAN protein expression by western blotting. In DLD-1 and HCT116 cells, ART did not affect RAN protein expression levels (Figures 27A and 27B). To investigate the effect of RAN on TCF/LEF promoter transcriptional activity under ART treatment, RAN was knocked down in DLD-1-TCF/LEF-Luc cells and HCT116-TCF/LEF-Luc cells, and also treated with or without ART. Western blot analysis showed that transfection of RAN siRNAs (#1, #2 and #3) successfully decreased the protein levels of RAN, compared with the mock (transfection of MISSION siRNA Universal Negative control) level (Figures 27C and 27D). In DLD-1-TCF/LEF-Luc cells, ART decreased TCF/LEF promoter transcriptional activity by 33.8% ($p<0.01$) compared with the mock value. RAN knock down by #1, #2 and #3 siRNA decreased TCF/LEF promoter transcriptional activity by 95.9%, 89.8% and 88.8%, respectively, compared with the mock value (Figure 27E). ART single treatment (mock cells) decreased TCF/LEF promoter transcriptional activity by 33.8% ($p<0.01$) compared with the untreated ART value. The TCF/LEF promoter transcriptional activity showed no difference between ART alone and the combination with knocked-down RAN (#1, #2 and #3) (Figure 27E). In HCT116-TCF/LEF-Luc cells, similar results were obtained. RAN knock down by #1, #2 and #3 siRNA decreased TCF/LEF promoter transcriptional activity decreased by 66.6%, 72.8% and 71.5%, respectively, compared with the mock value (Figure 27F). ART single treatment (mock cells) decreased TCF/LEF promoter transcriptional activity by 43.8% ($p<0.001$) compared with the

untreated ART value. The TCF/LEF promoter transcriptional activity showed no difference between ART alone and the combination with knocked-down RAN (#1, #2 and #3) (Figure 27F).

RAN translocate the protein with NLS sequence through Importin. Importin is essential for transferring protein into the nucleus. Since RAN is ART binding protein, I evaluated whether the localization of Importin was affected. However, expression levels and location of Importin using immunofluorescence was not changed by ART treatment in DLD-1 and HCT116 cells (Figures 28A and 28B).

6 – 2. Discussion

In the present study, ART was shown to inhibit the promoter transcriptional activity of TCF/LEF in human colon cancer cells. In addition, ART suppressed intestinal polyp development *in vivo* through inhibition of the mRNA and protein expression levels of c-Myc and Cyclin D1, both are regulated by the TCF/LEF transcriptional factor. Moreover, RAN was identified as a novel ART binding protein. My data suggested that ART reduces TCF1/TCF7 nuclear translocation by binding to RAN and inhibits translocation of TCF/LEF transcriptional factor to the nucleus (Figure 29).

This is the first report that shows an inhibitory effect of ART on the TCF/LEF promoter transcriptional activity. ART is a well-known antimalarial drug and is low side effects. Meanwhile, ART, at the research level, has been used to induce cancer cell death at a high-dose, more than 50 µM. ART is reported to induce cancer cell death via induction of apoptosis and ferroptosis, a type of apoptosis induced by accumulation of lipid peroxidation products and reactive oxygen species when ART binds to intracellular iron (47, 48). The concentrations of ART I used are much lower than the concentration

that induces cell death. Therefore, it is assumed that it will be possible to use ART as a safety cancer chemopreventive agent.

I also showed that ART can suppress intestinal polyp formation in a hereditary intestinal mouse carcinogenesis model (Min mice). In a rat cancer prevention study of ART, colon carcinogenesis was induced by DMH, and daily oral administration of ART (50 mg/kg BW and 150 mg/kg BW) for 8 weeks resulted in a significant decrease of the number of aberrant crypt foci, precancerous lesions, while suppressing the Wnt signaling and cell proliferation (15). Min mice are known to develop intestinal polyps through deletion of both alleles of the *Apc* gene and resultant activation of the Wnt signaling. TCF/LEF transcriptional activity plays a pivotal role on the Wnt signaling. So far, the use of various drugs has been reported to suppress the excessive Wnt signaling, such as TCF/LEF transcriptional activity and its downstream factor expression, and decrease the number of polyps in Min mice (49-51). There have been no reports from drugs that were used as antimalarials. Moreover, since there was no effect on body weight and organ weight, ART did not contribute to developmental disorders. In addition, ART did not affect c-Myc and Cyclin D1 expression levels in mucosa portion. From this, it is conceivable to suppress the Wnt signaling that was excessive due to the gene mutation. Inhibition of the Wnt signaling by ART is supported by other data from my results that ART treatment significantly suppressed both c-Myc and Cyclin D1 mRNA and protein expression *in vitro* and *in vivo*.

In most CRC, c-Myc and Cyclin D1 are highly expressed due to Wnt/β-catenin related gene (*APC* and *β-catein*) mutation (52). In this study using DLD-1 cells (*APC* mutant) and HCT116 cells (*β-catein* mutant), ART treatment significantly suppressed TCF/LEF transcriptional activity that was excessive due to gene mutations. This

suggested that ART contributes to proteins or mechanisms existing downstream from the mutated gene in the Wnt signaling, such as nuclear localization of β-catenin. When evaluating inhibition of Wnt signaling, β-catenin was often analyzed as the main target (53, 54). For the reason, it was evaluated that ART would affect the protein expression and intracellular localization of β-catenin. Indeed, ART did not change β-catenin protein levels and non-phospho β-catenin (active form) protein levels. However, interestingly, ART suppressed TCF1/TCF7 protein expression levels in the nucleus. A similar result has been reported elsewhere, that celecoxib (COX-2 selective inhibitor) did not change β-catenin protein levels in HCT116 cells, but suppressed TCF1 and TCF4 protein expression levels (55). My results lead us to think that decreasing TCF1/TCF7 protein levels in the nucleus may be the clue to reveal the mechanism of TCF1/TCF7 transcriptional activity suppression.

It might have been a detour, but I next searched for binding proteins of ART. As is usual in many general drugs, target proteins for ART are not clearly known. I used FG beads because several reports have successfully identified proteins that bind to compounds using FG beads (56, 57). In the knockdown experiment using siRNA, tubulin β chain (TUBB) and RAN were finally selected as binding proteins. Finally, I successfully found novel target proteins of ART. Among them, a strong candidate was RAN. RAN co-operates on the protein with NLS sequence, and translocates the protein from cytoplasm to the nucleus (58). TCF1/TCF7 and TCF4 possess an NLS sequence (59), therefore, they can be transported into the nucleus in a RAN-dependent manner. However, ART only inhibited TCF1/TCF7 transnuclearization. This could be explained by some speculation that many TCF4 could make a complex with β-catenin and therefore be able to translocate into the nucleus in a RAN-independent manner. On the

other hand, it has not been reported that TCF1/TCF7 forms a complex with β-catenin in the cytoplasm and translocates into the nucleus. Thus, I thought that most TCF1/TCF7 could be transported into the nucleus in a RAN-dependent manner. As a result, localization of TCF1/TCF7 was affected by ART that bound to RAN. RAN is highly expressed in several cancer type. Therefore, RAN is also considered as an anticancer target (60, 61). From this, it can be expected that ART can be applied to prevention and therapy via RAN in the future.

In this study, I showed that the peroxide structure in the ART is an important site to inhibit TCF/LEF promoter transcriptional activity. After cleavage of the peroxide structure, it changes to be a negative charged oxygen molecule, and easily bind to a positively charged substance. Thus, it is speculated that ART could bind to the positively charged amino acids, such as arginine and lysine, in the RAN protein. It is reported that arginine at 76th amino acid residue in RAN protein caused defect in nuclear transport (62), and this arginine might be a potential site for ART binding.

To identify ART binding proteins, I evaluated the difference of TCF/LEF promoter transcriptional activity value obtained between siRNA and ART treatment. When Ran was knocked down using siRNA, the suppression effect of ART on the Wnt signal disappeared in DLD-1 and HCT116 cells. Taking everything into consideration, the data implied that inhibitory effects of artesunate were caused by its binding to inhibition of RAN.

7. Conclusion

In this study, I performed a detailed mechanism analysis to the drugs, EM and ART, which selected by my own screening system using a FDA-approved drug library. I showed that EM suppressed NF-κB signaling and inflammation-related factors *in vitro* and reduced the number of intestinal polyps *in vivo*. Meanwhile, I showed that ART suppresses Wnt signaling and cell growth-related factors *in vitro* and reduced the number of intestinal polyps *in vivo*. Furthermore, RAN was identified as an ART binding protein using FG beads. I believe that I provided the seed of the cancer chemopreventive agents that could be a candidate of drugs able to use in the clinical interventional trial.

8. Acknowledgements

9. References

1. Bray F, Ferlay J, Soerjomataram I, Siegel RL, Torre LA, Jemal A. Global cancer statistics 2018: GLOBOCAN estimates of incidence and mortality worldwide for 36 cancers in 185 countries. *CA Cancer J Clin.* 2018; **68**: 394-424.

2. Komiya M, Fujii G, Takahashi M, *et al*. Prevention and intervention trials for colorectal cancer. *Japanese J Clin Oncol* 2013; **43**: 685-694.

3. Miyamoto S, Narita T, Komiya M, Fujii G, Hamoya T, Nakanishi R, Tamura S, Kurokawa Y, Takahashi M and Mutoh M. Novel screening system revealed that intracellular cholesterol trafficking can be a good target for colon cancer prevention. *Sci Rep*. 2019; **9**: 6192.

4. Yamamoto M, Kondo A, Tamura M, *et al*. Long-term therapeutic effects of erythromycin and newquinolone antibacterial agents on diffuse panbronchiolitis. *Jpn J Thorac Dis* 1990; **28**: 1305-1313.

5. Kudoh S, Azuma A, Yamamoto M, *et al*. Improvement of survival in patients with diffuse panbronchiolitis. *Am J Respir Crit Care Med* 1998; **157**: 1829-1832.

6. Liu T, Zhang L, Joo D and Sun SC. NF-κB signaling in inflammation. *Signal Transduct Target Ther*. 2017;**2**:17023.

7. Yamaya M, Azuma A, Takizawa H, *et al*. Macrolide effects on the prevention of COPD exacerbations. *Eur Respir J* 2012; **40**: 485-494.

8. Umeki S. Anti-inflammatory action of erythromycin. Its inhibitory effect on neutrophil NADPH oxidase activity. *Chest* 1993; **104**: 1191-1193.

9. Desaki M, Takizawa H, Ohtoshi T, *et al*. Erythromycin suppresses nuclear factor B and activator protein-1 activation in human bronchial epithelial cells. *Biochem Biophys Res Commun* 2000; **267**: 124-128.

10. Di Donato JA, Mercurio F, Karin M. NF-κB and the link between inflammation and cancer. *Immunol Rev* 2012; **246**: 379-400.

11. Angel P, Karin M. The role of Jun, Fos and the AP-1 complex in cell-proliferation and transformation. *Biochim Biophys Acta*. 1991; **1072**: 129-157.

12. Karin M. The regulation of AP-1 activity by mitogen-activated protein kinases. *J Biol Chem* 1995; **270**: 16483-16486.

13. Jiang F, Zhou JY, Zhang D, Liu MH, Chen YG. Artesunate induces apoptosis and autophagy in HCT116 colon cancer cells, and autophagy inhibition enhances the artesunate-induced apoptosis. *Int J Mol Med*. 2018; **42**: 1295-1304.

14. Xiao Chen, Yin Kwan Wong, Teck Kwang Lim, Wei Hou Lim, Qingsong Lin, Jigang Wang, and Zichun Hua1,3 Artesunate Activates the Intrinsic Apoptosis of HCT116 Cells through the Suppression of Fatty Acid Synthesis and the NF-κB Pathway. *Molecules*. 2017; **22**: 1272.

15. Kumar VL, Verma S, Das P. Artesunate suppresses inflammation and oxidative stress in a rat model of colorectal cancer. *Drug Dev Res*. 2019; **30**. doi: 10.1002/ddr.21590.

16. Schneikert J1, Behrens J. The canonical Wnt signalling pathway and its APC partner in colon cancer development. *Gut*. 2007; **56**: 417-425.

17. Fodde R, Smits R, Clevers H. APC, signal transduction and genetic instability in colorectal cancer. *Nat Rev Cancer*. 2001; **1**: 55-67.

18. Akakabe Y, Nyuugaku T. An efficient conversion of carboxylic acids to one-carbon degraded aldehydes via 2-hydroperoxy acids. *Biosci Biotechnol Biochem* 2007; **71**: 1370-1371.

19. Hamberg M, Sanz A, Castresana C. Alpha-oxidation of fatty acids in higher plants.

Identification of a pathogen-inducible oxygenase (piox) as an alpha-dioxygenase and biosynthesis of 2-hydroperoxylinolenic acid. *J Biol Chem* 1999; **274**: 24503-24513.

20. Wentworth P, Jr, McDunn JE, Wentworth AD, *et al*. Evidence for antibody-catalyzed ozone formation in bacterial killing and inflammation. *Science* 2002; **298**: 2195-2199.

21. Niho N, Takahashi M, Kitamura T, *et al*. Concomitant suppression of hyperlipidemia and intestinal polyp formation in *Apc*-deficient mice by peroxisome proliferator-activated receptor ligands. *Cancer Res* 2003; **63**: 6090-6095.

22. Shimizu S, Miyamoto S, Fujii G, *et al*. Suppression of intestinal carcinogenesis in *Apc*-mutant mice by limonin. *J Clin Biochem Nutr* 2015; **57**: 39-43.

23. Tomono S, Miyoshi N, Ohshima H. Comprehensive analysis of the lipophilic reactive carbonyls present in biological specimens by LC/ESI-MS/MS. *J Chromatogr B Analyt Technol Biomed Life Sci* 2015; **988**: 149-156.

24. Onuma W, Tomono S, Miyamoto S, *et al*. Irsogladine maleate, a gastric mucosal protectant, suppresses intestinal polyp development in *Apc*-mutant mice. *Oncotarget* 2016; **7**: 8640-8652.

25. Tadashi Kondo, Setsuo Hirohashi, Application of highly sensitive fluorescent dyes (CyDye DIGE Fluor saturation dyes) to laser microdissection and two-dimensional difference gel electrophoresis (2D-DIGE) for cancer proteomics, *Nature Protocols*. 2006;**1**:2940–2956.

26. Mutoh M, Takahashi M, Wakabayashi K. Roles of prostanoids in colon carcinogenesis and their potential targeting for cancer chemoprevention. *Curr Pharm Des* 2006; **12**: 2375-2382.

27. Wang SW, Sun YM. The IL-6/JAK/STAT3 pathway: potential therapeutic strategies in treating colorectal cancer (Review). *Int J Oncol* 2014; **44**: 1032-1040.

28. Xiao W, Hodge DR, Wang L, *et al*. NF-kappaB activates IL-6 expression through cooperation with c-Jun and IL6-AP1 site, but is independent of its IL6-NF-kappaB regulatory site in autocrine human multiple myeloma cells. *Cancer Biol Ther* 2004; **3**: 1007-1017.

29. Allport VC, Slater DM, Newton R, *et al*. NF-κB and AP-1 are required for cyclo-oxygenase 2 gene expression in amnion epithelial cell line (WISH). *Mol Hum Reprod* 2000; **6**: 561-565.

30. Li L, Wang L, Wu Z, *et al*. Anthocyanin-rich fractions from red raspberries attenuate inflammation in both RAW264.7 macrophages and a mouse model of colitis. *Sci Rep.* 2014; **4**: 6254.

31. Fumimori T, Honda S, Migita K, *et al*. Erythromycin suppresses the expression of cyclooxygenase-2 in rheumatoid synovial cells. *J Rheumatol* 2004; **31**: 436-441.

32. Masashi D, *et al.* Molecular Mechanisms of Anti-Inflammatory Action of Erythromycin in Human Bronchial Epithelial Cells: Possible Role in the Signaling Pathway That Regulates Nuclear Factor-κB Activation. *Antimicrob Agents Chemother*. 2004; **48**: 1581–1585.

33. Takashi I, *et al*. Clarithromycin Inhibits NF-κB Activation in Human Peripheral Blood Mononuclear Cells and Pulmonary Epithelial Cells. *Antimicrob Agents Chemother.* 2001; **45**: 44–47.

34. Verweij J, Pinedo HM. Mitomycin C: mechanism of action, usefulness and limitations. *Anticancer Drugs*. 1990; **1**:5-13.

35. Huang Z, Wu Y, Zhou X, *et al*. Clinical efficacy of mTOR inhibitors in solid

tumors: a systematic review. *Future Oncol* 2015; **11**: 1687-1699.

36. Fuwa H, Suzuki T, Kubo H, *et al*. Total synthesis and biological assessment of (-)-exiguolide and analogues. *Chemistry* 2011; **17**: 2678-2688.

37. Niho N, Mutoh M, Takahashi M, *et al*. Concurrent suppression of hyperlipidemia and intestinal polyp formation by NO-1886, increasing lipoprotein lipase activity in Min mice. *Proc Natl Acad Sci U S A*, 2005; **102**: 2970-2974.

38. Niho N, Takahashi M, Shoji Y, *et al*. Dose-dependent suppression of hyperlipidemia and intestinal polyp formation in Min mice by pioglitazone, a PPAR gamma ligand. *Cancer Sci* 2003; **94**: 960-964.

39. Niho N, Mutoh M, Komiya M, *et al*. Improvement of hyperlipidemia by indomethacin in Min mice. *Int J Cancer* 2007; **121**: 1665-1669.

40. Nakatsugi S, Fukutake M, Takahashi M, *et al*. Suppression of intestinal polyp development by nimesulide, a selective cyclooxygenase-2 inhibitor, in Min mice. *Jpn J Cancer Res* 1997; **88**: 1117-1120.

41. Shimizu S, Fujii G, Takahashi M, *et al*. Sesamol suppresses cyclooxygenase-2 transcriptional activity in colon cancer cells and modifies intestinal polyp development in $Apc^{Min/+}$ mice. *J Clin Biochem Nutr* 2014; **54**: 95-101.

42. Arthur JC *et al*. Intestinal inflammation targets cancer-inducing activity of the microbiota. *Science*. 2012; **338**: 120-123.

43. Zhang J *et al*. Oral antibiotic use and risk of colorectal cancer in the United Kingdom, 1989-2012: a matched case-control study. Gut. 2019; **68**: 1971-1978.

44. Komiya M, Fujii G, Miyamoto S, *et al*. Suppressive effects of the NADPH oxidase inhibitor apocynin on intestinal tumorigenesis in obese KK-A^y and *Apc* mutant Min mice. *Cancer Sci* 2015; **106**: 1499-1505.

45. Wang WJ, Yao Y, Jiang LL, H *et al*. Knockdown of lymphoid enhancer factor 1 inhibits colon cancer progression in vitro and in vivo. *PLoS One.* 2013; **8**: e76596.

46. Phuchareon J, McCormick F, Eisele DW, Tetsu O. EGFR inhibition evokes innate drug resistance in lung cancer cells by preventing Akt activity and thus inactivating Ets-1 function. *Proc Natl Acad Sci USA*. 2015; **112**: E3855-3863.

47. Jiang F, Zhou JY, Zhang D, Liu MH, Chen YG. Artesunate induces apoptosis and autophagy in HCT116 colon cancer cells, and autophagy inhibition enhances the artesunate-induced apoptosis. *Int J Mol Med.* 2018; **42**: 1295-1304.

48. Eling N, Reuter L, Hazin J, Hamacher-Brady A, Brady NR. Identification of artesunate as a specific activator of ferroptosis in pancreatic cancer cells. *Oncoscience.* 2015; **2**: 517-532.

49. Li Y, Cui SX, Sun SY, *et al*. Chemoprevention of intestinal tumorigenesis by the natural dietary flavonoid myricetin in APCMin/+ mice. *Oncotarget.* 2016; **7**: 60446-60460.

50. Junfang Z, Hailong C, Bing Z, *et al*. Berberine potently attenuates intestinal polyps growth in ApcMin mice and familial adenomatous polyposis patients through inhibition of Wnt signaling. *J Cell Mol Med*. 2013; **17**: 1484–1493.

51. Orner GA, Dashwood WM, Blum CA, Díaz GD, Li Q and Dashwood RH. Suppression of tumorigenesis in the Apc(min) mouse: down-regulation of beta-catenin signaling by a combination of tea plus sulindac. *Carcinogenesis.* 2003; **24**:263-267.

52. Polakis P. Wnt signaling and cancer. *Genes Dev.* 2000; **14**: 1837-1851.

53. Thacker PC, Karunagaran D. Curcumin and emodin down-regulate TGF-β signaling pathway in human cervical cancer cells. *PLoS One.* 2015; **10**: e0120045.

54. Wang Z, Li B, Zhou L, Yu S, *et al*. Prodigiosin inhibits Wnt/β-catenin signaling and exerts anticancer activity in breast cancer cells. *Proc Natl Acad Sci USA*. 2016; **113**: 13150-13155.

55. Takahashi-Yanaga F, Yoshihara T, Jingushi K, Miwa Y, Morimoto S, Hirata M, Sasaguri T. Celecoxib-induced degradation of T-cell factors-1 and -4 in human colon cancer cells.*Biochem Biophys Res Commun.* 2008; **377**: 1185-1190.

56. Aono Y, Horinaka M, Iizumi Y, Watanabe M, Taniguchi T, Yasuda S, Sakai T. Sulindac sulfone inhibits the mTORC1 pathway in colon cancer cells by directly targeting voltage-dependent anion channel 1 and 2. *Biochem Biophys Res Commun.* 2018; **505**: 1203-1210.

57. Iizumi Y, Oishi M, Taniguchi T, Goi W, Sowa Y, Sakai T. The flavonoid apigenin downregulates CDK1 by directly targeting ribosomal protein S9. *PLoS One.* 2013 29; **8**: e73219.

58. Kim YH, Han ME, Oh SO. The molecular mechanism for nuclear transport and its application. *Anat Cell Biol.* 2017; **50**: 77-85.

59. Hrckulak D, Kolar M, Strnad H, Korinek V. TCF/LEF Transcription Factors: An Update from the Internet Resources. *Cancers (Basel).* 2016; **8**: pii: E70.

60. Sheng C, Qiu J, Wang Y, *et al*. Knockdown of Ran GTPase expression inhibits the proliferation and migration of breast cancer cells. *Mol Med Rep.* 2018; **18**: 157-168.

61. Zaoui K, Boudhraa Z, Khalifé P, *et al*. Ran promotes membrane targeting and stabilization of RhoA to orchestrate ovarian cancer cell invasion. *Nat Commun.* 2019; **10**: 2666.

62. Kent HM *et al.* Engineered mutants in the switch II loop of Ran define the

contribution made by key residues to the interaction with nuclear transport factor 2

(NTF2) and the role of this interaction in nuclear protein import. *J Mol Biol*. 1999;
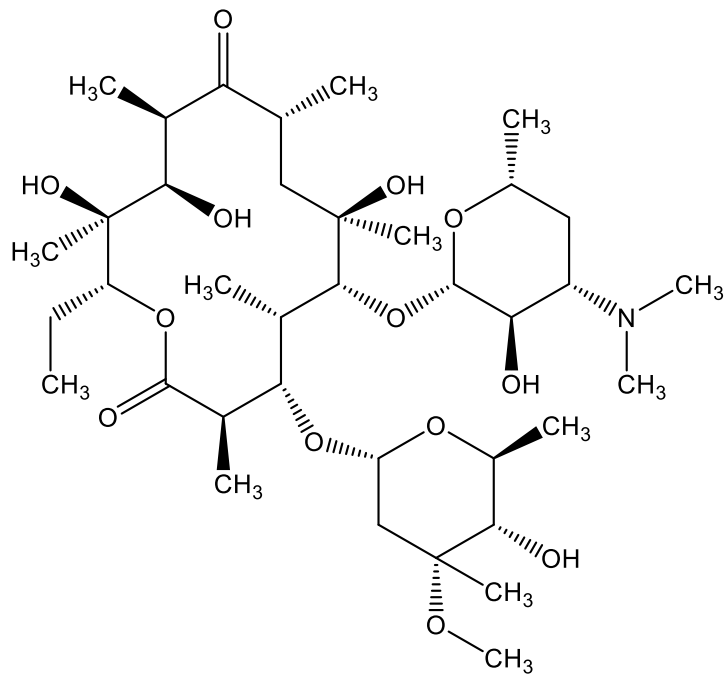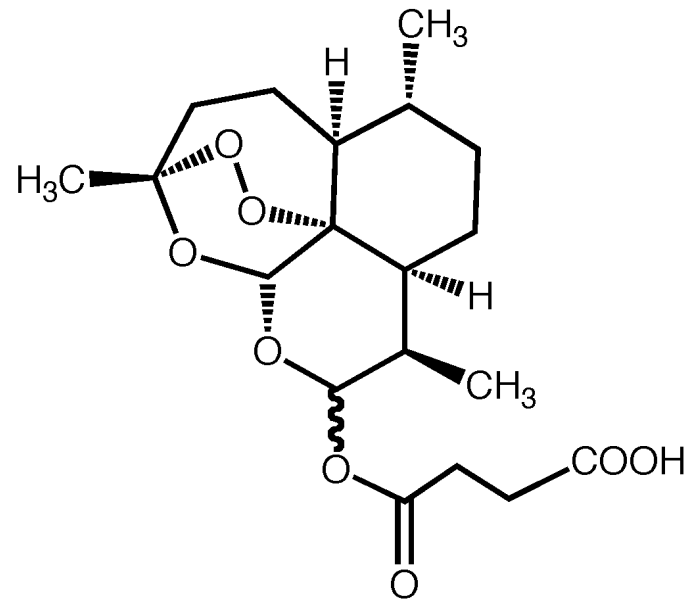
289: 565-577.

A

B

Figure 1. Chemical structure of erythromycin (A) and artesunate (B).
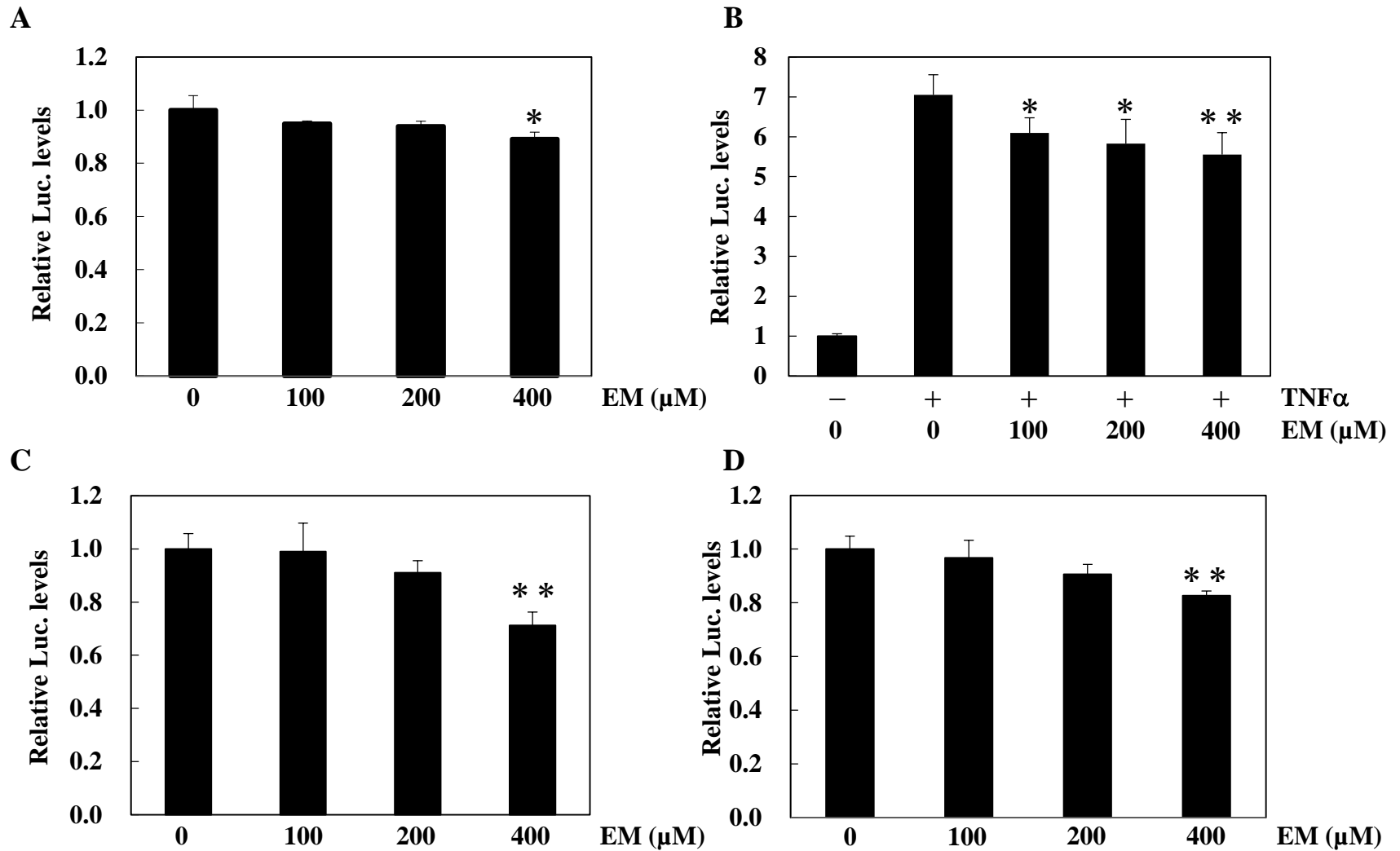
A

B

C

D

Figure 2. Effect of erythromycin on NF-κB promoter transcriptional activity in HCT116 cells.
HCT116-NF-κB-Luc cells were treated with erythromycin for 24 h (A). HCT116-NF-kB-Luc cells were treated with erythromycin and 10 ng/mL TNFα for 24 h (B). After transient NF-κB (C) and AP-1 (D) reporter plasmid transfection for 24 h, HCT116 cells were treated with EM for 24 h. NF-κB and AP-1 promoter transcriptional activity after 100, 200 and 400 µM EM treatment for 24 h. The basal luciferase activity of the control (0 µM EM) was set as 1.0. Data are shown as the mean $\pm$ SD, n = 4. *$p<0.05$, **$p<0.01$ *vs* control (0 µM EM) (A, C, D) and *vs* 10 ng/mL TNFα plus untreated EM (B). EM: erythromycin.
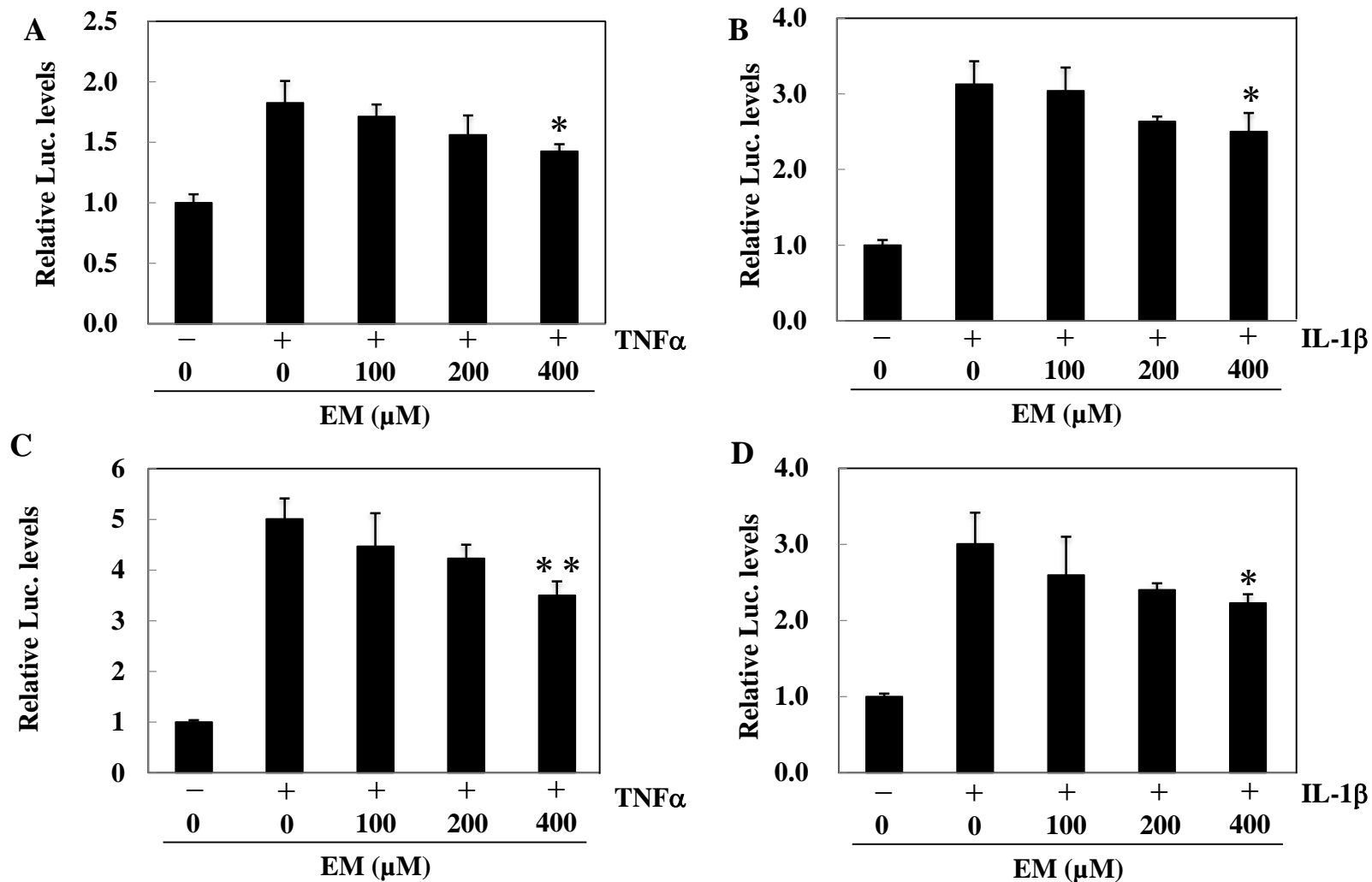
50

Figure 3. Effect of erythromycin on TNFα- and IL-1β-induced NF-κB promoter transcriptional activity in HCT116 and SW48 cells.
After transient NF-κB reporter plasmid transfection for 24 h, TNFα-induced (A) and IL-1β-induced (B) NF-κB promoter transcriptional activity after 100, 200 and 400 μM EM treatment for 24 h in HCT116 cells. After transient NF-κB reporter plasmid transfection for 24 h, TNFα-induced (C) and IL-1β-induced (D) NF-κB promoter transcriptional activity after 100, 200 and 400 μM EM treatment for 24 h in SW48 cells. The basal luciferase activity level of the control was set as 1.0. Data are shown as the mean ± SD, n = 3. *$p<0.05$, **$p<0.01$ *vs* TNFα or IL-1β plus untreated EM. TNFα : 10 ng/mL. IL-1β: 10 ng/mL.
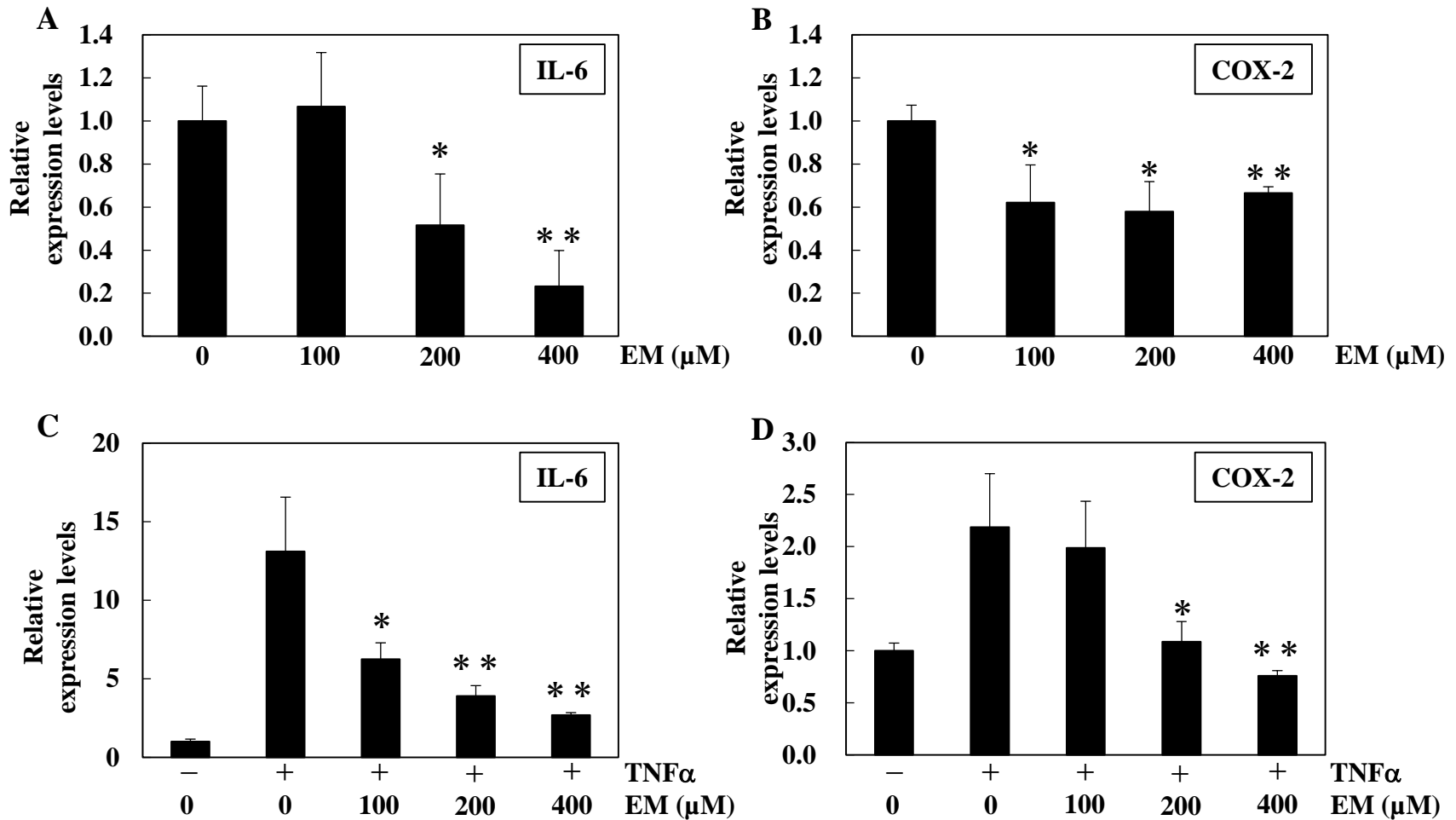
Figure 4. mRNA expression levels of inflammation-related factors in human colon cancer cells treated with or without erythromycin.
HCT116 cells were seeded in 24-well plates at a density of 2×10^5 cell/well and cultured in medium containing 100, 200 and 400 μM EM for 24 h. At 24 h after EM treatment, quantitative real-time PCR analysis was performed to determine IL-6 (A) and COX-2 mRNA expression levels (B). Furthermore, HCT116 cells were treated with 10 ng/mL TNFα and EM for 24 h to determine the effects of EM on IL-6 (C) and COX-2 mRNA expression levels (D). The basal mRNA expression levels of the control were set as 1.0. Data were normalized with GAPDH mRNA expression levels. Data are shown as the mean $\pm$ SD, n = 3. *$p < 0.05$, **$p < 0.01$ *vs* control (0 μM EM) (A, B) and *vs* 10 ng/mL TNFα plus untreated EM (C, D).
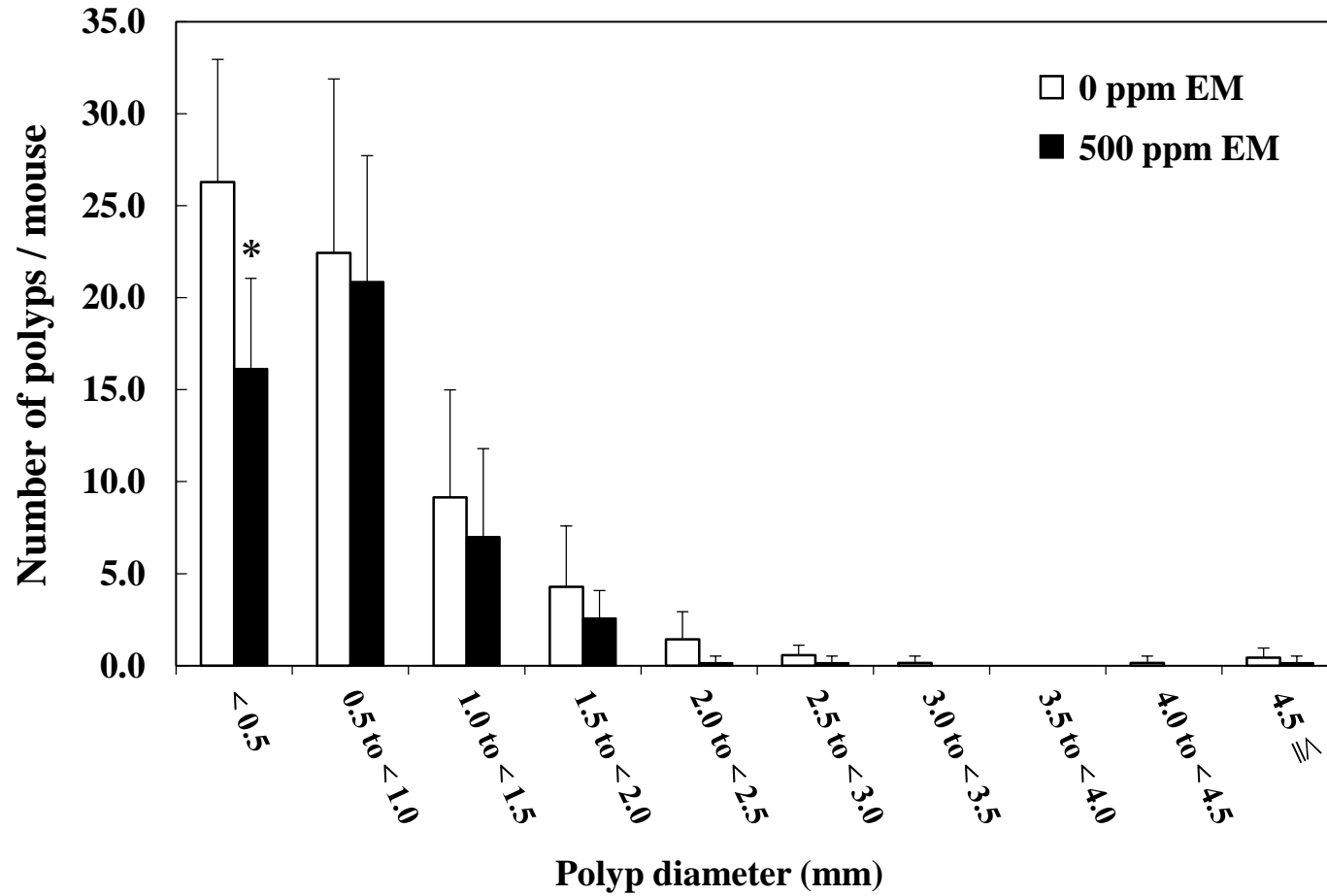
Figure 5. Effect of erythromycin on polyp size in Min mice.
Min mice were fed a basal diet (open box) or a diet containing 500 ppm EM (black-filled box) for 8 weeks. The number of polyps classified by size per mouse is shown as shown as the mean ± SD. *$p<0.05$ *vs* for each polyp diameter of 0 ppm EM.

A

IL-6

Relative expression levels

| 0 | 500 | 0 | 500 | EM |
| Mucosa | | Polyp | | (ppm) |

B

COX-2

Relative expression levels

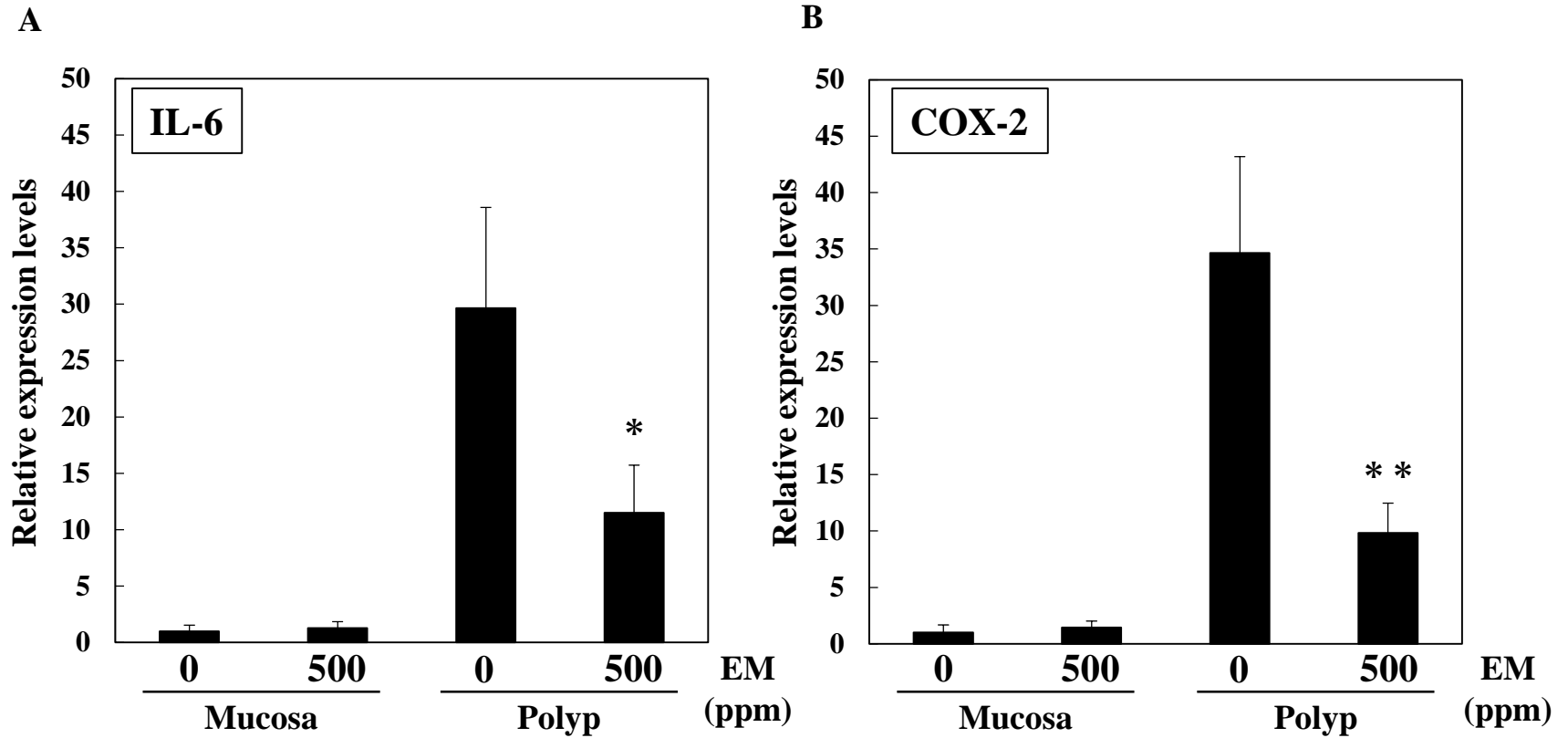| 0 | 500 | 0 | 500 | EM |
| Mucosa | | Polyp | | (ppm) |

54

Figure 6. mRNA expression levels of inflammation-related factors in the intestines of Min mice.
Quantitative real-time PCR analysis was performed to determine IL-6 mRNA (A) and COX-2 mRNA (B) expression levels in the non-polyp portions (mucosa) and polyp portions of the intestines of Min mice. Data were normalized with GAPDH mRNA expression levels. Each expression level in the mucosa without EM treatment was set as 1. Data are shown as the mean $\pm$ SD, n = 4 mice., *$p<0.05$, **$p<0.01$ *vs* for each portions of 0 ppm EM.
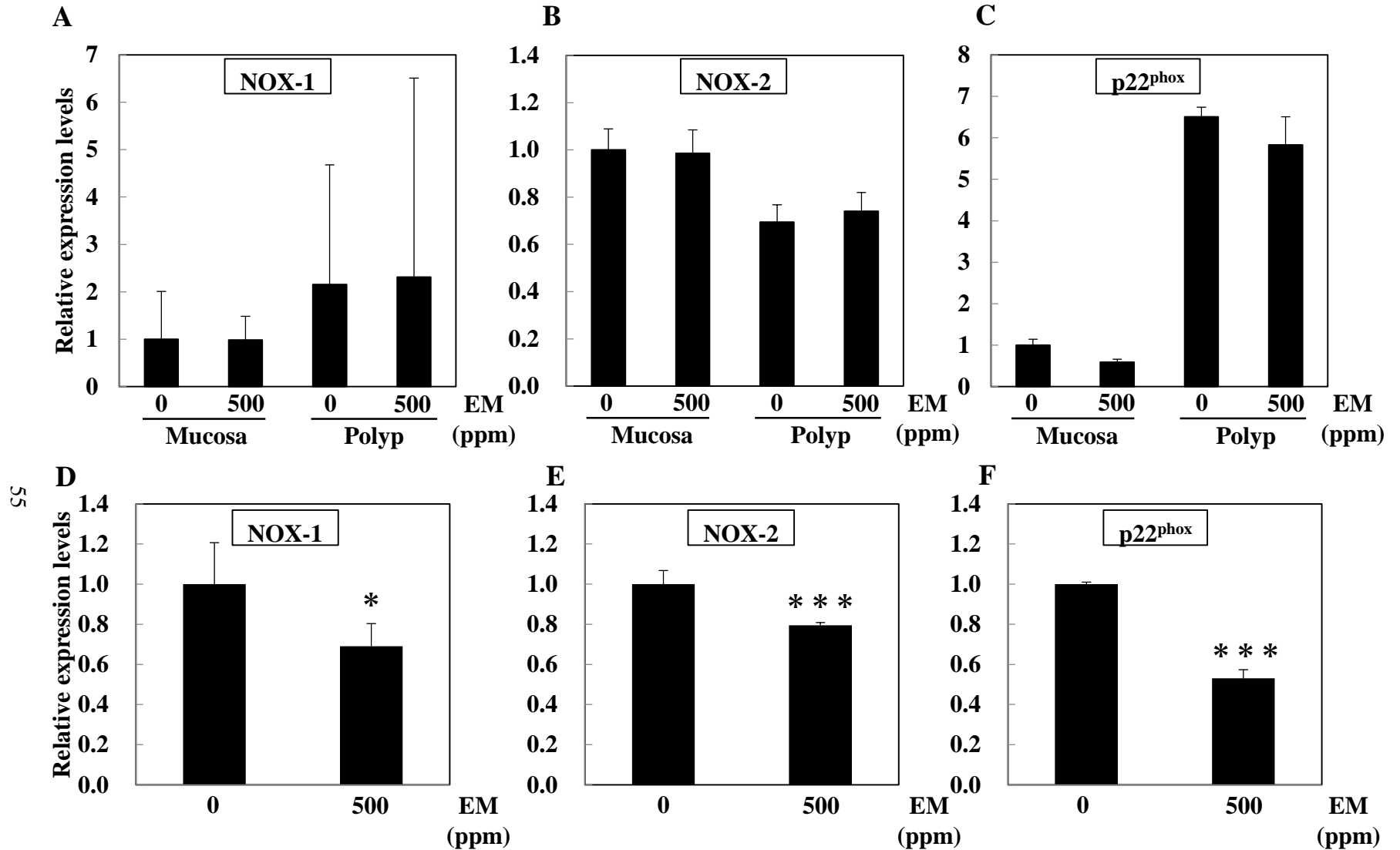
Figure 7. NADPH oxidase subunit mRNA levels in the intestines and livers of Min mice.
Quantitative real-time PCR analysis was performed to determine NOX-1 (A), NOX-2 (B) and p22 phox (C) mRNA expression levels in the intestines of Min mice. Quantitative real-time PCR analysis. was performed to determine NOX-1 (D), NOX-2 (E) and p22 phox (F) mRNA expression levels in the livers of Min mice. Data were normalized with GAPDH mRNA expression levels. Each expression level in the mucosa of 0 ppm EM treatment was set as 1 (A - C). The basal mRNA expression levels in the of 0 ppm EM treatment were set as 1.0. Data are shown as the mean $\pm$ SD, n = 4 mice. *$p<0.05$, ***$p<0.001$ *vs* for each portions of 0 ppm EM.
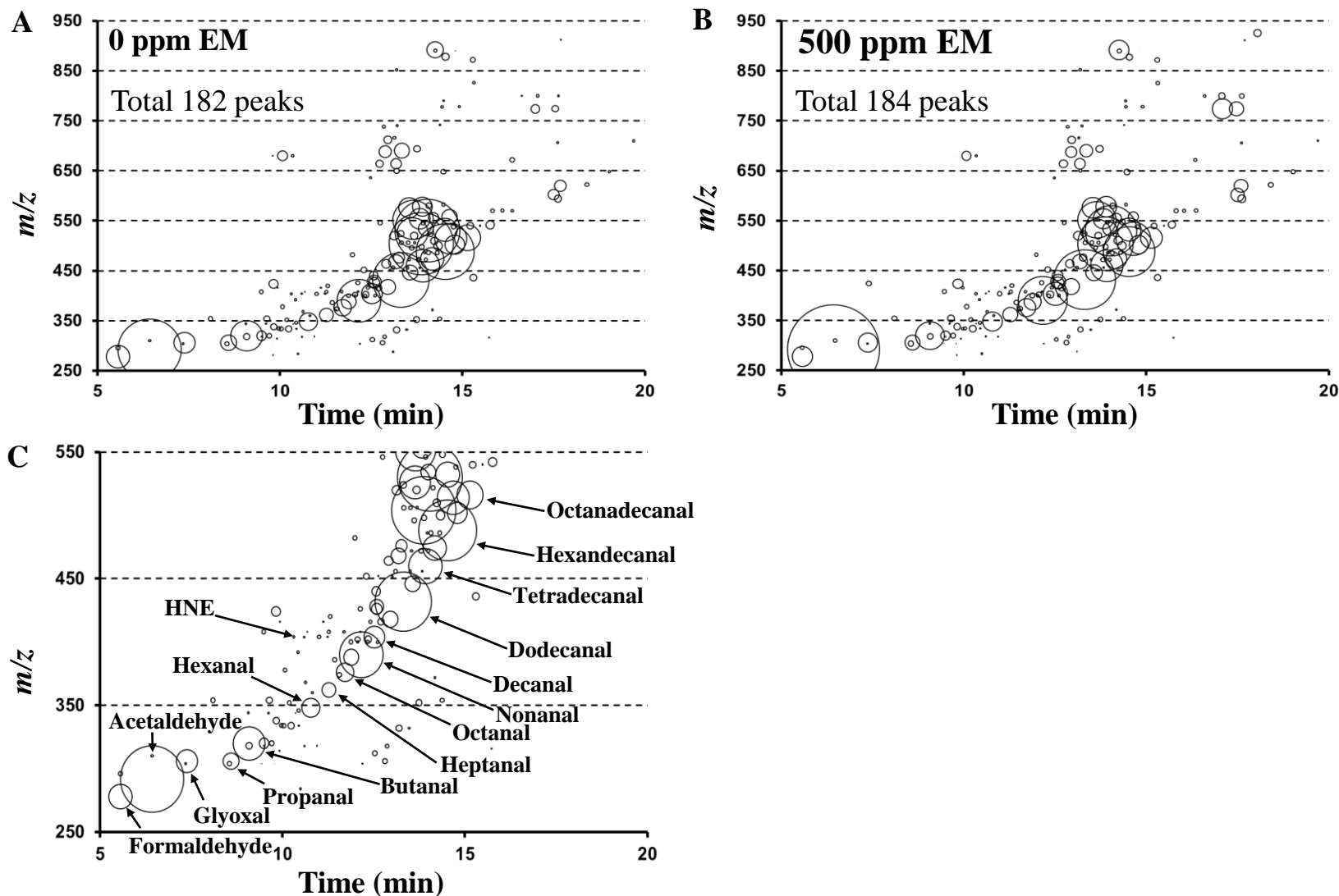
55

Figure 8. Corresponding RCs maps plotting free RCs detected in the liver samples of Min mice.

All free RCs detected in the liver samples taken from 0 (A) or 500 (B) ppm dried EM-treated Min mice are shown. The RCs are plotted as circles as a function of their retention times (horizontal axis) and m/z values (vertical axis). The areas of the circles represent the intensities of the peaks of the RCs relative to that of the IS. Figure 8C is an enlarged view of Figure 8B showing the m/z values within the range of 250 to 550, as well as the names of specific RCs identified by the analyses. The RCs abbreviations are listed in Materials and Methods.

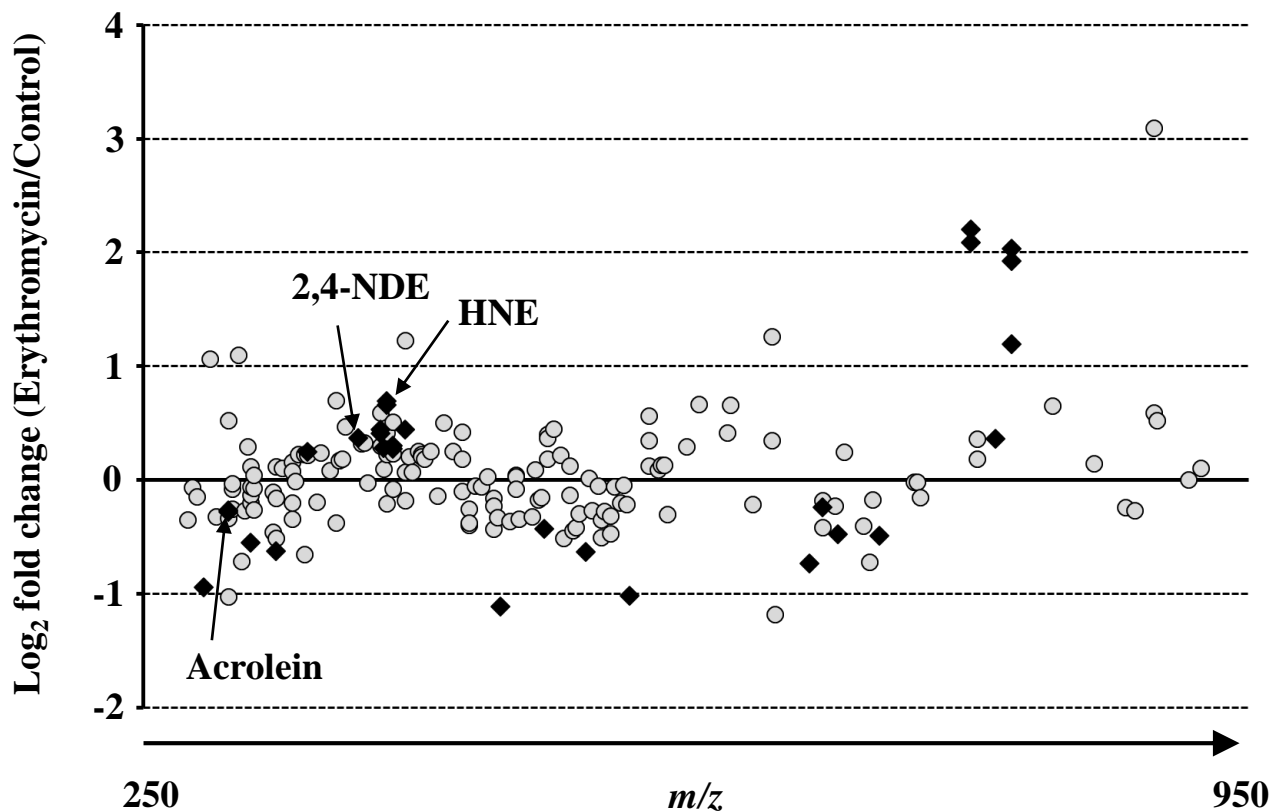**Figure 9. Relative RCs levels detected in the liver samples taken from erythromycin-treated Min mice compared with those detected in the liver samples taken from non-treated mice.**
The comparative RCs profiles of the liver samples from 500 ppm EM-treated Min mice. The closed diamonds indicate that the RCs levels were significantly different between non-treated and EM-treated mice ($p<0.05$).
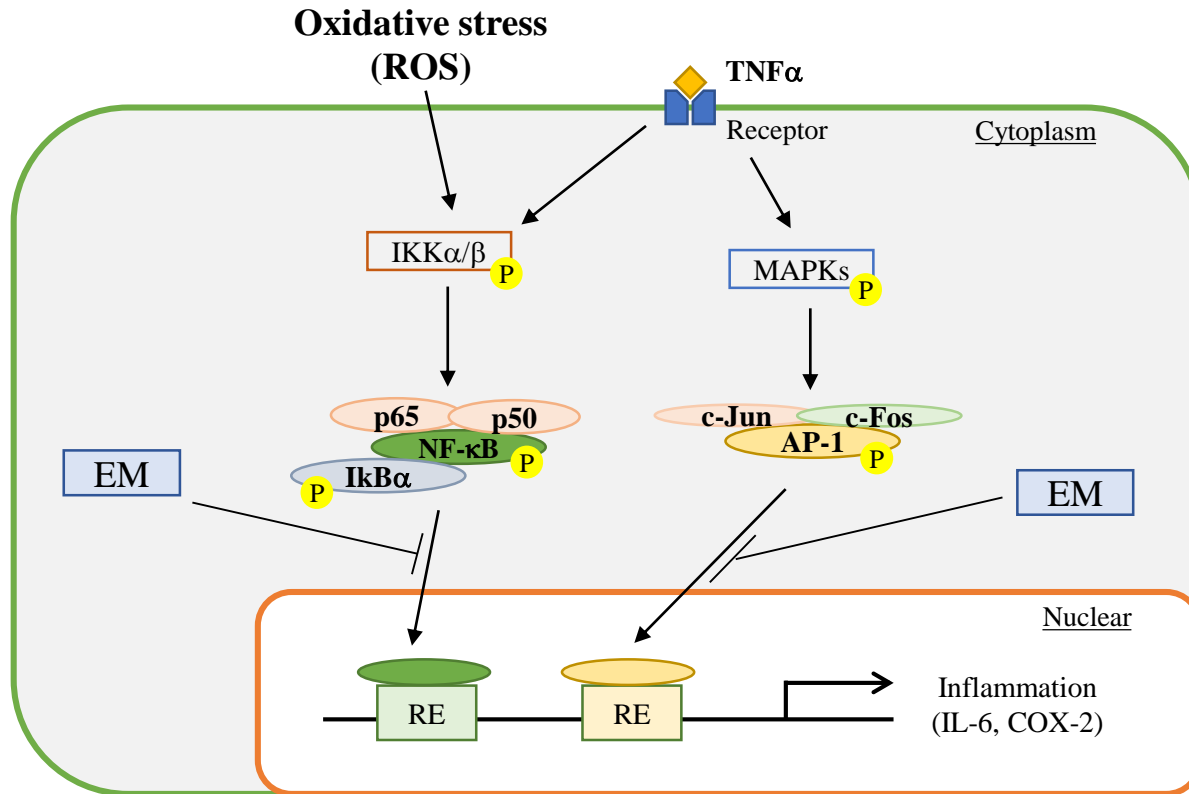
Figure 10. Schema of assumed NF-κB signaling suppression by erythromycin. EM: erythromycin; RE: response element.
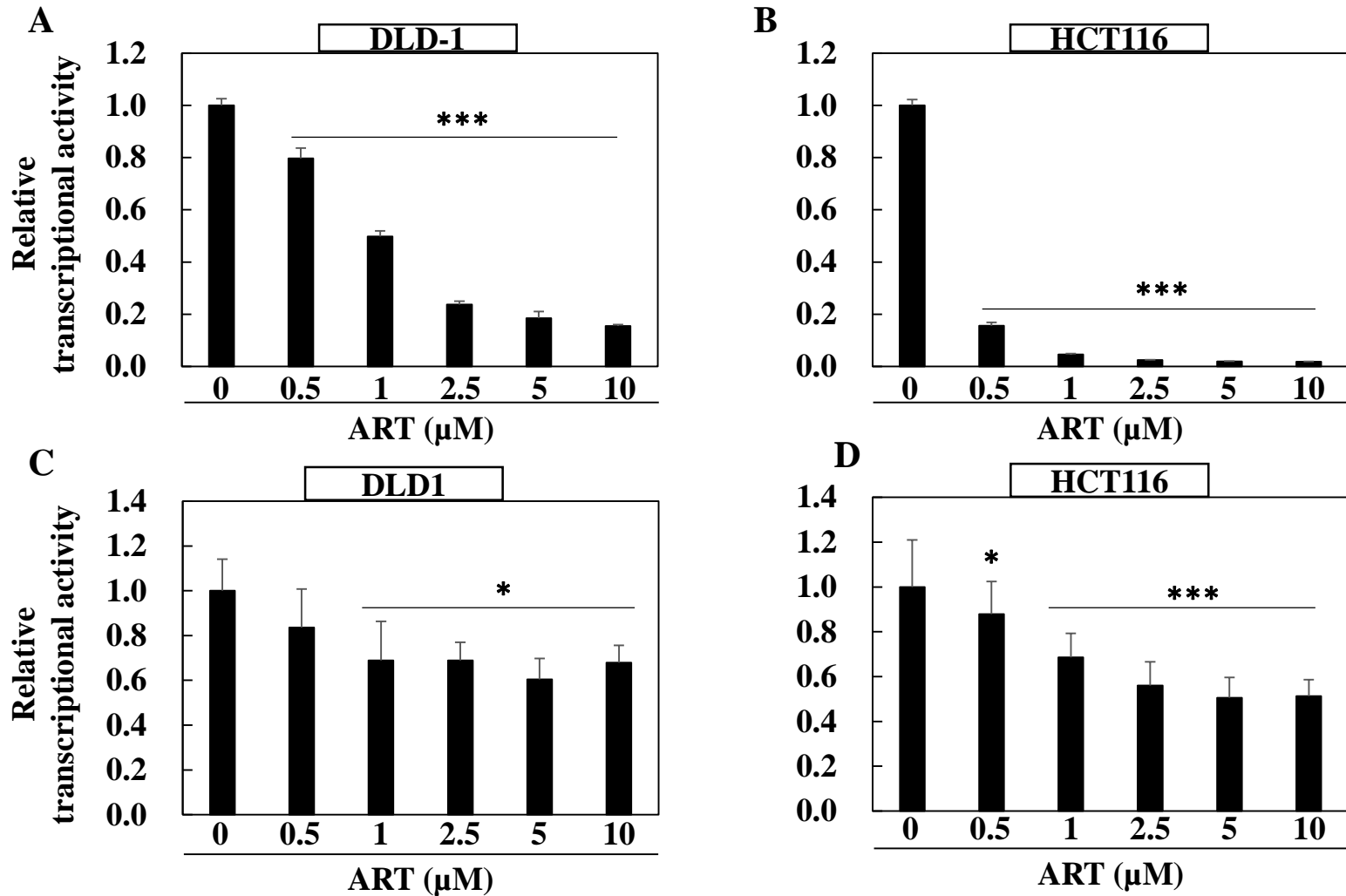
Figure 11. Effects of artesunate on TCF/LEF promoter transcriptional activity in colorectal cancer cells.
The DLD-1-TCF/LEF-Luc cells (A) and HCT116-TCF/LEF-Luc cells (B) were treated with ART for 24 h. After transient TCF/LEF reporter plasmid transfection for 24 h, DLD-1 (C) and HCT116 cells (D) were treated with ART for 24 h. TCF/LEF promoter transcriptional activity after 0.5, 1, 2.5, 5 and 10 µM ART treatment for 24 h. The basal luciferase activity of the control (0 µM ART) was set as 1.0. Data are shown as mean $\pm$ SD, n = 4. $*p<$ 0.05 and $***p<$ 0.01 *vs* control (0 µM ART). ART, artesunate.

Figure 12. mRNA expression levels of cell proliferation-related factors after artesunate treatment in colorectal cancer cells.
DLD-1 and HCT116 cells were seeded in 12-well plates at a density of 4×10^5 cells/well and cultured in medium containing 0.5, 1, 2.5, 5 and 10 µM ART for 24 h. At 24 h after ART treatment, c-Myc mRNA expression levels were evaluated in DLD-1 (A) and HCT116 cells (B) by quantitative real-time PCR analysis. Cyclin D1 mRNA were also evaluated in DLD-1 (C) and HCT116 cells (D). The basal mRNA expression levels of the control (0 µM ART) were set as 1.0. Data were normalized with GAPDH mRNA expression levels. Data are shown as the mean $\pm$ SD (n = 4). *$p<0.05$, **$p<0.01$ and ***$p<0.001$ *vs* control (0 µM ART). ART, artesunate.

A

DLD-1

ART (μM)	0	0.5	1	2.5	5	10

c-Myc

Cyclin D1

β-actin

B

HCT116

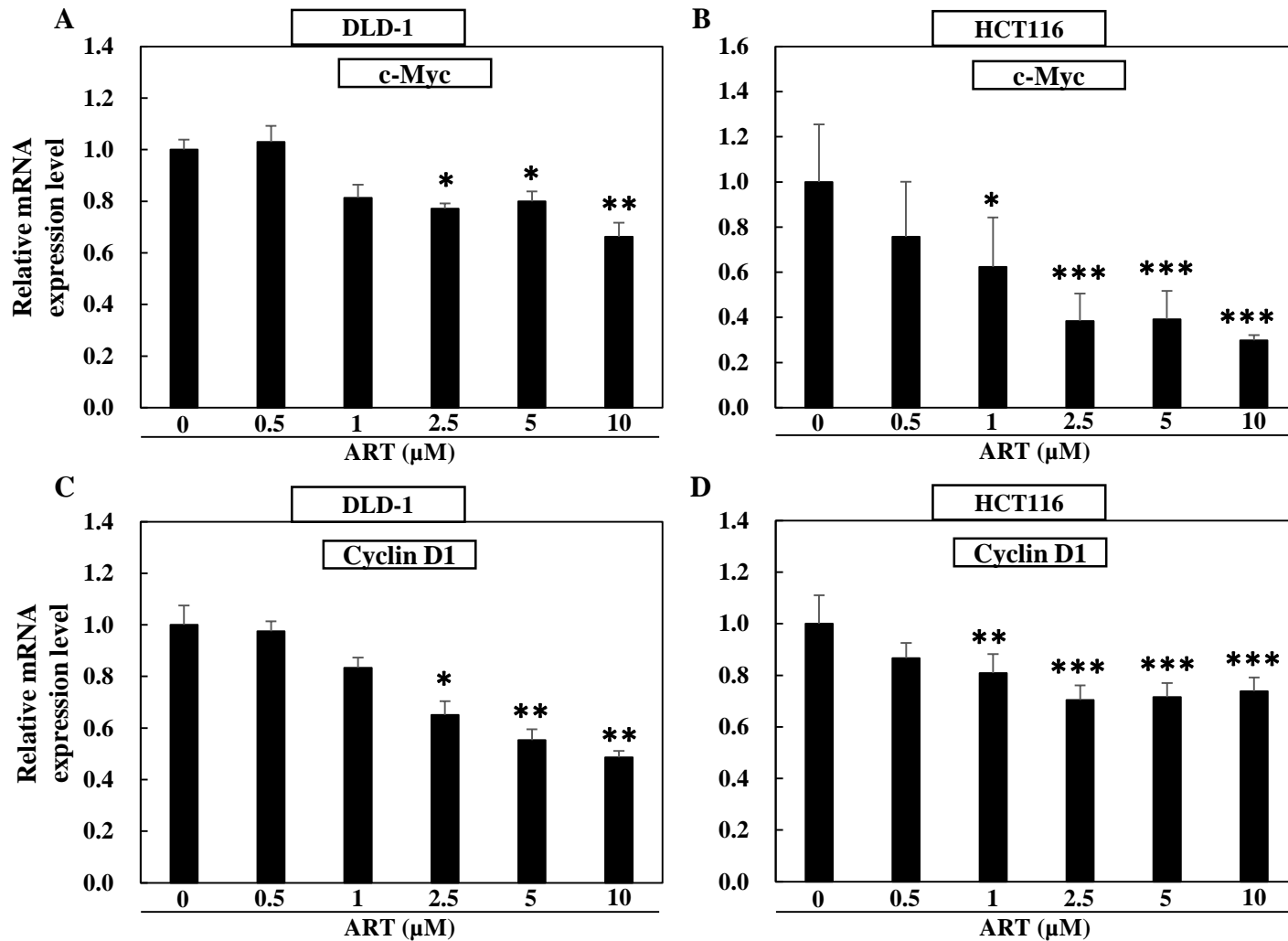| ART (μM)	0	0.5	1	2.5	5	10

c-Myc

Cyclin D1

β-actin
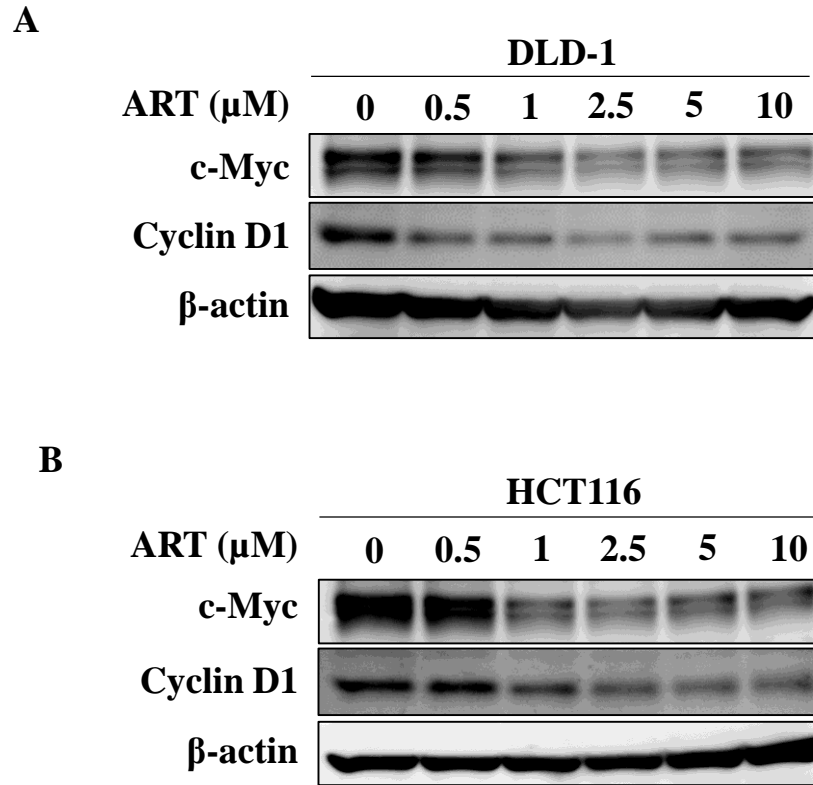
Figure 13. Protein expression levels of cell proliferation-related factors after artesunate treatment in colorectal cancer cells.
DLD-1 (A) and HCT116 cells (B) were seeded in 24-well plates at a density of 2×10^5 cell/well and treated with indicated doses of ART for 24 h. 15 μg of whole cell extract was added, and electrophoresis was performed. After then, the elution was analyzed by western blot using anti-c-Myc, anti-cyclin D1 and anti-β-actin antibodies. β-actin was used as a control.
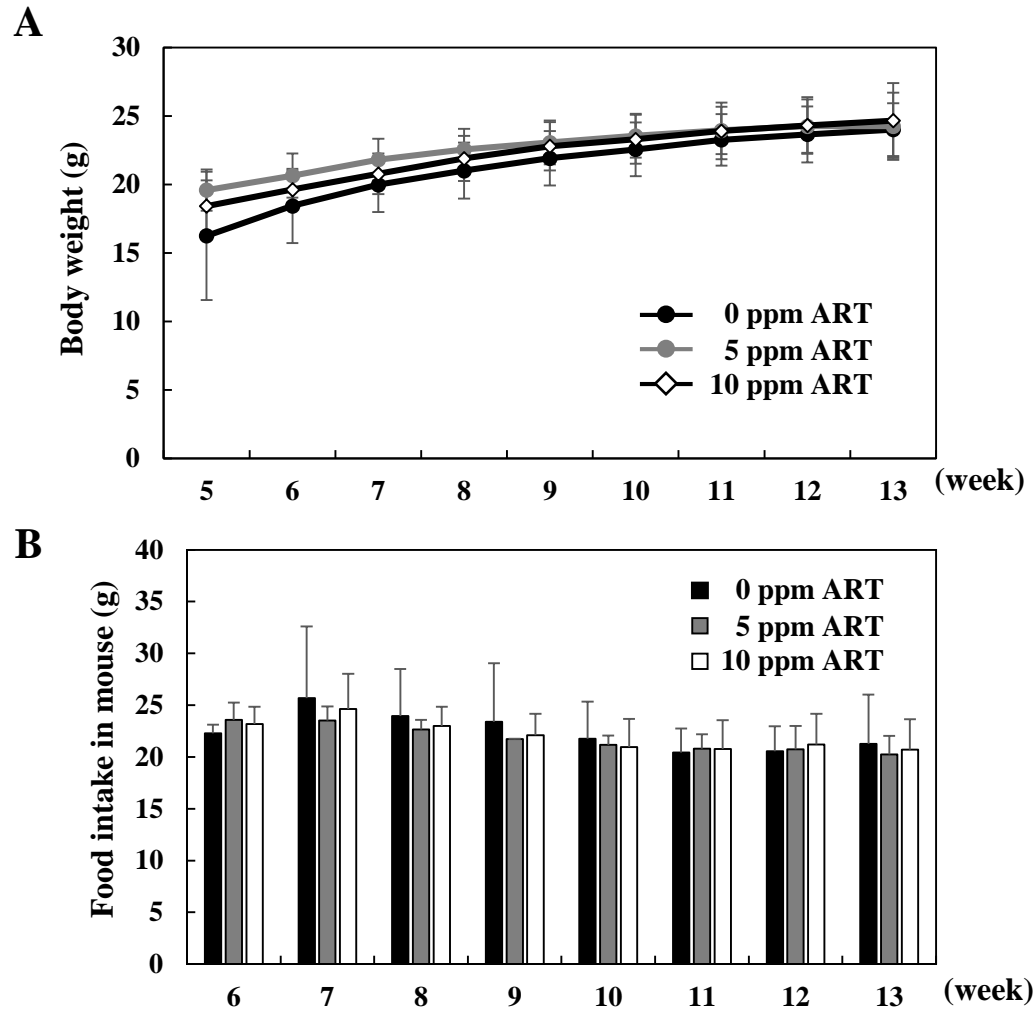
Figure 14. Effect of artesunate on body weight and food intake in Min mice.
Min mice were fed a basal-diet or a diet containing 5 ppm or 10 ppm artesunate from 5 to 13 weeks . The weekly body weight (A) and weekly food intake (B) per mouse are shown as the mean $\pm$ SD.
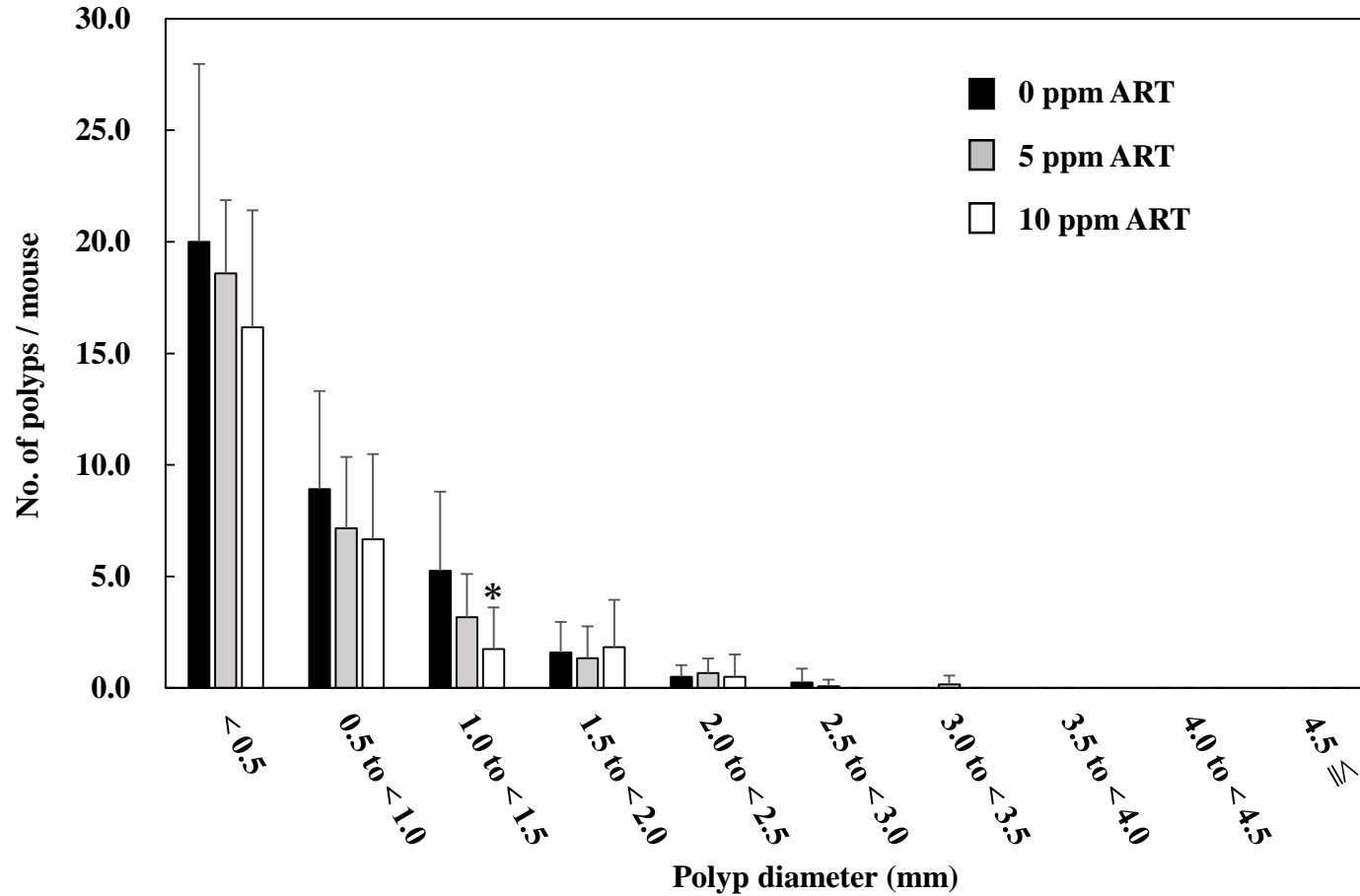
Figure 15. Effect of artesunate on polyp size.
Min mice were fed a basal-diet (Black-filled box) or a diet containing 5 ppm (gray-filled box) or 10 ppm (Open box) artesunate for 8 weeks . The number of polyps classified by size per mouse is shown as shown as the mean ± SD. *$p<0.05$ *vs* for each polyp diameter of 0 ppm ART.

A

c-Myc

Relative mRNA expression level

						ART (ppm)
mucosa			polyp			
0	5	10	0	5	10	

B

Cyclin D1

						ART (ppm)
mucosa			polyp			
0	5	10	0	5	10	
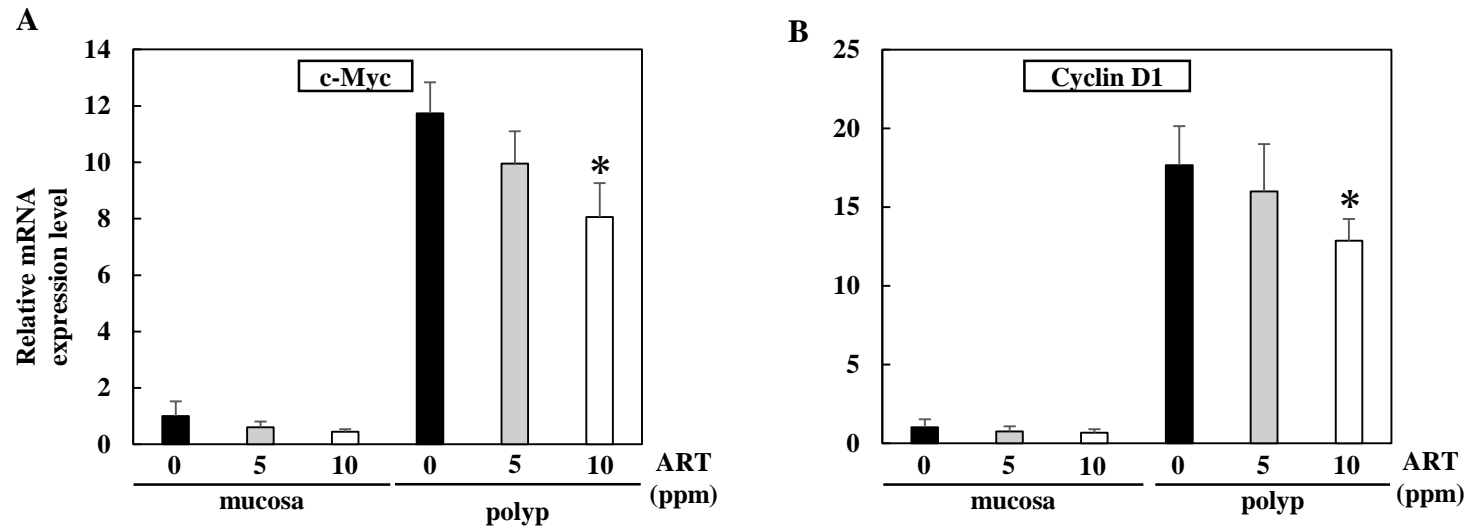
Figure 16. mRNA expression levels of cell proliferation-related factors after artesunate treatment in the intestines of Min mice.
Quantitative real-time PCR analysis was performed to evaluate expression levels of c-Myc mRNA (A) and cyclin D1 mRNA (B) in the non-polyp portions (mucosa) and polyp portions of the intestines of Min mice. Data were normalized with GAPDH mRNA expression levels. Each expression level in the mucosa without ART treatment was set as 1. Data are shown as the mean $\pm$ SD, n = 4 mice., *$p<0.05$ *vs* for each portions of 0 ppm ART. ART, artesunate.

Figure 17. Protein expression levels of Wnt/β-catenin signaling-related factors after artesunate treatment *in vitro*.
DLD-1 and HCT116 cells were seeded in 24-well plates at a density of 2×10^5 cell/well and treated with indicated dose of artesunate for 24 h. 15 µg of whole cell extract was added, and electrophoresis was performed. After then, the elution was analyzed by western blot using anti-total β-catenin, Non-phos β-catenin and anti-β-actin antibodies (A, B). The elution was analyzed by western blot using anti-TCF1/TCF7, anti-LEF1, anti-TCF4 anti-β-actin antibodies (C, D). β-actin was used as a control. Non-phos, Non-phosphorylated.

A

DLD-1

	Cyt.			Nuc.		
ART (µM)	0	1	10	0	1	10

Non phos
β-catenin

TCF1/TCF7

LEF1

β-tubulin

Lamin A+C

B

HCT116

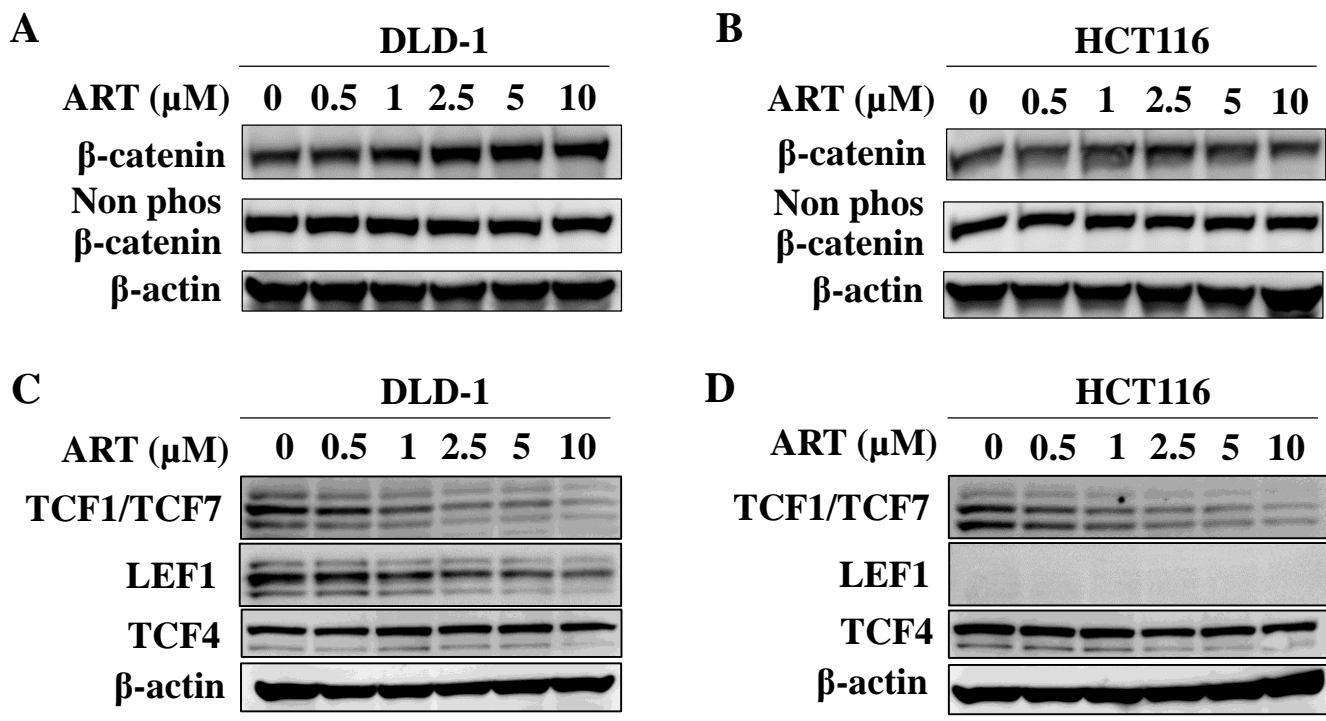|	Cyt.			Nuc.		
ART (µM)	0	1	10	0	1	10

Non phos
β-catenin

TCF1/TCF7

LEF1

β-tubulin

Lamin A+C
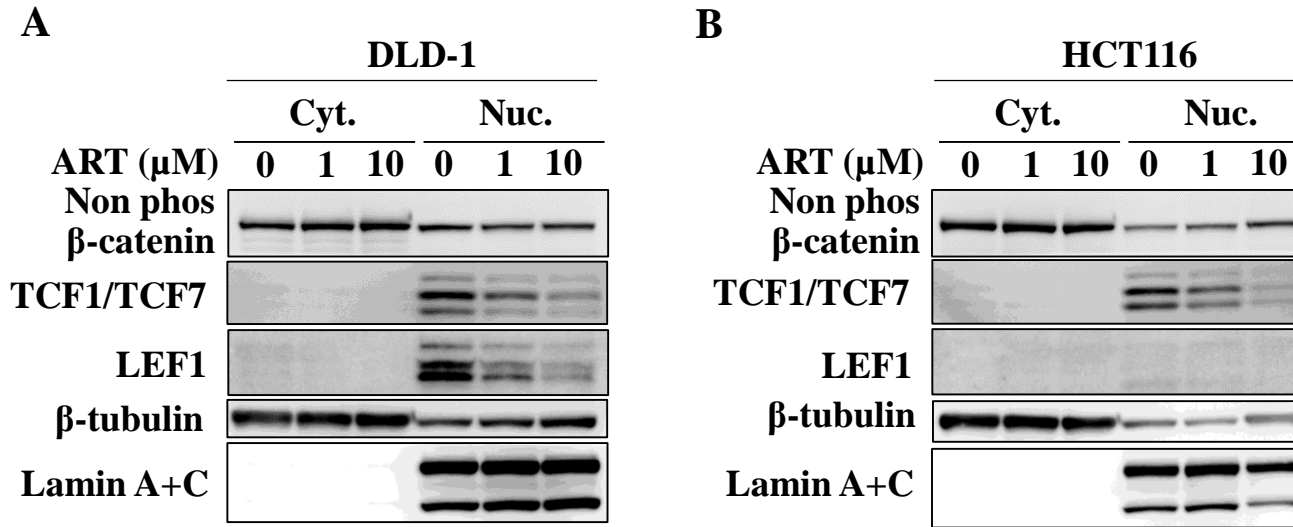
Figure 18. Protein expression levels of Wnt/β-catenin signaling-related factors after artesunate treatment in cytoplasmic and nuclear fraction.
After ART treatment, DLD-1 (A) and HCT116 cells (B) were separated in cytoplasmic and nuclear fraction using NE-PER nuclear and cytoplasmic extraction kit. The elution was analyzed by western blot using anti-Non-phos β-catenin, anti-TCF1/TCF7, anti-LEF1 anti-β-tubulin and anti-Lamin A+C antibodies. β-tubulin was used as a cyt. control. Lamin A+C was used as a nun. control. Cyt., cytoplasmic fraction; Nun., nuclear fraction; Non-phos, Non-phosphorylated.
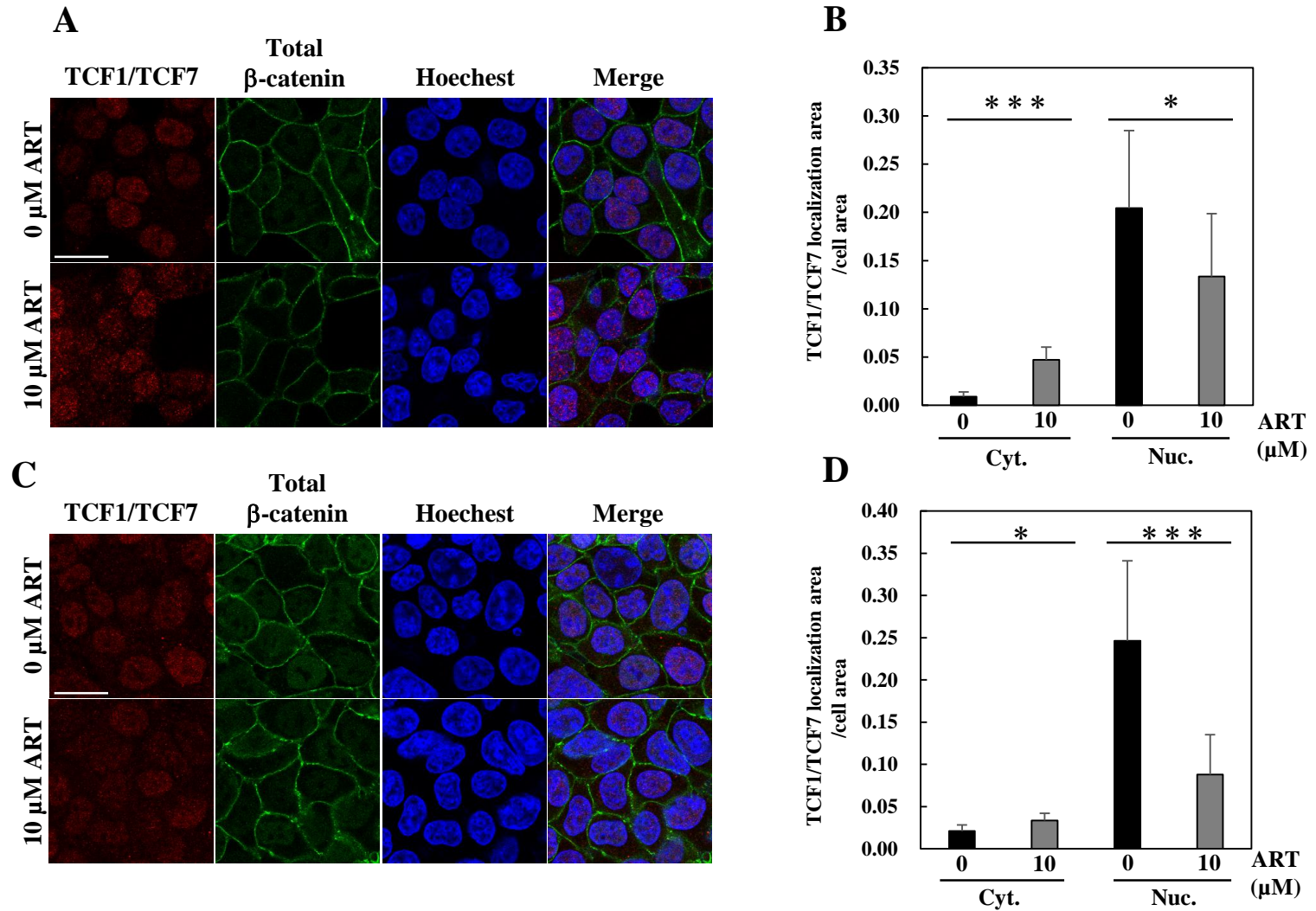
Figure 19. Effect of artesunate on TCF1/TCF7 localization.

Localization of TCF1/TCF7 and β-catenin protein was evaluated by immunofluorescence assay. HCT116 (A) and DLD-1 cells (C) were seeded in 8-well chamber slides, and the cells were treated with 10 μM artesunate. The cells analyzed by confocal microscopy for the localization of TCF1/TCF7 (red), total b-catenin (green) and nuclear (Hoechest, bule). Scale bars; 20 µm. In HCT116 (B) and DLD-1 cells (D), the intracellular localization area of TCF1/TCF7 are measured with ImageJ software. The whole intracellular area was set as 1.0. n = 10 cells., *p <0.05 and ***p <0.001 *vs* 0 for each fraction control (0 µM ART). Cyt., cytoplasmic fraction; Nun., nuclear fraction.
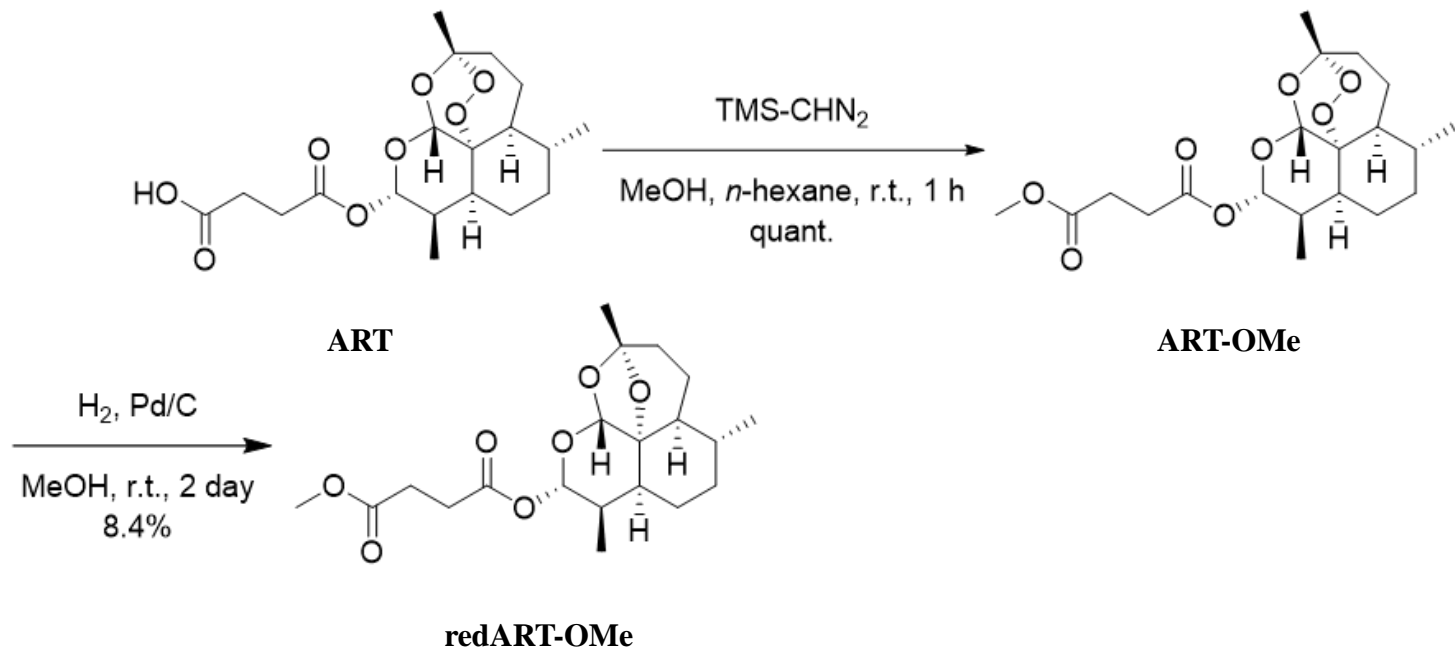
Figure 20. Scheme of synthesis procedure of ART isomer structure, ART-OMe and redART-OMe.
ART-OMe was synthesized from ART using TMS-CHN$_2$ to convert the hydroxy group contained in the carboxyl group to a methyl group. Therefore, redART-OMe was synthesized from ART-OMe using H$_2$ and Pd/C to convert peroxide structure to ether structure. Pd/C, palladium on carbon.

A DLD1

B HCT116

C DLD1
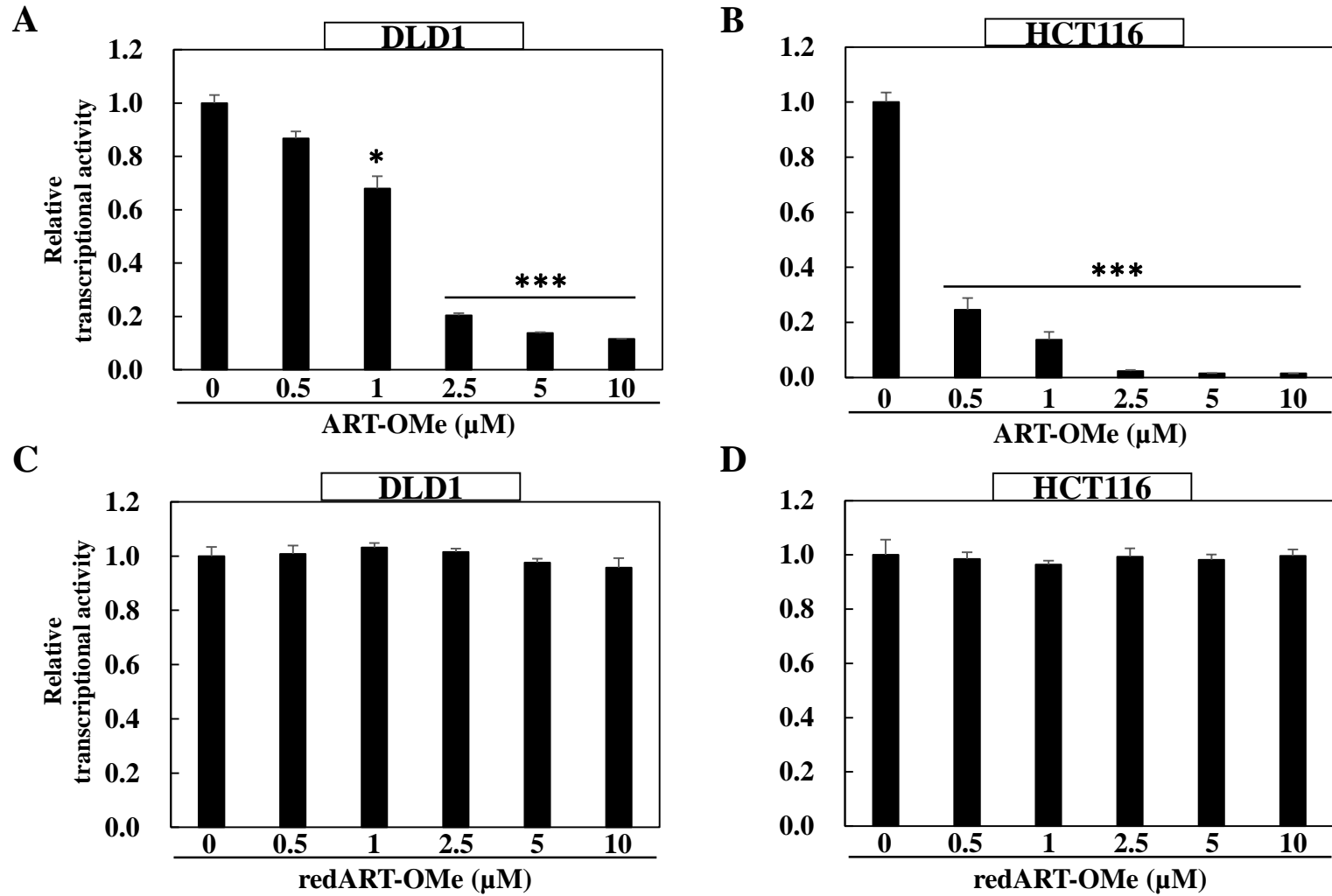
D HCT116

Figure 21. Effect of two synthesized isomer on TCF/LEF cells.
The DLD-1-TCF/LEF cells (A, C) and HCT116-TCF/LEF cells (B, D) were treated with indicated dose of ART-OMe or redART-OMe for 24 h. The basal luciferase activity of the control (0 µM ART-OMe (A, B) and redART-OMe (C, D)) was set as 1.0. Data are shown as mean $\pm$ SD, n = 4. *$p < 0.05$ and ***$p < 0.01$ *vs* control control (0 µM ART-OMe (A, B) and redART-OMe (C, D)) .
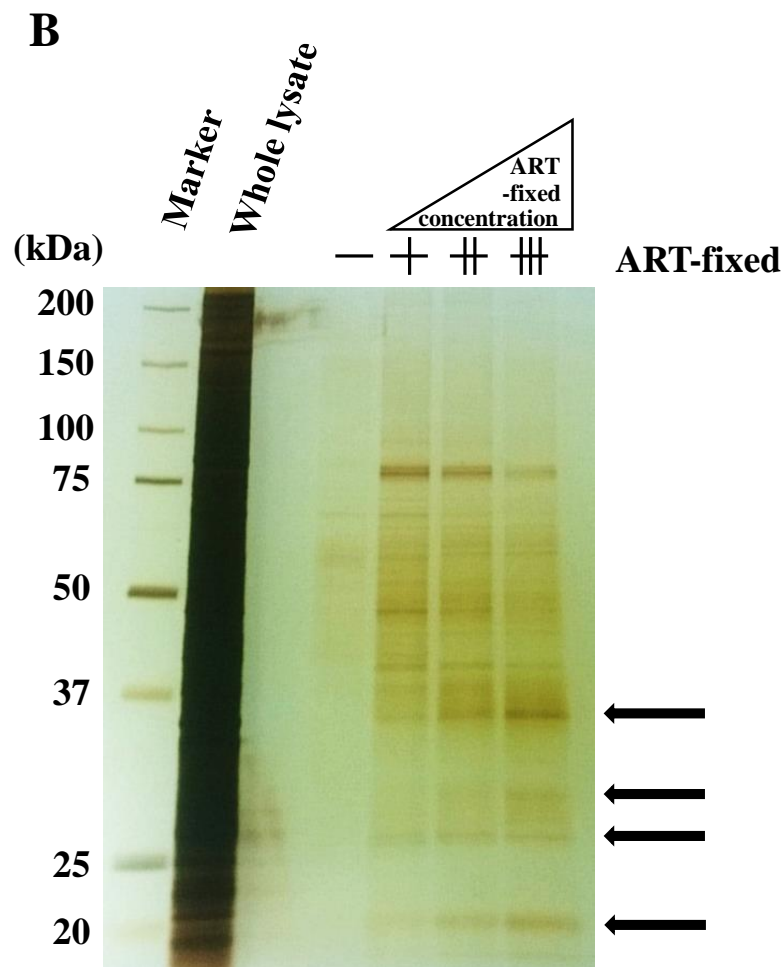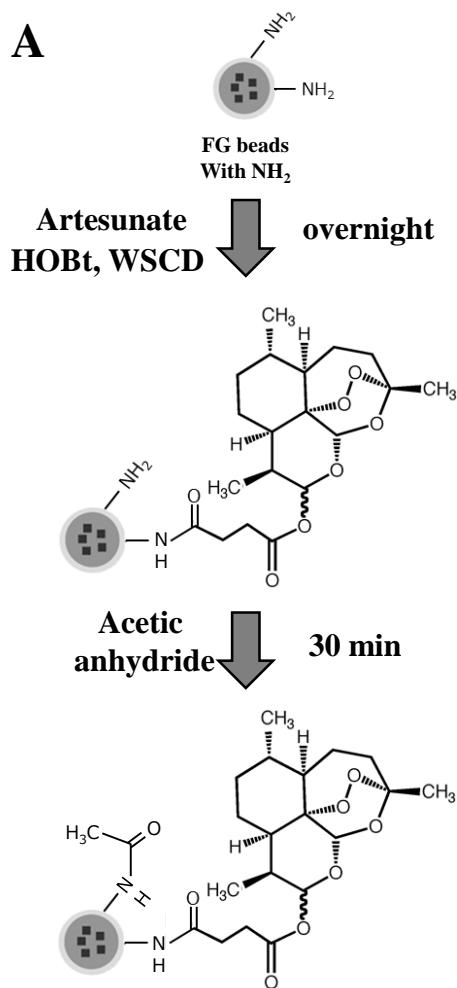
Figure 22. Search for artesunate-binding proteins using FG beads.
(A) Scheme for the fixation of artesunate onto magnetic FG beads with NH_2. FG beads with NH_2 and artesunate are chemically bonded using HOBt. After that, the exposed NH_2 on the FG beads was masked with acetic anhydride. (B) Empty beads or ART-fixed beads were incubated with 200 µg of whole cell lysate of HCT116 cells, and the beads or ART binding protein were electrophoresed. Thereafter, the protein was detected by silver staining. The ART fixed concentration was prepared by changing the ART concentration added to the beads. The arrow was the detected protein.

70

A

DLD-1

Relative transcriptional activity

1.20
1.00
0.80
0.60
0.40
0.20
0.00

− + − + ART

MOCK siLEF1

B

HCT116

1.20
1.00
0.80
0.60
0.40
0.20
0.00

− + − + ART

MOCK siLEF1

71
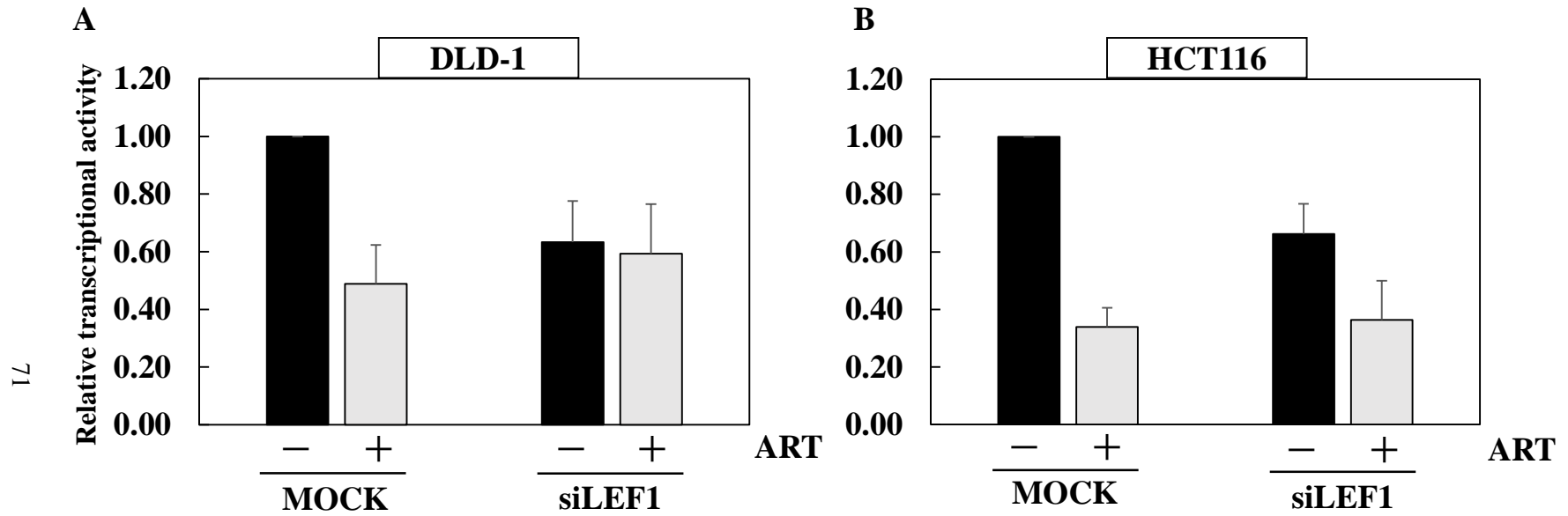
Figure 23. Effect of LEF1 knockdown on the TCF/LEF promoter transcriptional activity treated with artesunate.
0.5 µM ART was cotreated for 24 hours on DLD-1 TCF/LEF-Luc cells (A) and HCT116 TCF/LEF-Luc cells (B) in which control (mock) and LEF1 were knocked down with siRNA. The basal luciferase activity of the control (mock cells with 0 µM ART) was set as 1.0. Data are shown as mean ± SD, n = 3.
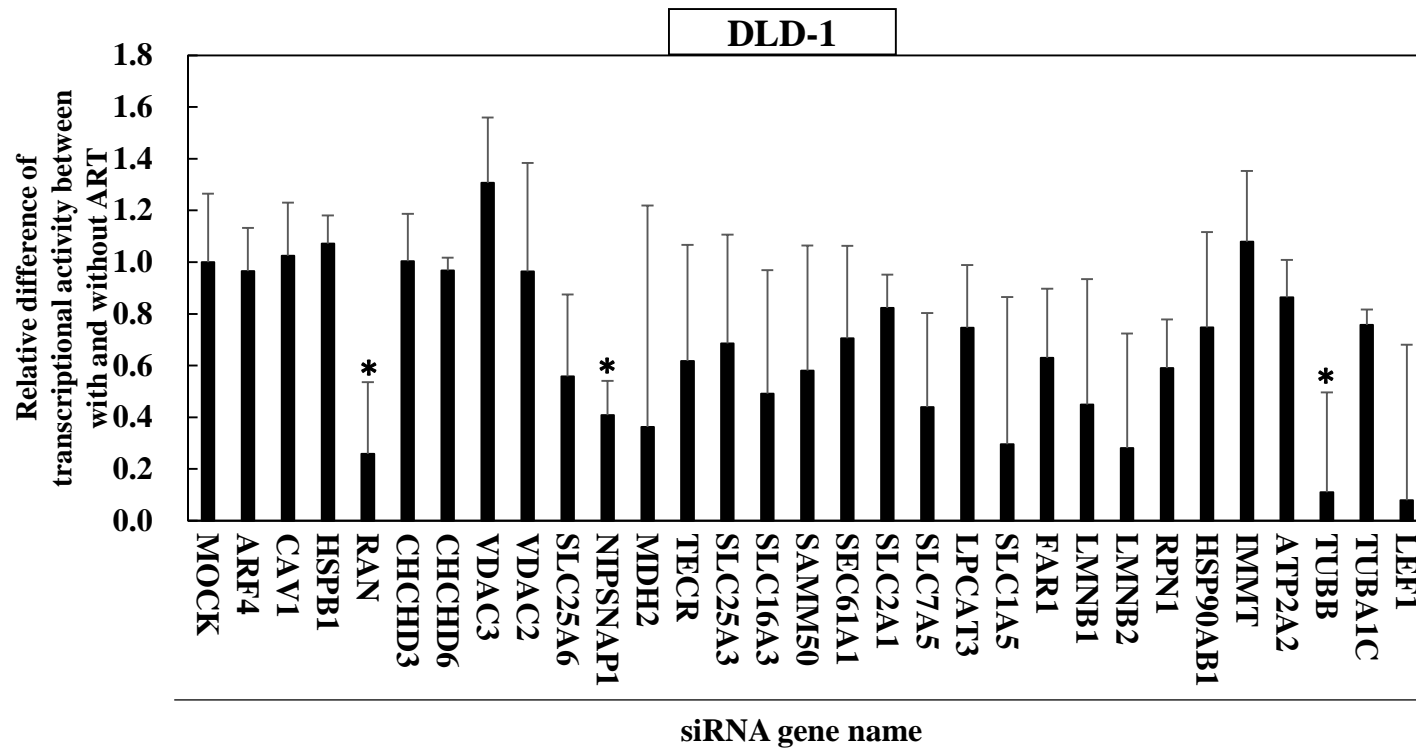
Figure 24. Difference of promoter transcriptional activity obtained between siRNA and ART treatment in DLD-1 cells.
In the DLD-1-TCF/LEF-Luc cells, to knock down each protein, transfection was performed by mixing three siRNA primers. After that, each cell was treated with 0.5 µM ART for 24 h. And evaluated the difference of the TCF/LEF promoter transcriptional activity between no treatment in candidate gene knock-down cells treated and ART treatment in candidate gene knock-down cells. The difference of the luciferase activity in Mock is set as 1.0. Data are presented as the mean $\pm$ SD (n = 3). *$p < 0.05$ *vs* MOCK cells.
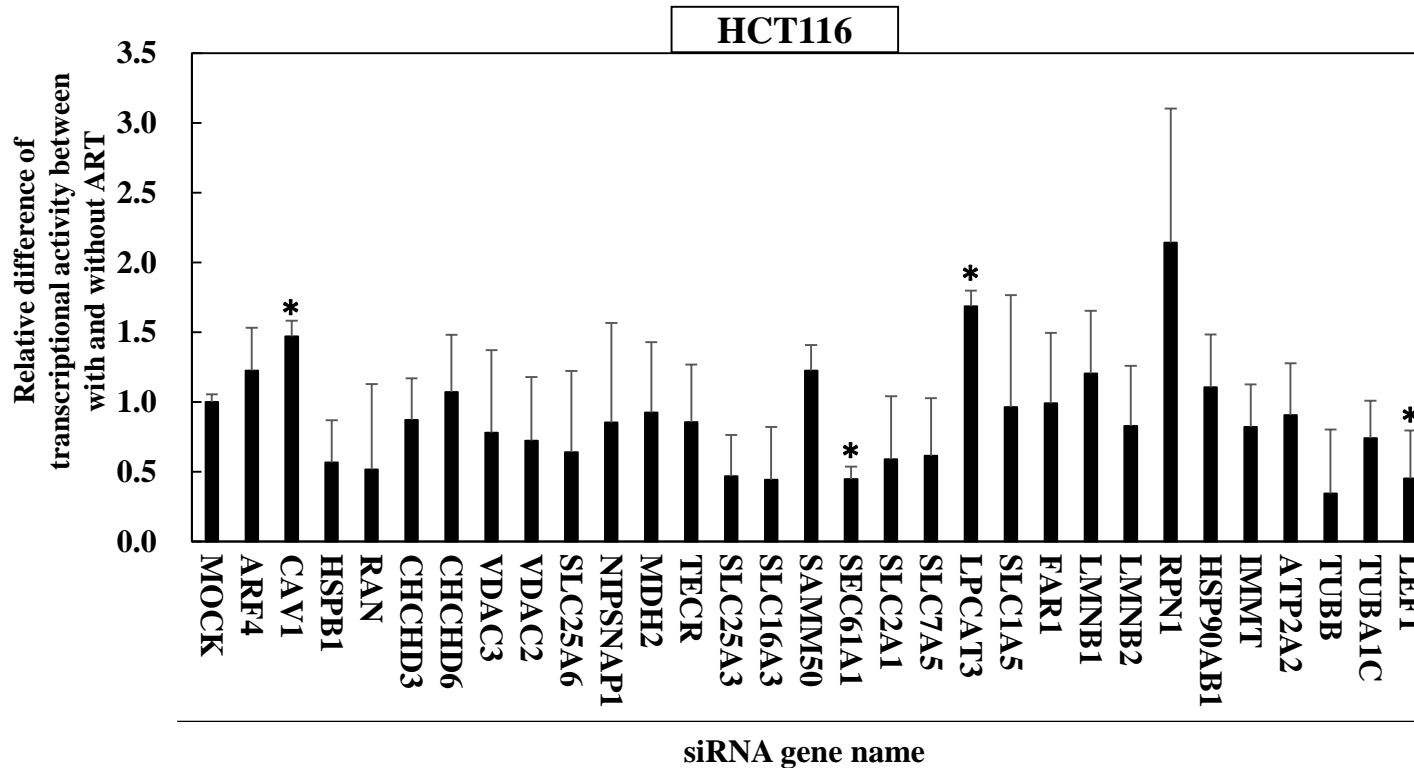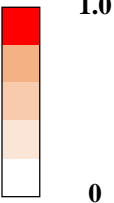
Figure 25. Difference of promoter transcriptional activity obtained between siRNA and ART treatment in HCT116 cells.
In the HCT116-TCF/LEF-Luc cells, to knock down each protein, transfection was performed by mixing three siRNA primers. After that, each cell was treated with 0.5 µM ART for 24 h. And evaluated the difference of the TCF/LEF promoter transcriptional activity between no treatment in candidate gene knock-down cells treated and ART treatment in candidate gene knock-down cells. The difference of the luciferase activity in Mock is set as 1.0. Data are presented as the mean $\pm$ SD (n = 3). *$p < 0.05$ *vs* MOCK cells.

A

Gene name	DLD-1	HCT116
MOCK		
LEF1		
ARF4		
CAV1		
HSPB1		
RAN		
CHCHD3		
CHCHD6		
VDAC3		
VDAC2		
SLC25A6		
NIPSNAP1		
MDH2		
TECR		
SLC25A3		
SLC16A3		
SAMM50		
SEC61A1		
SLC2A1		
SLC7A5		
LPCAT3		
SLC1A5		
FAR1		
LMNB1		
LMNB2		
RPN1		
HSP90AB1		
IMMT		
ATP2A2		
TUBB		
TUBA1C		

The ratio of luc. value — 1.0 / 0

B
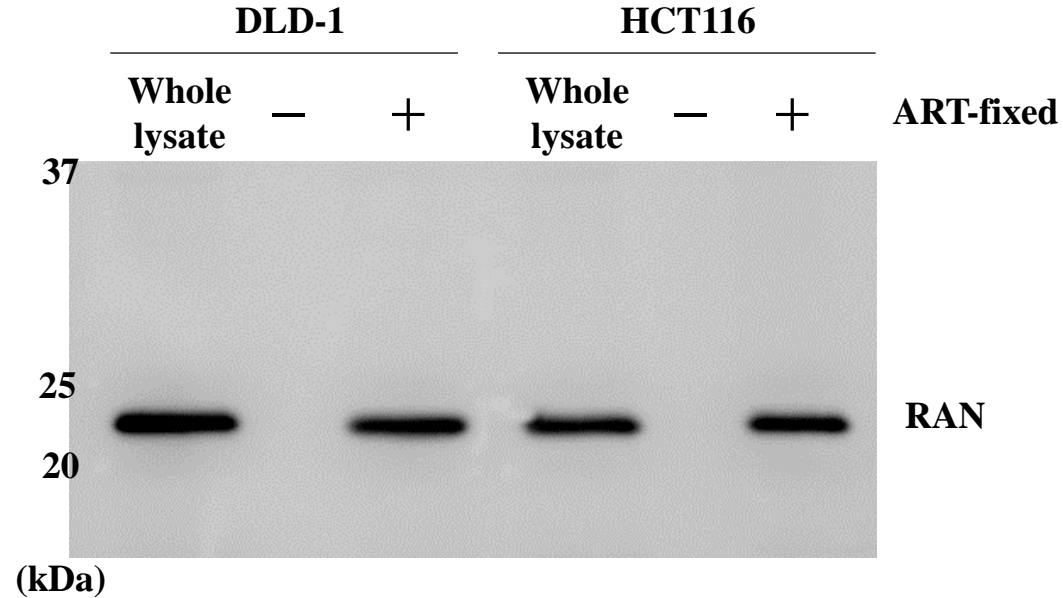
Figure 26. Identification for artesunate-binding proteins.
Using the Figure 24 and 25 results, I showed the importance of the protein required for ART to suppress TCF / LEF transcriptional activity using heat maps (A). Each colors represent mean value from 4 samples. (B) Empty beads or ART-fixed beads were incubated with 200 µg of whole cell lysate of DLD-1 cells or HCT116 cells, and the beads or ART binding protein were electrophoresed. The elution was analyzed by western blot using anti-RAN antibody. ART, artesunate. Luc, luciferase.

74
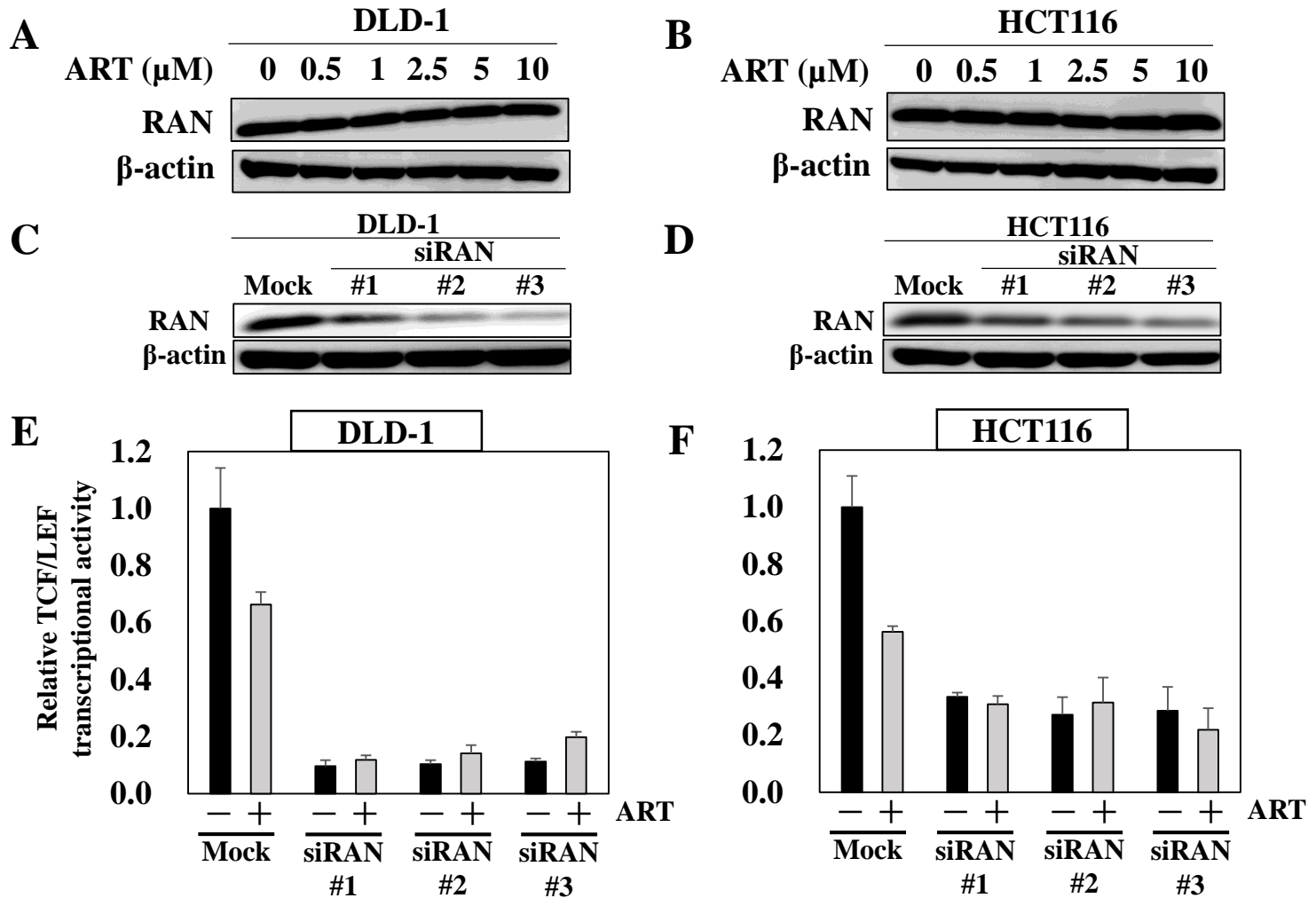
Figure 27. RAN knockdown inhibited the suppression effect of TCF / LEF transcriptional activity by artesunate.
DLD-1 (A) and HCT116 cells (B) were seeded in 24-well plates at a density of 2×10^5 cell/well, and treated with indicated dose of artesunate for 24 h. DLD-1-TCF/LEF-Luc cells and (C) HCT116-TCF/LEF-Luc cells (D) were transfected with mock (control siRNA) or RAN siRNAs (#1, #2 and #3), and cultured for 72 h. 15 µg of whole cell extract was added, and electrophoresis was performed. After then, the elution was analyzed by western blot using anti-RAN and anti-β-actin antibodies. β-actin was used as a control (A - D). DLD-1-TCF/LEF-Luc cells and (E) HCT116-TCF/LEF-Luc cells (F) were transfected with mock (control siRNA) or RAN siRNAs (#1, #2 and #3), and cultured for 72 h. After that both cells treated with 0 µM (ART −) or 0.5 µM ART (ART+) for 24 h. The basal luciferase activity of the control (mock cells plus 0 µM ART) was set as 1.0. Data are shown as mean $\pm$ SD, n = 4.
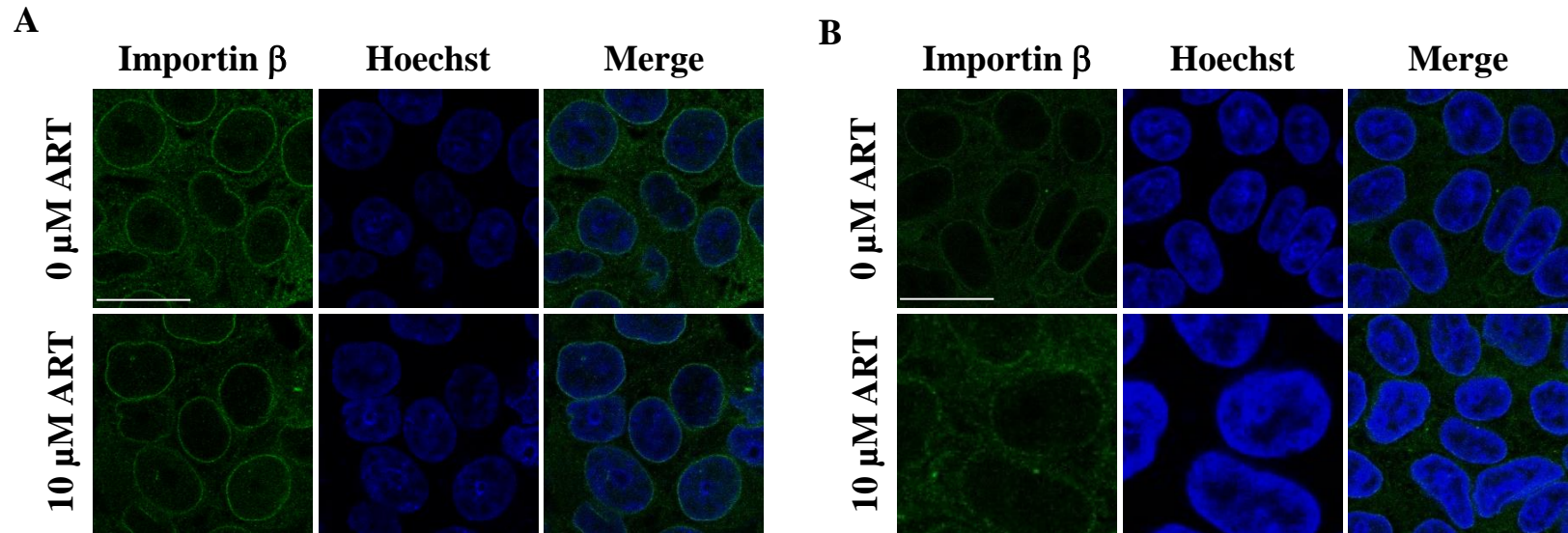
Figure 28. Effect of artesunate on Importin β localization.
Localization of Importin β protein was evaluated by immunofluorescence assay. HCT116 (A) and DLD-1 cells (B) were seeded in 8-well chamber slides, and the cells were treated with 10 µM ART. The cells analyzed by confocal microscopy for the localization Importin β (green) and nuclear (Hoechest, bule). Scale bars; 20 µm.
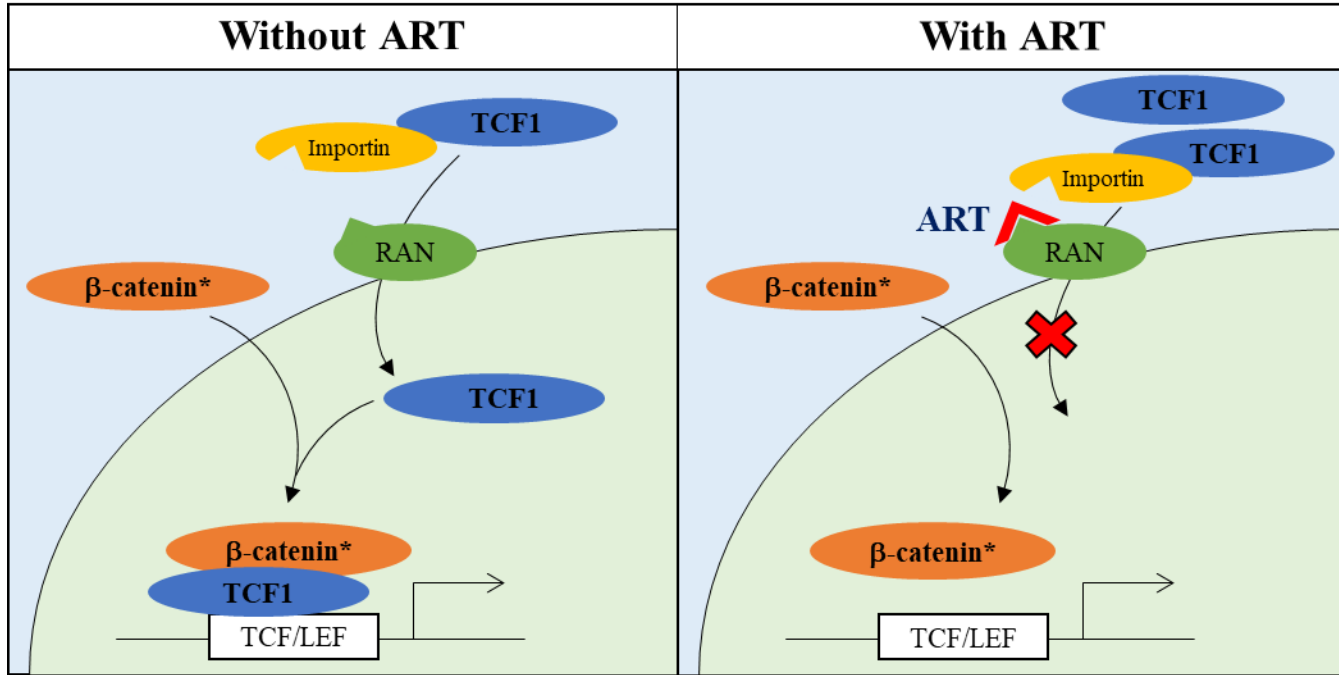
Figure 29. Schema of assumed WNT signaling suppression by artesunate.

Table 1. Primer sequences

Name	Sequence (5'→3')
human IL-6-F	CACCCCTGACCCAACCACAAAT
human IL-6-R	TCCTTAAAGCTGCGCAGAATGAGA
human COX-2-F	GATACTCAGGCAGAGATGATCTACCC
human COX-2-R	AGACCAGGCACCAGACCAAAGA
human c-Myc-F	TCAAGAGGTGCCACGTCTCC
human c-Myc-R	TCTTGGCAGCAGGAAGTCCTT
human Cyclin D1-F	CTGTGCTGCGAAGTGGAAACC
human Cyclin D1-R	GTCCAGGTAGTTCATGGCCAGC
human GAPDH-F	CCACCCATGGCAAATTCC
human GAPDH-R	TGGGATTTCCATTGATGACAA
mouse IL-6-F	TGTTCTCTGGGAAATCGTGGA
mouse IL-6-R	AAGTGCATCATCGTTGTTCATACA
mouse COX-2-F	GTGCCAATTGCTGTACAAGC
mouse COX-2-R	TACAGCTCAGTTGAACGCCT
mouse NOX1-F	TCCCTTTGCTTCCTTCTTGA
mouse NOX1-R	CCAGCCAGTGAGGAAGAGTC
mouse NOX2-F	GGGGTGTTGAAGGTCTCAAA
mouse NOX2-R	TGTTACCAACTGGGACGACA
mouse p22^{phox}-F	CGTGGCTACTGCTGGACGTT
mouse p22^{phox}-R	TGGACCCCTTTTTCCTCTTT
mouse c-Myc-F	GCTCGCCCAAATCCTGTACCT
mouse c-Myc-R	TCTCCACAGACACCACATCAATTTC
mouse Cyclin D1-F	TGACTGCCGAGAAGTTGTGC
mouse Cyclin D1-R	CTCATCCGCCTCTGGCATT
mouse GAPDH-F	TTGTCTCCTGCGACTTCA
mouse GAPDH-R	CACCACCCTGTTGCTGTA

Table 2. Antibodies List

Antibody		Clone, Cat#	Vendor	City, State, Country
β-actin	Mouse monoclonal	A2228	Sigma-Aldrich	St. Louis, MO
β-catenin	Mouse monoclonal	610154	BD Transduction Laboratories	San Jose, CA, USA
β-tubulin	Mouse monoclonal	ab179513	Abcam	Cambridge, MA, USA
c-Myc	Rabbit monoclonal	ab32072	Abcam	Cambridge, MA, USA
Cyclin D1	Rabbit monoclonal	2978T	Cell Signaling Technology, Inc.	Danvers, MA, USA
Lamin A+C	Rabbit monoclonal	ab232730	Abcam	Cambridge, MA, USA
LEF1	Rabbit monoclonal	2230T	Cell Signaling Technology, Inc.	Danvers, MA, USA
Non-phospho β-catenin (Ser33/37/Thr41)	Rabbit monoclonal	8814S	Cell Signaling Technology, Inc.	Danvers, MA, USA
TCF1/TCF7	Rabbit monoclonal	2203S	Cell Signaling Technology, Inc.	Danvers, MA, USA
TCF4	Rabbit monoclonal	ab76151	Abcam	Cambridge, MA, USA

Table 3. siRNA target sequence (part 1)

NCBI gene symbol	No.	siRNA Target Sequence (5'→3')	Product Id	Product Name
ARF4	#1	CAAGACAACCATTCTGTATAA	SI04307142	Hs_ARF4_7
	#2	AACGTTAAATGAAATTGGATA	SI04159029	Hs_ARF4_5
	#3	CTGCTTGTACCAGCCAGAGAA	SI04313281	Hs_ARF4_8
ATP2A2	#1	CAACTGGAGTTAACACCGAAA	SI03053337	Hs_ATP2A2_9
	#2	AAGGTGATACTTGTTCCCTTA	SI02626680	Hs_ATP2A2_6
	#3	CAGACACTAACTTTAGCGATA	SI00156807	Hs_ATP2A2_3
CAV1	#1	AAGCAAGTGTACGACGCGCAC	SI00299642	Hs_CAV1_10
	#2	AAATTAAGAGCTTCCTGATTG	SI02654617	Hs_CAV1_13
	#3	CACCTGTAAACCTGAGTCGTA	SI04381482	Hs_CAV1_17
CHCHD3	#1	CAGGATGCATTCTACAAAGAA	SI00345345	Hs_CHCHD3_1
	#2	CCGCTCTGGCCACCCAGTATA	SI04138435	Hs_CHCHD3_5
	#3	ACACTCTTGAGTATTAGTAAA	SI04232641	Hs_CHCHD3_8
CHCHD6	#1	CAGGGTGTCCTTCGGAGTGGA	SI00345450	Hs_CHCHD6_4
	#2	ACGCCGTGACACCTTCTACAA	SI00345443	Hs_CHCHD6_3
	#3	CTCGGACCTGGTCAAGGCATA	SI04364822	Hs_CHCHD6_6
FAR1	#1	AGCGAACTCACCCAACCTAAA	SI04261481	Hs_MLSTD2_6
	#2	TGGATGGATGATGGCCTAGTA	SI04207546	Hs_MLSTD2_5
	#3	CAAGTTGCGGAATATACGTTA	SI04263119	Hs_MLSTD2_7
HSP90AB1	#1	TACGTTGCTCACTATTACGTA	SI03110100	Hs_HSP90AB1_3
	#2	CACAACGATGATGAACAGTAT	SI03055304	Hs_HSP90AB1_1
	#3	CAGAAGACAAGGAGAATTACA	SI03062990	Hs_HSP90AB1_2
HSPB1	#1	ACCCGACTGGAGGAGCATAAA	SI02650606	Hs_HSPB1_7
	#2	TCCGCGACTGGTACCCGCATA	SI04231129	Hs_HSPB1_10
	#3	AAGGACGAGCATGGCTACATC	SI00300496	Hs_HSPB1_1
IMMT	#1	TCGGGATGACTTTAAACGAGA	SI04246347	Hs_IMMT_6
	#2	AAGCATTAGAACATCACAGAA	SI00447237	Hs_IMMT_4
	#3	GCCCGTTTCTATGCTGTTCAA	SI04226628	Hs_IMMT_5
LEF1	#1	CCCGAAGAGGAAGGCGATTTA	SI00114947	Hs_LEF1_3
	#2	CCCATCAGATGTCAACTCCAA	SI05392289	Hs_LEF1_9
	#3	CTGGTCTGCAAGAGACAATTA	SI03099719	Hs_LEF1_5
LMNB1	#1	AACGCGCTTGGTAGAGGTGGA	SI00300671	Hs_LMNB1_2
	#2	CCCGAGCATCCTCAAGTCGTA	SI04187463	Hs_LMNB1_7
	#3	AGGGAAGGGTTTCTCTATTAA	SI02656269	Hs_LMNB1_6
LMNB2	#1	CCGGAAGATGCTGGACGCCAA	SI02652223	Hs_LMNB2_2
	#2	CGCCTACAAGTTCACGCCCAA	SI04278295	Hs_LMNB2_7
	#3	TCGGCAATAGCTCACCGTTTA	SI02652244	Hs_LMNB2_5
LPCAT3	#1	CTGGATACTATTACACTGCCA	SI04320477	Hs_MBOAT5_3
	#2	CTGGGCTTCAATGGCTTTGAA	SI00328790	Hs_C3F_4
	#3	CACGTGGGACAAATGGCTTAA	SI04143496	Hs_MBOAT5_1
NIPSNAP1	#1	CCGCTCCCTCTTTGTTCACAA	SI04326742	Hs_NIPSNAP1_6
	#2	CAGAATGGGTCCCAACATCTA	SI00659015	Hs_NIPSNAP1_1
	#3	CTCACAGATAGGAGAGCTCTA	SI04335149	Hs_NIPSNAP1_7
PDIA3	#1	AAGCTGCAGCTACCAGATTAA	SI02654771	Hs_GRP58_5
	#2	AAGGAATAGTCCCATTAGCAA	SI02654778	Hs_GRP58_6
	#3	TAGCTGCACTGTTTATGGAAA	SI00075642	Hs_GRP58_1
RAN	#1	AACGACCTTCGTGAAACGTCA	SI04950512	Hs_RAN_9
	#2	ATCCATTGTCTTCCACCGAAA	SI04950519	Hs_RAN_10
	#3	ATCACAATATTCAGTGGTGAA	SI04950505	Hs_RAN_8
RPN1	#1	TGGGAGATTCTTCACAGTCAA	SI00706874	Hs_RPN1_2
	#2	ACCCATGTGCTTCATCCGTAT	SI04221791	Hs_RPN1_7
	#3	CAGGATGTTTATTACCGGGAT	SI03175074	Hs_RPN1_5

Table 3. siRNA target sequence (part 2)

NCBI gene symbol	No.	siRNA Target Sequence (5'→3')	Product Id	Product Name
SAMM50	#1	AACAATGAAGGCAGTATGGTA	SI03019079	Hs_SAMM50_1
	#2	CCCATTGGTGATAAGCCGTCA	SI04322885	Hs_SAMM50_5
	#3	ATCGCTCGGTTGGAACTTAAT	SI04183039	Hs_SAMM50_3
SEC61A1	#1	AAGATTCAGTTTAAGGAGAAA	SI00714133	Hs_SEC61A1_3
	#2	TTCTCTCTTCATTGCAACTAA	SI04327400	Hs_SEC61A1_7
	#3	CCCGGTCCATGCAGTTGTATA	SI04318321	Hs_SEC61A1_6
SLC16A3	#1	CCGGAGCATCATCCAGGTCTA	SI00720419	Hs_SLC16A3_1
	#2	GCCCGTGTTCGTGGTGAGCTA	SI04134774	Hs_SLC16A3_5
	#3	GCCGGCAACGCTTGCTATTTA	SI04362435	Hs_SLC16A3_7
SLC1A5	#1	CAGCCTTTCGCTCATACTCTA	SI00079709	Hs_SLC1A5_1
	#2	CACGCTGCCGCTGATGATGAA	SI00079730	Hs_SLC1A5_4
	#3	CCGGTCCTGTACCGTCCTCAA	SI00079723	Hs_SLC1A5_3
SLC25A3	#1	CAAGGGCATATTTAACGGATT	SI04307422	Hs_SLC25A3_8
	#2	CTGGCGCACATCACTATATTT	SI03211761	Hs_SLC25A3_5
	#3	TGCTTTGAACGTACTGTTGAA	SI04248664	Hs_SLC25A3_7
SLC25A6	#1	AACCAAGAGAACCACGTAGAA	SI02776879	Hs_SLC25A6_5
	#2	CTCAACCGTGCGGACCATCAA	SI04434150	Hs_SLC25A6_8
	#3	CGTGTTCTAAGTATTTATTTA	SI02780232	Hs_SLC25A6_6
SLC2A1	#1	CCGGGCCAAGAGTGTGCTAAA	SI00089264	Hs_SLC2A1_2
	#2	CAGCTGGATGAGACTTCCAAA	SI03068436	Hs_SLC2A1_5
	#3	CTGAAGTCGCACAGTGAATAA	SI04750368	Hs_SLC2A1_9
SLC7A5	#1	GAACATTGTGCTGGCATTATA	SI03101000	Hs_SLC7A5_6
	#2	TGGGCTTGTGACATTCGTGAA	SI00725536	Hs_SLC7A5_4
	#3	ACGCACGACGTCAGCCTCTTA	SI00725515	Hs_SLC7A5_1
TECR	#1	CGCCACCATTGCGGAGATCAA	SI04337459	Hs_GPSN2_7
	#2	GACGGTCTTCCTAACAGAGTA	SI03216724	Hs_GPSN2_5
	#3	CTGGATCGGTTTCGCCATCAT	SI00430528	Hs_GPSN2_1
TUBA1C	#1	CAAGGTTGGCATTAATTACCA	SI04352600	Hs_TUBA1C_1
	#2	GAGGATGAGGGTGAAGAGTAT	SI04368609	Hs_TUBA1C_2
	#3	CTGTAAATGTCTATTGCCGTA	SI02654071	Hs_TUBA6_3
TUBB	#1	CCGCATCTCTGTGTACTACAA	SI03650444	Hs_TUBB_10
	#2	CCCATTCCATTTGTCCAGTTA	SI03077249	Hs_TUBB_8
	#3	GCGGATCAGCGTCTACTACAA	SI02780883	Hs_TUBB3_5
VDAC2	#1	CCGGTTCATCTAATACAGACA	SI03082912	Hs_VDAC2_10
	#2	AAAATACAAGTGGTGTGAGTA	SI00302148	Hs_VDAC2_5
	#3	TGGTTTCTAGTTGGTTATCTA	SI02631013	Hs_VDAC2_6
VDAC3	#1	AACGTACTGTGACCTAGGAAA	SI03030090	Hs_VDAC3_6
	#2	AACTGACTCTTGATACCATAT	SI00302155	Hs_VDAC3_5
	#3	ACCCTTCGACCAGGAGTCAAA	SI03039631	Hs_VDAC3_8

Table 4. The number of intestinal polyps/mouse in Min mice treated with or without erythromycin

Erythromycin (ppm)	No. of mice	No. of polyps/mouse				
		Small intestine			Colon	Total
		Proximal	Middle	Distal		
0	7	7.9 ± 4.3	20.3 ± 5.6	35.9 ± 16.1	0.7 ± 1.0	64.7 ± 21.3
500	7	2.3 ± 1.4**	17.7 ± 5.2	28.3 ± 11.2	0.1 ± 0.4	47.0 ± 13.5

Data are presented as the means ± SD (n = 7).
Significant difference in comparison with control group (0 ppm EM) **$p < 0.01$.

Table 5. The levels of RCs detected in the Liver (pmol/mg wet tissue)

Compounds	Control	Erythromycin
Acetaldehyde	36657.2 ± 7070.5	76880.8 ± 82777.6
Acrolein	1165.5 ± 125.7	947.3 ± 116.7**
Glyoxal	12360.8 ± 1624.5	10380.5 ± 2136.9
Propanal	5919.6 ± 488.3	5606.8 ± 1121.5
Crotonaldehyde	1491.8 ± 223.7	1301.3 ± 236.5
Butanal	3157.6 ± 385.8	3005.2 ± 426.6
Pentanal	671.1 ± 81.8	728.6 ± 120.5
2-Hexenal	156.3 ± 26.5	155.2 ± 35.3
Hexanal	8403.2 ± 1651.6	9859.4 ± 1288.6
2-Heptenal	110.2 ± 27.2	97.8 ± 18.9
Heptanal	2125.4 ± 730.4	2508.1 ± 718.7
2-Octenal	81.2 ± 12.4	91.0 ± 12.7
Octanal	4857.5 ± 1324.8	5532.1 ± 1051.9
2,4-NDE	299.8 ± 37.8	385.9 ± 45.3*
2-Nonenal	1043.5 ± 98.0	1306.1 ± 270.5
Nonanal	13480.2 ± 3013.7	16970.2 ± 2868.9
2,4-DDE	239.7 ± 27.0	326.6 ± 80.9*
HNE	217.5 ± 47.1	341.5 ± 75.7**
Decanal	2169.8 ± 674.4	2897.8 ± 723.2
2-Undecenal	75.6 ± 10.3	104.0 ± 15.8***
Undecanal	1254.8 ± 256.5	1450.8 ± 319.4
Dodecanal	19945.8 ± 5636.9	23770.4 ± 3946.5
Tridecanal	2362.8 ± 833.7	2820.3 ± 857.4
Tetradecanal	1319.5 ± 359.0	1275.9 ± 386.1
Pentadecanal	5275.3 ± 2039.9	4198.6 ± 2320.0
Hexadecanal	9318.7 ± 2994.8	7359.1 ± 2736.5
8,11,14-HpDTE	261.6 ± 76.5	213.3 ± 81.1
8,11-HpDDE	349.3 ± 141.2	373.4 ± 88.9
8-HpDE	329.9 ± 34.3	291.3 ± 127.0
Heptadecanal	1075.1 ± 401.5	969.1 ± 372.1
Octadecanal	2176.8 ± 1025.5	1532.6 ± 773.6

Data are presented as mean ± SD (n=5).
Significant difference in comparison with control group (0 ppm EM) *$p<0.05$, **$p<0.01$, ***$p<0.001$.

Table 6. The weight of organs in Min mice treated or untreated with artesunate

	Organ name	Control (n = 12)	ART 5 ppm (n = 12)	ART 10 ppm (n = 12)
	Body	25.09 ± 1.83	25.58 ± 1.73	25.69 ± 2.47
	Liver	1.24 ± 0.09	1.25 ± 0.11	1.25 ± 0.15
weight(g)	Spleen	0.12 ± 0.05	0.10 ± 0.03	0.12 ± 0.06
	Kidney	0.16 ± 0.02	0.17 ± 0.01	0.16 ± 0.02
	Visceral fat	0.36 ± 0.13	0.42 ± 0.12	0.40 ± 0.16

Data are presented as the means ± SD.

No significant differences were detected in the weight of each organ treated or untreated with artesunate.

Table 7. The number of intestinal polyps/mouse in Min mice treated with or without artesunate

Treatment (ppm)	No. of mouse	Small intestinal			Colon	Total
		Proximal	Middle	Distal		
0	12	2.4 ± 1.6	9.3 ± 3.6	24.4 ± 7.1	0.3 ± 0.5	36.5 ± 9.7
5	12	2.6 ± 1.4	9.2 ± 3.1	19.3 ± 4.4*	0.2 ± 0.4	31.3 ± 4.3
10	12	2.1 ± 1.5	7.4 ± 4.9	17.4 ± 6.5*	0.1 ± 0.3	27.0 ± 10.3*

Data are presented as the means ± SD.

Significant difference in comparison with 0 ppm artesunate treatment *$p < 0.05$.

Table 8. The list of top 50 proteins detected only with ART-fixed beads

Accession	Score	coverage(%)	Num. of Peptide
Q16891|MIC60_HUMAN	1119	57	165
Q9NX63|MIC19_HUMAN	506	45	42
Q9BQE3|TBA1C_HUMAN	503	35	69
P07437|TBB5_HUMAN	354	35	43
P68371|TBB4B_HUMAN	289	35	45
Q13509|TBB3_HUMAN	269	32	33
Q13885|TBB2A_HUMAN	264	35	41
P45880|VDAC2_HUMAN	175	26	24
P11166|GTR1_HUMAN	142	10	13
P04843|RPN1_HUMAN	141	37	35
Q9NVI7|ATD3A_HUMAN	134	20	19
Q9BPW8|NIPS1_HUMAN	94	24	24
Q9Y512|SAM50_HUMAN	94	29	28
Q9Y277|VDAC3_HUMAN	88	17	14
Q9NX63|MIC19_HUMAN	83	31	7
Q9BRQ6|MIC25_HUMAN	74	27	8
Q99720|SGMR1_HUMAN	64	17	6
Q8NC51|PAIRB_HUMAN	59	12	4
Q9UJZ1|STML2_HUMAN	58	16	8
Q96LW7|BINCA_HUMAN	53	18	4
Q03135|CAV1_HUMAN	52	10	2
Q8WVX9|FACR1_HUMAN	52	15	8
P00338|LDHA_HUMAN	50	9	4
P12236|ADT3_HUMAN	49	24	12
Q07021|C1QBP_HUMAN	46	8	3
Q00325|MPCP_HUMAN	46	13	7
Q01650|LAT1_HUMAN	43	12	14
P61619|S61A1_HUMAN	43	16	14
O15260|SURF4_HUMAN	42	6	10
O43175|SERA_HUMAN	42	8	4
Q8TB61|S35B2_HUMAN	40	9	8
P30049|ATPD_HUMAN	39	13	2
P08238|HS90B_HUMAN	38	3	3
O15427|MOT4_HUMAN	37	12	9
O14828|SCAM3_HUMAN	36	12	5
P06454|PTMA_HUMAN	36	9	1
Q15758|AAAT_HUMAN	35	10	6
P55854|SUMO3_HUMAN	34	20	2
Q03135|CAV1_HUMAN	33	21	5
Q14722|KCAB1_HUMAN	32	3	2
P27824|CALX_HUMAN	32	3	2
P16615|AT2A2_HUMAN	31	11	15
P40926|MDHM_HUMAN	31	7	2
Q99805|TM9S2_HUMAN	31	5	3
Q99653|CHP1_HUMAN	30	24	5
Q15459|SF3A1_HUMAN	30	2	2
P50402|EMD_HUMAN	29	11	3
P22626|ROA2_HUMAN	29	2	1
P62826|RAN_HUMAN	29	10	3
P60660|MYL6_HUMAN	29	14	2